UNIVERSITY OF MINNESOTA

CENTER FOR TRANSPORTATION STUDIES

RESEARCH REPORT

Thermal and Mechanical Fatigue Effects On GFRP Rebar-Concrete Bond

Department of Civil Engineering

Catherine French•Dr. Carol Shield•Annie Christine Retika

Technical Report Documentation Page

1. Report No.	2.	3. Recipient's Accession No.
CTS 97-10		

4. Title and Subtitle	5. Report Date
Thermal and Mechanical Fatigue Effects on GFRP Rebar-Concrete Bond	December, 1997
	6.

7. Author(s)	8. Performing Organization Report No.
Annie Christine Retika, Dr. Carol Shield, Dr. Catherine French	

9. Performing Organization Name and Address	10. Project/Task/Work Unit No.
Department of Civil Engineering 500 Pillsbury Drive S. E. Minneapolis, MN 55455	11. Contract (C) or Grant (G) No. (C) (G)

12. Sponsoring Organization Name and Address	13. Type of Report and Period Covered
Center for Transportation Studies 200 Transportation and Safety Building 511 Washington Ave. S.E. Minneapolis, MN 55455	Final Report 1995 14. Sponsoring Agency Code

15. Supplementary Notes

16. Abstract (Limit: 200 words)

This report summarizes an experimental program conducted to investigate the thermal and mechanical fatigue effects on the bond between Glass Fiber-Reinforced Plastic (GFRP) rebars and concrete. Variables included in the study were rebar diameter (No. 6 and No. 4 GFRP, No. 6 steel), material (steel and GFRP) and manufacturer (two different manufactures for the GFRP rebar). For comparison, specimens were also fabricated using steel rebar as a control. The embedment lengths were chosen so that a splitting failure was assured in all specimens.

A total of 30 inverted half-beam specimens were cast in 15 beams. Six specimens were mechanically tension-tension cycled, twelve specimens were thermally cycled and twelve were used as control specimens (no thermal or mechanical fatigue). During thermal fatigue, the rebars were also subjected to a constant tensile load to simulate dead load.

During the bond tests, specimens were loaded continuously until failure while monitoring load, free-end slip, and loaded end slip. The results were evaluated to compare the bond performance of GFRP rebar to steel rebar, and to determine the effects of thermal and mechanical fatigue on bond.

It was found that mechanical fatigue has more detrimental effect on steel that on GFRP specimens while thermal fatigue has more effect on GFRP than on steel specimens. The effect of thermal fatigue was more in GFRP M2 than in M1 specimens. The difference in bond performance between No. 6 and No. 4 GFRP M1 cannot be determined form this study due to inferior product quality of the No. 4 M1 bars.

17. Document Analysis/Descriptors	18. Availability Statement
thermal and mechanical fatigue Glass Fiber-Reinforced Plastic	No restrictions. Document available from: National Technical Information Services, Springfield, Virginia 22161

19. Security Class (this report)	20. Security Class (this page)	21. No. of Pages	22. Price
Unclassified	Unclassified		

Thermal and Mechanical Fatigue Effects On GFRP Rebar-Concrete Bond

Prepared by

Annie ChristineRetika
Dr. Carol Shield
Dr. Catherine French

Final Report Prepared for

UNIVERSITY OF MINNESOTA
CENTER OF TRANSPORTATION STUDIES

April 1997

ACKNOWLEDGEMENTS

The University of Minnesota Center of Transportation Studies provided funding for the project. Generous material donations, provided by Rebarfab, Inc., Corrosion Proof Products, and PolyStructures, Inc., were greatly appreciated.

The financial support of oil overcharge funds distributed through the Minnesota Department of Administration is acknowledged, but the authors assume complete responsibility for the contents herein.

TABLE OF CONTENTS

List of Tables

List of Figures

ABSTRACT

This report summarizes an experimental program conducted to investigate the thermal and mechanical fatigue effects on the bond between Glass Fiber-Reinforced Plastic (GFRP) rebars and concrete. Variables included in the study were rebar diameter (No.6 and No.4 GFRP, No.6 steel), material (steel and GFRP) and manufacturer (two different manufacturers for the GFRP rebar). For comparison, specimens were also fabricated using steel rebar as a control. The embedment lengths were chosen so that a splitting failure was assured in all specimens.

A total of 30 inverted half-beam specimens were cast in 15 beams. Six specimens were mechanically tension-tension cycled, twelve specimens were thermally cycled and twelve specimens were used as control specimens (no thermal or mechanical fatigue). During thermal fatigue, the rebars were also subjected to a constant tensile load to simulate dead load.

During the bond tests, specimens were loaded continuously until failure while monitoring load, free-end slip, and loaded end slip. The results were evaluated to compare the bond performance of GFRP rebar to steel rebar, and to determine the effects of thermal and mechanical fatigue on bond.

It was found that mechanical fatigue has more detrimental effect on steel than on GFRP specimens while thermal fatigue has more effect on GFRP than on steel specimens. The effect of thermal fatigue was more in GFRP M2 than in M1 specimens. The difference in bond performance between No.6 and No.4 GFRP M1 cannot be determined from this study due to inferior product quality of the No.4 M1 bars.

Chapter 1: Introduction

1.1 GENERAL

For more than 100 years, steel bars have performed quite well as a reinforcing medium in concrete structures except where members have been exposed to aggressive environments such as coastal and marine structures, bridges, chemical plants, and wastewater treatment facilities. The corrosion problem has become a tremendous concern since extensive salting of bridges and highways began in the late 1960's [1].

Several methods have been used to prevent the corrosion of steel reinforcement such as the use of admixtures to improve the impermeability of concrete and the use of epoxy-coated steel rebars. However, extensive premature corrosion of epoxy-coated rebars has been found in new bridges, which indicates a shortcoming of this technique [2]. The localized corrosion in the epoxy coated rebar (caused by localized cracking of the coating) is probably worse than the corrosion in the uncoated steel rebar, because the localized corrosion goes deeper into the bar instead of spreading on the surface of the rebar.

As a result, in the last 15 years there has been an increase in the use of alternative reinforcing materials for concrete in harsh environments. The recent advancements in the field of plastics and fiber composites have resulted in the development of fiber-reinforced plastic (FRP) rebars that surpass the strength and fatigue properties of steel.

Many questions still remain about the suitability of using FRP rebars in concrete structures due to the lack of information and design guidelines. Of particular importance is understanding the effect of thermal fatigue on the bond strength between the FRP rebars and the concrete, especially for structures in Minnesota where there are large annual temperature

swings. Thermal fatigue is important because the coefficient of thermal expansion of Glass Fiber-Reinforced Plastic (GFRP) rebar is similar to that of concrete in the longitudinal direction, but is five times as large as that of concrete in the transverse direction [3]. The objective of the current project was to study the thermal and mechanical fatigue effects on the bond between GFRP rebars and concrete.

1.1.1 How GFRPs are manufactured

In the United States, GFRP rebars are manufactured by pultrusion. In this process, strands of slightly twisted glass fiber are drawn through a catalyzed vinyl ester resin bath, then carefully aligned and pulled through a heated steel die which strips away excess resin and produces the desired rod diameter, with final rod composition approximately 30% thermosetting resin and 70% glass fiber by volume. A band of glass fibers is wound around the rod in a spiral, creating the final indented surface that is intended to provide mechanical bond between the rebar and concrete [4].

Besides glass fiber, other types of fiber that currently predominant the composite industry are kevlar (aramid) and graphite (carbon). The choice of resins is limited to polyester and epoxy resins, because these two matrix systems are utilized for the bulk of current structural composites [5]. Epoxy resins are typically stronger and have better chemical resistance than polyester resins, especially for resisting the effects of an alkaline and saline environment [6]. However, polyester is acceptable in its resistance for typical chemicals such as de-icing salts or other chemicals spilled by trucks passing over bridges [5].

Some mechanical properties, such as tensile strength and modulus, are primarily dependent upon the fibers, while the interlaminar shear strength is primarily dependent upon the matrix. Tensile strength of FRP bar is sensitive to rebar diameter. The ultimate tensile strength of FRP rebars decreases as the rebar diameter increases due to inadequacies in interlaminar shear transfer from outer fibers to the core fibers [7].

1.1.2 Advantages and Weaknesses of FRP Rebars

FRP rebars have several important advantages as well as drawbacks over conventional reinforcing steel. The main advantages are as follows [8]:

Corrosion resistant - FRP rebars resist the corrosive effects of acids, salts, and similar aggressive materials under a wide range of temperatures.

High Strength - The ultimate strength of GFRP rebars is reported at over 100 ksi. The high strength of these bars is adequate for reinforcement in concrete structures.

Low Weight - The specific gravity of FRP rebars is one-fourth that of steel. The light weight of plastic rebars reduces transportation costs and enables easier handling on construction sites.

Non-conductivity - Plastic rebars have excellent electrical insulating properties, therefore they are ideal for applications where electric or electromagnetic insulation is required in concrete structures, such as in airports to eliminate radar interference problems.

Economy - The cost of GFRP rebars is slightly higher than that of epoxy-coated steel rebars. However, other features of GFRP rebars, such as light weight and longer service life, could make them more economical than epoxy-coated steel rebars.

Weaknesses of FRP rebars

Fiber-Reinforced Plastic rebars would not be suitable for applications in which the possibility of a high-temperature fire existed [4]. The flexural strength for the FRP rebars decreases significantly at temperatures in excess of 400 °F.

Another consideration is that although FRP rebars have ultimate strengths greater than that of commonly used Grade 60 steel rebars, their stiffness is only about one-fourth that of steel [4]. The lower stiffness affects deflection and crack width parameters of a structural member. And unlike steel rebars, GFRP rebars fail in a brittle manner with little or no ductility. This is illustrated in Figure 1.1 which shows the comparison of the stress-strain curves between steel and GFRP rebars.

Proper anchorage of FRP rebars in concrete is also a major consideration. To fully utilize the high tensile strength of FRP rebars in reinforced concrete and to avoid extreme concrete cracking or even member failure, the bond between the rebar and the concrete has to be sufficient for the rebar to develop its ultimate tensile strength.

Durability of GFRP rebars still needs careful investigation. Ultraviolet radiation, thermal cycling, and moisture can cause a breakdown of the matrix resulting in loss of strength of the whole composite [6]. Moreover, concrete alkalinity is a concern because glass fibers are very vulnerable in alkaline environments. Silica (largest component in glass fiber) and alkalis react chemically, resulting in dissolution of silica accompanied by a rapid and severe strength loss [9].

1.2 BACKGROUND

The following sections provide background regarding bond behavior and summarizing previous research on the bond of GFRP rebars.

1.2.1 Measure of Bond Strength

The bond strength between reinforcing bar and concrete primarily depends on concrete compressive strength, reinforcing bar diameter and spacing, embedment length, and concrete cover. Bonding is provided by chemical adhesion between the two materials, the friction due to surface roughness of the bars, the mechanical anchorage of the bar surface deformation, and shrinkage pressure of the hardened concrete against the rebars [10]. Bond strength of FRP rebars will also depend on fiber volume ratio, fiber and resin types, and rebar surface condition (smooth vs. ribbed vs. sand coated) [11].

There are various measures of bond strength. But the most widely used is the average bond stress, which can be calculated as the load divided by the surface area of the bar embedded in the concrete, or:

$$u = \frac{P}{\pi d_b l} \tag{1.1}$$

where, u is the nominal bond stress, P is the maximum applied force, d_b is the rebar diameter, and l is the embedment length.

1.2.2 Modes of Failure

There are three types of failure observed in bond tests:

Tensile failure: The ultimate tensile strength of the rebar is developed because the rebar embedment length is larger than what is required to develope its ultimate strength.

Pullout failure: This type of failure occurs if adequate confinement is provided in the form of transverse steel, large cover, or a combination thereof. The confinement allows the tensile stress in the concrete to be resisted. In contrast to steel reinforced concrete, where the steel bar shears the concrete located between bar deformations, in FRP reinforced concrete, concrete shears the surface deformations of the FRP bar, causing large slippage and bond failure [10]. This difference is illustrated in Figure 1.2 in which the shearing of the concrete is shown by the dashed lines.

Splitting failure: If sufficient concrete cover and/or transverse confinement are not provided to resist the radial tensile stress in concrete, a splitting failure occurs, in which the bar exerts pressure on the surrounding concrete, forcing the covering concrete to split. This is the type of failure most often observed in bridge decks or other members without transverse reinforcement. Therefore, for the current study transverse reinforcement was not used and the development length as well as the cover were chosen to assure that a splitting failure would occur.

1.2.3 Type of Bond Test Specimen

There are three types of specimens typically used in bond research: pullout, inverted half-beam, and splice type specimens.

Pullout specimens consist of a test bar cast uniaxially in a small block or cylinder of concrete as illustrated in Figure 1.3. These specimens do not accurately reflect the state of

stress in a concrete beam or deck because during the pullout test the concrete surrounding the rebars is put into compression, reducing the possibility of cracking and increasing the bond strength, while in reality the concrete surrounding the rebar of a real structure is under tension, thus allowing cracking at lower stresses and reducing friction [12]. However, the tests are very economical and allow preliminary relative comparisons.

Inverted half-beam specimens are used as a more realistic bond test. A typical specimen is shown in Figure 1.4 along with the shear and moment distribution. The specimen allows the test bar to be in an area of flexural tension under a moment gradient and constant shear, as illustrated. If P is the load in the exposed bar, l_1 is the distance between P and the low horizontal reaction, R_3, and l_2 is the distance between the two vertical reactions, R_1 and R_2, then R_1 (and R_2) equals Pl_1/l_2, which is the constant shear developed in the specimen. The longer l_2 is, the smaller the shear. The specimen has zero moment at the free end and a maximum moment of Pl_1 at the loaded end.

The bar is bonded over a specific embedment length and unbonded near the free end and the loaded end (Figure 1.4). The unbonded region near the loaded end is called the lead length, and its purpose is to prevent conical pullout failure. Relative slip between the reinforcement and the concrete can be measured at both ends.

Splice type bond specimens are considered the most realistic and costly. They consist of full scale beams with two point loads (Figure 1.5). As can be seen, two bars are spliced in an area of constant moment and zero shear. The specimen fails in bond in the splice region. This test provides comparison of deflection and overall structural performance, however the slip between the rebar and the concrete cannot be measured.

1.2.4 Background on Development Length

Development length, as defined in ACI318-95, is the length of embedded reinforcement required to develop the design strength of reinforcement at a critical section. For deformed bars or deformed wire in tension, the formula relating the development length to the bar diameter is given by:

$$\frac{l_d}{d_b} = \frac{3}{40}\frac{f_y}{\sqrt{f'_c}}\frac{\alpha\beta\gamma\lambda}{\left(\frac{c+K_{tr}}{d_b}\right)} \tag{1.2}$$

where l_d is the development length, d_b is the bar diameter, f_y is the yield stress of the bar, f'_c is the concrete compressive strength, c is the spacing or cover dimension, K_{tr} is the factor representing the contribution of confining reinforcement, and α, β, γ and λ are factors accounting for the reinforcement location, coating, size, and concrete type, respectively. All of these variables will affect the bond strength between the rebar and the concrete.

Because GFRP bars fail in a brittle manner (i.e., without yield), this equation cannot be applied directly to determine the development length of GFRP bars. Even though some equations have been proposed for the development lengh of GFRP bars (as will be mentioned in the next section), more further investigation is still needed to develop design guidelines for GFRP bars.

1.2.5 Previous Research

In this section, highlights of previous bond studies regarding FRP-reinforced concrete will be presented. Although several investigators have studied the feasibility of using FRP bars

as reinforcement in concrete, prior to the current project, no work had been done to investigate the effects of thermal or mechanical fatigue on the bond between FRP rebars and concrete.

Brown and Bartholomew at Widener University [4] conducted experimental work on FRP-reinforced concrete to study its flexural behavior through destructive testing of concrete beams and its bond strength through cylinder-pullout specimens. Twenty-four pullout specimens were tested, in which 3/8 in. diameter FRP rebars were embedded a specified length into standard 6x12 in. concrete cylinders. The test parameters included embedment length (4 in. and 6 in.) and concrete compressive strength, which varied from 1160 psi to 4200 psi at the age of testing. No information was provided on material type and properties of the GFRP bars.

It was found that in the tests conducted with lower f'_c , bond failure resulted when slippage of rebar occurred, with little surface cracking of the concrete. On the other hand, in specimens with higher f'_c, little slippage occurred, while specimens exhibited cracking and splitting of the concrete.

Bond strength in this study was measured as the nominal bond force per unit embedment length, which was calculated from the pullout force (P) divided by the rebar embedment length (l). To overcome the difficulty of varying concrete compressive strengths, k values were calculated as the nominal bond force per unit embedment length normalized with respect to the square root of f'_c, or:

$$k = \frac{P}{l\sqrt{f_c'}} \tag{1.3}$$

The researcher concluded that specimens with similar embedment lengths had similar k factors, regardless of f'_c. The overall average k value from all tests was 20.37. For comparison,

the k value for steel (calculated using the ACI318-89 average bond stress equation multiplied by bar circumference) was found to equal 30. Thus, it was concluded that the FRP rebars in this study had a bond strength approximately two-thirds that of steel bars. From flexural tests, it was also observed that FRP-reinforced beams exhibited ductile failure modes.

Pleimann at the University of Arkansas [14] conducted cylinder pullout tests with No.2, No.3, and No.4 GFRP bars, varying embedment lengths from 4 to 12 in. in 2 in. increments. The FRP was E-glass with vinylester resin. From tensile tests of the GFRP bars, the mean tensile strength was found to be 170 ksi, and the modulus of elasticity was 7700 ksi. Each bar size and embedment length combination was investigated for 28 day concrete compressive strengths of 3000, 4500, and 6000 psi.

Four pullout tests were done with No.2 bars, 19 tests with No.3 bars, and 21 tests with No.4 bars. No data was available on the pullout loads of the specimens. For each test, the k factor was calculated using Eqn.(1.3). For No.2 bars, the mean k value was 24.86 with 95% reliability value (RV) being 18.14 (95%RV means 95% of the data will fall between 2 standard deviation away from the mean, given a bell curve distribution). For No.3 bars the k value was 29.19 with 95% RV of 21.92, and for No.4 bars the k value was 32.70 with 95% RV of 24.23. The change in k with bar size indicates a scale factor relative to bond strength, showing that bond strength of the fiberglass rebars improves with size.

It was concluded that the ultimate tensile strength and the modulus of elasticity of the GFRP bars may be safely assumed to be 160 ksi and 7.5×10^3 ksi, respectively. This value of ultimate strength is considerably high because the bars tested in this research were small, and

for GFRP bars the ultimate strength decreases with an increase in bar size. It was also concluded that the development length may be safely assumed to be:

$$l_d = \frac{f_u A_b}{20\sqrt{f_c'}} \tag{1.4}$$

where, l_d is the development length, f_u is the ultimate strength of the rebar, A_b is the area of the rebar, and f'_c is the concrete compressive strength.

Faza and GangaRao at West Virginia University [11] conducted four-point bending tests and cantilever bond tests on concrete beams reinforced with FRP bars. Variables in the bond tests were bar size and embedment length. Twelve specimens were tested: No.8 rebar (l=16 and 24 in.) and No.3 rebar (l=8, 12, 16, and 24 in.) in 4200 psi concrete. No information was provided on material properties of the GFRP bars. The bond test set up was similar to that of inverted half-beam specimens. All of the specimens with No.8 rebar demonstrated a splitting failure, with u equal to 465 psi and 400 psi for 16 in. and 24 in. embedment length, respectively. All of the specimens with No.3 bar experienced tensile failure except the 16 in.embedment length, which failed in the grip. More bond studies were recommended.

From the bending test, it was observed that FRP reinforced beams developed sudden cracks with widths larger than the corresponding ones in steel reinforced beams. The crack pattern in terms of crack width and their distribution was vastly improved by using sand coated rebars due to a better bond between the sand coated rebar and the concrete [11].

Daniali at Lamar University [10] investigated the bond strength of FRP bars and their modes of failure using beam specimens. The FRP bars were made of vinylester resin and

type E-glass fibers with a glass content of 60-70% by weight. The concrete compressive strength at 28 days was 4500 psi. Variables considered were bar diameter and development lengths: No.4 with 8, 12, and 16 in. embedment; No.6 with 12, 18, and 24 in. embedment; No.8 with 20, 25, and 30 in. embedment. A total of 27 beam specimens were tested.

The specimens were 8x18 in. by 10 ft. long reinforced with one No.4, No.6 or No.8 bar and four No.2 FRP bars to keep shear reinforcement in place. The stirrups were made of No.3 FRP bars. A concrete cover of $3d_b$ was used for No.4 bars, $2d_b$ for No.6 bars, and $1.75d_b$ for No.8 bars (the reason for using different cover was not mentioned).

The full tensile strength was developed in all No.4 specimens. Only No.6 specimens with 24 in. embedment could develop their full tensile strength, while others with 12 and 18 in. embedment lengths had pullout and splitting failures, respectively, at $90\%f_u$. All beams with No.8 bars had pullout failure at a load of 70 to 90% of f_u. The crack patterns were the same in identical specimens and very wide prior to failure.

Larralde and Silva at Drexel University [12] conducted twelve cylinder-pullout tests to study the bond of GFRP rebars and concrete, using No.3 and No.5 GFRP rebars with 3 and 6 in. embedment lengths, and 4000 psi 28 day concrete strength. The FRP rebars were made from type S-glass and vinylester resin with spiral deformation pattern. The average modulus of elasticity and ultimate strength were 7500 ksi and 80 ksi respectively.

Load and displacement measurements were taken at each load stage, and were used to calculate the corresponding normal stress, nominal bond stress, and slip. It was found that the slip at failure was much larger for FRP rebars than that of steel rebars.

It was observed that for the change in embedment length from 3 to 6 in., the pullout force increased significantly, but the calculated bond strength decreased. This reduction was attributed to the nonlinear distribution of bond stress along the embedment length.

Ehsani, Saadatmanesh, and Tao at the University of Arizona [2] conducted a study on bond behavior of GFRP rebars using 48 beam and 18 pullout specimens. Rebars were constructed of E-glass fibers with 60% glass content by weight, with polyester matrix and spiral deformation pattern. The variables included in the study were concrete strength, bar diameter, embedment length, clear cover distance, and concrete casting depth. Bar sizes chosen were No.3, 6 and 9 GFRP bars, tested with 4000 and 8000 psi concrete (28-day target strength).

During the beam tests, slip between the rebar and concrete was recorded at the loaded and free ends of the rebar. From the load-slip curves, it was observed that the loaded-end slip increased with the increase of load at the beginning of the loading. However, the free end slip did not take place until the adhesion resistance between rebar and concrete was broken [2].

Three modes of failure were observed: splitting of concrete, rebar pullout and rebar fracture. Splitting failure was observed in specimens with small concrete cover ($1d_b$), which could not sustain the circumferencial tensile stresses. Pullout failure occured for shorter embedment lengths, and was signalled when both loaded and free end slips increased rapidly with only a slight increase in load. Rebar fracture was observed for longer embedment lengths and large covers. Splitting failure and rebar pullout are controlled by concrete strength, but rebar fracture is only controlled by the tensile capacity of the rebars.

The results showed an increase in ultimate bond stress with an increase in concrete strength, but the increase was not proportional to the square root of f'_c, as assumed with steel rebar. It also showed that the higher the casting position of the rebar, the lower the ultimate bond stress. This is attributed to the "top bar effect", that is for a bar cast with more than 12 in. of concrete below it, there is a possible void underneath the bar that can cause a higher water/cement ratio of the concrete surrounding the bar. This is due to the bleeding of water and air trapped beneath the top bar.

The recommended development length to develop the full tensile strength of No.3, 6 and 9 rebars were 8, 18, 30 in., respectively. It was realized that the pullout tests gave a higher ultimate bond stress due to elimination of concrete flexural cracks and therefore may result in unconservative development lengths. Also, the loaded-end slip was reduced in pullout specimens due to compression on the concrete surface which in turn limits the cracking.

Chaallal and Benmokrane at University of Sherbrooke [3,15], conducted 24 cylinder pullout tests to evaluate the bond strength of GFRP rebar and to determine the optimal anchored length required to develop full tensile load capacity of the GFRP rebar. The pullout tests were performed on No.4, 5, and 6 GFRP rebars (made of type E-glass fiber and polyester resin) and on conventional steel rebars for comparison purposes. The concrete compressive strength at 28 days was 4500 psi and the development length was either 5 times or 10 times the rod diameter.

Optimal anchored lengths to develop f_u and $0.7f_u$ were presented. The optimal length to develop $0.7f_u$ was provided for the sake of comparison with conventional steel reinforcement, with yield load, f_y, comparable to $0.7f_u$. It was observed that the bond strength of GFRP rebar

varied from 62 to 84% of that of steel bars (averaged over all bar sizes tested). The anchored length to develop f_u was found to be $20d_b$ while that to develop $0.7f_u$ was $10d_b$.

From the load-slip curve, it was observed that the curve was linear up to 70 to 85% of the peak load, nonlinear from there to the peak load, and dropped quickly following the peak load. In the nonlinear part, the resistance to pullout is provided by the frictional force between the rod and the concrete and by a force provided by mechanical interlock with the surface deformation of the rod. The drop of the curve following the peak load indicates that as slip increases, the bond strength decreases sharply due to shearing of surface deformations.

Extensive tension tests were also performed on No.4, No.5 and No.6 GFRP bars. It was observed that the GFRP bar behaves linearly up to failure, with an average ultimate tensile strength of 100 ksi, modulus of elasticity of 6000 psi, and ultimate strain of 1.8%.

In addition, some tests were conducted to determine the coefficient of thermal expansion, α, both in longitudinal and transverse directions. The result showed that α_L was similar to that of concrete and α_T was five times that of concrete. But regardless of the high value of α_T, no evidence of strength loss due to debonding was noticed in the flexural tests at low temperature (-30 °C).

Although no work had been done to investigate fatigue effects on the bond of FRP-reinforced concrete beams, a study was conducted by **Budelmann, Kepp and Rostasy in Germany** on the fatigue behavior of bond-anchored unidirectional GFRP rebar [16]. The FRP bars were type E-glass fibers (70% by volume) in a polyester matrix and anchored in a cylindrical steel tube which was filled with a quartz sand/polyester resin mortar. The bar was 0.3 in. in diameter and bonded through a short embedment length (0.8 in.) in the anchorage

tube. In the fatigue test, 2 million cycles of load were imposed with upper stress levels between 50 to 60% of the bar strength. The stress amplitudes varied between 4.4 to 14.5 ksi. It was found that the bond slip grows slightly with the number of cycles and accelerates considerably shortly before bond failure occurs.

From pullout tests conducted on the non-cycled specimens, it was observed that up to the peak load, the bond strength grows linearly and the slip is small, due to the adhesion component of the bond. After the peak load, the bond stress decreases, due to low friction component of the bond.

1.2.6 Summary of Previous Research

Table 1.1 summarizes the bond test results from previous research, in terms of bar size, embedment length, concrete compressive strength, cover, maximum pullout load (in kips and $\%f_u$), failure remarks, and k value. The pullout loads were listed as $\%f_u$ to see how much tensile strength were developed in the bars for specific embedment lengths.

The table is divided into three groups: a) pullout test, b) inverted half-beam test, and c) beam test. The pullout test was subdivided into cylinder and block specimens while the inverted half beam test were subdivided into specimens with and without stirrups and specimens with top bar. Some of the inverted half beam specimens from reference 2 had tensile failures at a percentage of f_u below 100. The reason for these failures was not mentioned in the paper.

To see the distribution of the results from previous research, a graph of maximum loads (in kips and $\%f_u$) versus development length (in terms of bar diameter) was constructed for each group of the table (Figure 1.6). Data from specimens with rebar failure (i.e., tensile failure, rebar that broke in the grip, and rebar delamination) were not included in the graphs. Lines

were drawn between data points of specimens with the same bar size and similar concrete strength. As can be seen, the maximum load tends to increase with an increase in the development length even though the increase did not follow any regular pattern. The plotted data shows a large variability, which is due to the non-uniformity of the GFRP bars being a composite material.

1.3 OBJECTIVE AND SCOPE

The objective of the current study conducted at the University of Minnesota was to investigate the thermal and mechanical fatigue effects on bond between FRP rebars and concrete. The load-slip behavior was measured experimentally to investigate these effects on bond and to study the difference of load distribution and transfer among all specimens.

A total of 30 specimens were cast in 15 inverted half-beam specimens. All beams were made from one batch of concrete to eliminate the effect of concrete strength variability. The target concrete compressive strength at 28 days was 4300 psi. Two bar diameters (No.4 and 6) with No.6 GFRP bars from two different manufacturers were tested to investigate the difference in bond performance. Specimens were also made from No.6 steel bars for comparison. Only No.6 GFRP and No.6 steel bars were compared for mechanical fatigue effect. All type of bars were tested for thermal fatigue effects, i.e. No.4, No.6 GFRP (from 2 manufacturers), and No.6 steel.

This study adds to the current knowledge to provide a better understanding of the bond between GFRP bars and concrete. Chapter 2 summerizes the experimental program. Chapter 3 presents the test results and evaluations. The major conclusions are presented in Chapter 4.

Chapter 2: Experimental Program

This chapter describes the experimental program used to determine the effects of thermal and mechanical fatigue on the bond between GFRP bars and concrete using inverted half-beam specimens. Thirty specimens made from one batch of concrete were tested. Six specimens were mechanically tension-tension cycled, twelve specimens were thermally cycled, and twelve specimens were used as control specimens (no fatigue effects). The control specimens were subjected to a constant load of $5\%f_u$ (ultimate strength of the rebar) to simulate dead load. The same constant loading was applied to the thermal fatigue specimens during temperature cycling.

Bond behavior was evaluated on the basis of measured ultimate bond strength and bar slip relative to concrete. Slip was measured both at the loaded end and free end of the bar.

2.1 TEST VARIABLES

Variables included in the study were rebar diameter (No.6 and 4 GFRP, No.6 steel), material (steel and GFRP) and manufacturer (two manufacturers for GFRP rebars). The development lengths were designed to ensure splitting failures in all specimens. Section 2.1.1 describes how the embedment lengths were selected. The selection of lead length is explained in Section 2.1.2.

2.1.1 Selection of Development Lengths

A series of pilot specimens were cast to estimate the development lengths to be used for the actual test bars. The purpose was to avoid rebar fracture in bond specimens

due to excessive embedment lengths. Concrete for these specimens was ordered from a ready mix plant, with the same mix design to be used in the later study. Because ready-mix concrete strength observed in past projects far exceeded nominal values, a concrete strength of 8 ksi was assumed in determining embedment lengths so as to avoid rebar fracture in the tests.

2.1.1.1 Steel Bars

For the steel bars, the development length was estimated using the equation developed by Orangun, Jirsa, and Breen for bars without transverse reinforcement [14]:

$$l_d = \frac{\frac{d_b f_s}{4\alpha\sqrt{f_c'}} - 50}{1.2 + 3\frac{C}{d_b}} \tag{2.1}$$

where, l_d is the development length (in.), d_b is the nominal bar dimeter (in.), f_s is the maximum steel stress developed before the bond fails (psi), f_c' is the concrete compressive strength (psi), C is the lesser of the side cover (C_s) and bottom cover (C_b) (in.), and α is a function of $C_s/C_b d_b$, taken from Fig. 4 of Reference [14] as 1.25. This equation was also used by Grundhoffer in determining the development length of steel bars in his study [13]. Based on an f_c' of 8 ksi, the embedment lengths were chosen using this equation such that the ratio of stress at pullout to yield stress (f_s/f_y) for the steel bars would equal approximately one.

Table 2.1 lists the steel stress ratio (f_s/f_y), where f_s was calculated using the OJB equation with different combinations of development lengths and concrete strengths. A ratio bigger than 1 means the steel stress is greater than f_y and the bar will yield. Concrete

strengths of 4.5, 6, and 8 ksi were evaluated to account for the possible range of concrete strengths to be obtained from the ready mix plant. From this table, $8d_b$ and $10.67d_b$ development length were selected for the steel pilot specimens because the stress ratio at f_c' of 8 ksi for these lengths were approximately one.

2.1.1.2 GFRP Bars

For GFRP bars, the development lengths were estimated by rearranging Eqn.(1.3) to yield:

$$l = \frac{P}{k\sqrt{f_c'}} = \frac{A_b f}{k\sqrt{f_c'}} = \left(\frac{\pi d_b f}{4k\sqrt{f_c}}\right) d_b \qquad (2.2)$$

where, P is the maximum pullout load (lbs), l is the development length (in.), A_b is the nominal area of the rebar (in^2), d_b is the bar diameter (in.), f is the maximum bar stress developed before the bond fails (psi), f'_c the is concrete compresive strength (psi), and k is the nominal bond strength, U, normalized with respect to $\sqrt{f_c'}$.

The k value for No.4 GFRP bar was taken from the pullout test results of Pleimann [14] who conducted the largest number of tests with No.4 GFRP specimens. The mean k value reported was 32.70 with 95% reliability value being 24.23. Because development length is inversely proportional with k (Eqn. (2.2)), a smaller k value will result in a larger (more conservative) development length. Therefore, in estimating the development length for the No.4 GFRP bar, the k value used was 25, which corresponds to the 95% reliability value above.

For No.6 GFRP bars, the k value used in estimating l_d was based on the data from previous research (Table 1.1). Only results from inverted half beam and beam tests were

included because the cylinder tests gave very high k values (78 and 63) resulting from concrete under compression during the test. The average k from previous research was found to be 32.67. It was decided to use k equals 30 for No.6 GFRP bars to give a conservative development length.

In his bond study, Chaalal [3,15] suggested a reduction of 30% in usable strength of GFRP for use in design due to the brittle failure. Using this reduction, the embedment lengths for the GFRP bars were chosen such that the ratio of bar stress at pullout to 70% of the ultimate bar stress, $f/(0.7f_u)$, would be approximately one. The value of f_u used was 90 ksi for both bar sizes. This value was chosen based on information given by one of the GFRP manufacturers, who reported an average of 90 ksi for No.6 bars and 70 to 110 ksi range for No.4 bars (which gave an average of 90 ksi).

A development length table (Table 2.2) was then made for No.6 and No.4 GFRP bars. In this table, the bar stress ratio is listed in two ways: as a ratio to ultimate strength, f/f_u, (tabulated in the left column) and as a ratio to $0.7f_u$, $f/(0.7f_u)$, (tabulated in the right column). This separation was made to compare the stress ratio on GFRP bars to that of steel bars, because $0.7f_u$ *(63 ksi)* is comparable to f_y of steel (60 ksi). Thus, development lengths can be chosen such that the same stress ratio can be developed in GFRP and steel bars. A stress ratio greater than 1 in the left column would mean the bar would likely be fractured.

From these tables, development lengths of $13.33d_b$ and $16d_b$ were chosen for the No.6 GFRP pilot specimens because the stress ratios in the left column for these lengths

are below 1 and the stress ratios in the right column correspond well to the steel stress ratio for $8d_b$ and $10.67d_b$ development lengths listed in Table 2.1.

Development lengths of $10d_b$ and $12d_b$ were chosen for the No. 4 GFRP pilot specimens because the stress ratios in the left column are all below 1. In the next section, only results from the specimen with $12d_b$-develepment length was presented because the specimen with $10d_b$-development length was damaged prior to testing.

2.1.1.3 Results of Pilot Specimens

All of the pilot specimens experienced splitting failure as expected. The results are tabulated in Table 2.3 in terms of concrete strength, maximum load, measured stress ratio (f_s/f_y or f/f_u) and expected stress ratio (f_s/f_y or f/f_u from Eqn.(2.1) and (2.2) respectively). As can be seen, the measured and expected stress ratios were very close together except for steel with $8d_b$ development length and No.6 GFRP with $16d_b$ development length which had a stress ratio lower than the expected ratio.

It was also noticed that the maximum load decreased with an increase in development length (from $13.33d_b$ to $16d_b$) in both GFRP M1 and M2 specimens. In steel specimens, however, the maximum load increased significantly with an increase in development length (from $8d_b$ to $10.67d_b$) which is typical for bond tests. The unexpected results observed in GFRP specimens may be due to the variability in the bond between GFRP bars and concrete.

The development length tables for steel and GFRP (Table 2.1 and Table 2.2 respectively) were used in conjunction with the results of the pilot specimens (Table 2.3) in determining the development lengths for the later study. From Table 2.1 and 2.2, the

development lengths with ratios of f_s/f_y or $f/0.7f_u$ of approximately one at f_c' of 8 ksi are $9.33d_b$ for steel, $13.33d_b$ for No.6 GFRP and $11d_b$ for No.4 GFRP.

Because the service load stresses in GFRP bars are expected to remain well below 50% of their ultimate strength [10], the development lengths for GFRP bars were also chosen so that the stress ratio f/f_u on the left column of Table 2.2 was about 0.50. This was done to keep the maximum bar stress far enough from the ultimate stress considering that GFRP bars fail in a brittle manner. From Table 2.2, the development lengths with f/f_u of approximately 0.5 at f_c' of 4.5 ksi were $13.33d_b$ for No.6 GFRP and $11d_b$ for No.4 GFRP (by interpolation). The associated stress ratios in the right column ($f/0.7f_u$) for these lengths were 0.73 and 0.74, which correspond closely to a stress ratio of 0.75 for development length steel (Table 2.1). The pilot specimens also indicated a stress ratio of approximately 0.50 for No.6 GFRP with $13.33d_b$ development length. Therefore, the development lengths chosen for the bond specimens in the later study were $13.33d_b$ for No.6 GFRP, $11d_b$ for No.4 GFRP, and $9.33d_b$ for No.6 steel bars.

2.1.2 Selection of Lead Length

Lead length is defined as the distance from the loaded end concrete face to the beginning of the development length. Its purpose is to prevent conical pullout failure in bond specimens. The lead length used for the pilot specimens was 0.5 in., the same as that used in the previous bond study of epoxy-coated steel bars by Grundhoffer [8]. This length was selected because it gave bond stress results closest to the predicted bond stress based on the Orangun, Jirsa, and Breen equation, (Eqn 2.1), [8].

Because all pilot specimens had splitting failures and failure loads close to those predicted (except for steel with $8d_b$ embedment and No.6 GFRP with $16d_b$), the 0.5 in. lead length was maintained for the later bond study.

2.2 SPECIMEN LABEL

Each specimen was labeled as follows:

Specimen Label: FB#AM

F	=	T for thermal fatigue specimens M for mechanical fatigue specimens C for control specimens
B	=	G for GFRP specimens S for steel specimens
#	=	4 for No.4 GFRP rebars 6 for No.6 GFRP or steel rebars
A	=	A,B,C (replication)
M	=	blank for steel M1 for first GFRP manufacturer M2 for second GFRP manufacturer

2.3 MATERIALS

2.3.1 Test bars

The GFRP rebars were manufactured by Corrosion Proof Products and PolyStructures, Inc. The former will be referred as GFRP M1 and the latter as GFRP M2. Figure 2.1 shows a photograph of the test bars. GFRP M1 has a grip mounted at the end of the bar (provided by the manufacturer) while GFRP M2 has no grip. For testing

purposes, an aluminum grip was later fabricated for GFRP M2 bars and the details can be found in Section 2.5.2.2.

Deformations on both types of GFRP bars are created by a strand of glass fibers wrapped around the bar in a helical pattern. The average spacing between strands was 1.75 in. for No.6 GFRP M1, 0.75 in. for No.6 GFRP M2, and 1.5 in. for No.4 GFRP M1. The spacing was more uniform in GFRP M1 than in GFRP M2. In addition, GFRP M1 has a sand coating, while GFRP M2 only has plastic grit particles on its surface.

From diameter measurements taken with a caliper on ten places for each bar type (both at the normal and indented surface), the averages were found to be 0.79 in. (normal) and 0.76 in. (indented) for No.6 GFRP M1, 0.84 in. and 0.76 in. for No.6 GFRP M2, and 0.54 in. and 0.53 in. for No.4 GFRP M1. As can be seen, the indentations of GFRP M2 were larger than those of GFRP M1.

The range in diameter measurements at the normal surface were 0.78 to 0.81 in. for No.6 GFRP M1, 0.8 to 0.85 in. for GFRP M2, and 0.54 to 0.56 in. for No.4 GFRP M1. At the indented surface, the ranges were 0.75 to 0.77 in. for No.6 GFRP M1, 0.74 to 0.78 in. for GFRP M2, and 0.525 to 0.529 in. for No.4 GFRP M1. As can be seen, GFRP M1 diameter was more uniform than that of GFRP M2.

Steel bars used in this experiment were Grade 60 steel with type N deformation pattern. They were manufactured by RebarFab, Inc. Six diameter measurements was taken along the rebar to yield an average of 0.72 in. at the normal surface and 0.82 in. at the rib. The range was 0.720 to 0.721 in. at the normal surface and 0.819 to 0.823 in. at the rib. As can be seen, the steel bars have more deformation than the GFRP M1 or M2 bars.

For the No. 6 GFRP bars from M1 and M2, three tension tests were conducted according to the procedure in Appendix A to determine the ultimate tensile strength and modulus of elasticity. The results are listed in Table 2.4. The average ultimate strengths were 68.3 and 86.6 ksi for No.6 GFRP M1and No. 6 GFRP M2 rebars respectively, with values ranging from 57.3 to 81.7 ksi for GFRP M1 and 81.6 to 93.8 ksi for GFRP M2. The average modulus of elasticity were 5500ksi for both No.6 GFRP M1 and No. 6 GFRP M2 rebars respectively. All GFRP M1 bars and two M2 bars failed ininterlaminar shear in the grip. One GFRP M2 bar failed in tension between the grips.

2.3.2 Concrete

Concrete was delivered from a ready-mix plant. The intention was to use a concrete mix currently specified for bridge deck construction in the State of Minnesota. Type 3Y33 MNDOT mix was ordered with 6% air entrainment and a target strength of 4300 psi at 28 days. The measured slump was 1.75 in (target slump was 3 in.).

The bond tests were performed when the specimens were between 4 to 8 months old. By this age, it was assumed that the concrete compressive strength would remain constant. From twenty three 6x12 in. cylinders tested, the average concrete compressive strength was found to be 5630 psi with a standard deviation of 430psi.

2.4 TEST SPECIMENS

Test specimens used were inverted half-beam specimensas described earlier in Section 1.2.3. They were 12 in. wide, 18 in. deep and 48 in. long. Each beam had two bars

extending from opposite end faces, so that two separate tests could be done on each beam. Drawings of the beam cross section for each bar type are shown in Figures 2.2 to 2.4 with a typical elevation view shown in Figure 2.5. As can be seen, no transverse reinforcement was used because it was not required for shear strength and also to promote a splitting failure in bond specimens, which is the anticipated failure mode in bridge decks.

Some auxiliary longitudinal reinforcement was added in the tension region near the corners of the beam (Figures 2.2 to 2.4). The purpose of these steel rebars was to prevent flexural failure in the unbonded region of the test beam. Two No.5 steel bars were used as auxiliary reinforcement in the No.6 GFRP specimens and two No.4 steel bars were used in the No.4 GFRP and No.6 steel specimens (based on moment calculation). The addition of this reinforcement was not intended to affect the bond behavior. Exact location of this auxiliary reinforcement is given in Figures 2.2 to 2.4.

The concrete cover was chosen at $2d_b$ to promote splitting failure, because larger cover may result in bar pullout or rebar fracture [10]. The cover was taken as the distance from the edge of concrete to the surface of the bar. Development lengths were controlled by shielding portions of the rebar with PVC pipe (Figure 2.5), which was centered around the bar using masking tape. The PVC pipe was carefully sealed with silicon sealant to prevent concrete from seeping in between the test bar and the PVC pipe.

The length of bar extending out of the specimen was 14.75 in. on average for GFRP bars and 19.25 in. for steel bars. The length was longer for steel because the wedge gripping system used for steel required a longer bar length than the gripping system for the GFRP bars. The bars also protuded 0.25 in. from the back of specimen to allow the

measurement of free end slip. Two holes were made for lifting ports using 3/4 in. PVC pipes as shown in Figure 2.2 to 2.5.

2.5 PLACEMENT OF CONCRETE

2.5.1 Formwork

Concrete forms were constructed from 1/2 in. plywood and were bolted together to enable disassembly and reassembly. The bars were held inside the form by holes made on the faces of the form. Forms for GFRP M1 specimens were also cut at the loaded face to allow easy dissasembling at the time of stripping, because these bars had a grip preattached to the end of the bar. The forms were treated with Crete-Lease form release agent after the bars were installed. Care was taken to insure that the release agent was not applied to the surface of the bars.

2.5.2 Casting

The beams were cast with the bars in the side position to eliminate top bar effects and to facilitate the same concrete casting depth for both bars. The bars had 6 in. of concrete below them, thus simulating bottom bar condition. Concrete was poured in 2 lifts (using a crane and bucket) and each lift was vibrated with a concrete vibrator. The first lift was approximately 10 in. All specimens received the first lift before any received the second lift. Companion concrete cylinders were made after the first lift was poured.

2.5.3 Concrete Curing and Stripping of Forms

Specimens were cured by covering the forms with plastic sheets and placing wet burlap on top of the forms to help supply a humid environment. Concrete cylinders were

also cured in the same way. This condition was maintained for a week until the forms were stripped. After stripping the forms, specimens were flipped to their correct orientation (one bar at the top and the other at the bottom) and kept in the lab environment until they were tested.

2.6 TEST SETUP

2.6.1 Bond Test Frame

The test frame used for the bond test is shown in Figure 2.6. This figure shows the set up used for testing steel specimens. The same set up was used to test the GFRP specimens using a different bar gripping system as will be discussed in the next section.

Reaction 1 on the specimen was created by a concrete block with a rocker support resting on it. Reaction 2 was created by a tie-down beam placed across the specimen via four 1 in. tension rods tied to the structural floor. A reaction fixture, made from a roller mounted on a steel plate, was placed between the tie-down beam and the specimen. Reaction 3 was carried into the testing frame by a rocker mounted on a steel plate and by a neoprene pad. The bar load was applied with a 77 kip MTS actuator through a grip system designed for each bar type.

Reaction 1 was located 6 in. from the loaded end, reaction 2 was located 10.5 in. from the free end, and the centroid of reaction 3 was located 13 in. from the test bar. These reactions were referred to earlier as $R_1, R_2, R_3,$ and R_4 in Figure 1.4.

2.6.2 Grip Systems

2.6.2.1 Steel Grip

A wedge grip was used to pull the steel bars. This grip was placed between two steel tubes connected by two threaded rods as shown in Figure 2.6. The first tube was used to react against the grip while the second tube was used to connect the system to the actuator head. This arrangement required a longer length of bar compared to the gripping system used for GFRP.

2.6.2.2 GFRP M1 Grip

As mentioned earlier, GFRP M1 had a grip mounted at the end of the bar (Fig. 2.1) provided by the manufacturer. This grip was then connected to the actuator head through a clevis device made from steel plates as shown in Figure 2.7. A 3/4 in. threaded rod was inserted through the hole in this grip system when testing.

2.6.2.3 GFRP M2 Grip

Because GFRP bars are very weak in the transverse direction, the region of the bar in the grip must be protected against crushing [10]. Therefore, the grip for the GFRP bars was designed to grasp the bar in a manner that failure at the grip region would be avoided.

Figure 2.8 shows the schematic of the grip made for GFRP M2. The design was based on the work done by Professor Charles Dolan at the University of Wyoming who conducted research on finding suitable grips for testing GFRP bars [18]. The grip was made from T6061 Aluminum with a parabolic core. With this design, lateral pressure induced to the bar will be minimized because the parabolic shape has zero slope at the

smaller opening end if the bar is oriented along the central axis of the grip. The formula for the radius of parabolic surface was:

$$r_x = r_0 + 0.08\frac{x^2}{L} \tag{2.3}$$

where, L is the anchor length, r_x is the radius at any point along the anchor ($x = 0$ at the anchor opening), and r_0 is the radius of the anchor opening.

In order to leave a 1/16 inch clearance around the bar, r_0 was selected to be 0.5 in. because the maximum diameter of No.6 GFRP bars was 0.85 in. The anchor length (L) was selected to be 6 in. long based on Dolan's results.

The inside gap between the bar and the parabolic wall was filled with Sikadur 35, Hi-Mod LV epoxy poured in three lifts. The volume of epoxy poured in the first lift was about 14% of the total volume needed to fill the gap, the second lift was 43% of the volume, and the third lift was also 43% of the total volume. Every lift was allowed to cure for 3 hours before the next lift was poured.

To pour the epoxy, the specimen was supported along the long axis so that the bar was oriented vertically upward. The bottom of the grip was supported by a plastic tube, with a slit cut on its side to slide the tube around the bar. The grip was mounted with the smaller opening toward the concrete face and the bigger opening away from the concrete face. The length of bar sticking out of the top of the grip was about 1/8 in. To center the bar, a round-shaped cardboard disk was cut with the same outside diameter as the bottom end of the grip and with a hole made in the center with the same diameter as the bar. A 5-

minute epoxy was applied along the circumference of the bar at the location of the lower opening to ensure no Sikadur epoxy would leak out of the grip.

To pull the grip, a steel fixture was designed to match the exterior threads on the grip. As shown in Figure 2.9, one end of the fixture was connected to the grip by threads, while the other end was connected to the clevis device used for GFRP M1, which then connected to the actuator head. The drawing of the steel fixture is shown in Figure 2.10 in plan, cross-sectional, and side views.

2.6.3 Instrumentation

As mentioned in Chapter 1, the relative slip between rebar and concrete can be measured at the free end and the loaded end. Free end slip (FES) represents pure slip relative to concrete and does not include elongation of the bar. Loaded-end slip (LES) includes the pure slip and elongation of the bonded bar. It is measured by placing a displacement transducer on the external portion of the bar to monitor relative movement between a point on the bar and the concrete face. This measurement includes slip, elongation of the bonded bar, and elongation of the bar outside the concrete. Loaded-end slip is defined as the loaded end displacement minus the elongation of the bar outside the bonded region [13]. By subtracting FES from LES, the elongation of the bar within the bonded region can be obtained. The following sections describe how the free end and the loaded end instrumentation were placed on the bond specimen.

2.6.3.1 Free-end Slip

The free end slip was measured using a ±0.1 in. Linear Variable Differential Transformer (LVDT) as shown in Figure 2.11. In this figure, the LVDT rod was connected to the test bar using a small aluminum block epoxied to the bar. The LVDT was referenced to the concrete face using an aluminum fixture epoxied to the concrete face.

2.6.3.2 Loaded-end Slip

The loaded-end slip was measured using six ±0.1 in. LVDT's for the steel specimens or two ±1 in. LVDT's (calibrated to ±0.5 in.) and four ±0.1 in. LVDT's for the GFRP specimens. The larger LVDT range was selected for the GFRP specimens because the GFRP bars were expected to have a larger amount of slip than the steel bars.

LVDT's were mounted on two nylon frames as shown in Figure 2.12 (plan and elevation views). As can be seen, LVDT C1 and C2 were placed at the front frame (180° apart) while B1 and B2 (180° apart), B3 and B4 (180° apart) were placed at the back frame. The two LVDT's placed 180° apart at each side of the bar were used to average out any effects due to bending, which may result due to unequal gripping, unsymmetric bar section, initial bend in the bar, and specimen misalignment [8].

The frames were positioned around the bar using wood spacers which were cut to the required head and gage lengths. The gage length for both steel and GFRP specimens was 2 in. As shown in Figure 2.13, the head length is defined as the distance from the loaded end concrete surface to the loaded end slip instrumentation. The head length was measured to the nearest 32nd of an inch before the test. The average was 2 in. for steel

and 2.75 in. for GFRP specimens. Different head lengths were used for steel and GFRP bars to allow enough space for mounting the required LVDT.

The loaded-end slip (LES) was detemined from 2 different sets of LVDT's to compare the results. The equations used were as follows (Figure 2.12):

$$LES = \frac{C1 + C2}{2} - \frac{B1 + B2}{2}\frac{(L_H + L_L)}{L_G}$$

or (2.4)

$$LES = \frac{C1 + C2}{2} - \frac{B3 + B4}{2}\frac{(L_H + L_L)}{L_G}$$

where:
LES = loaded-end slip (in)
$C1$ = displacement of LVDT C1 (in)
$C2$ = displacement of LVDT C2 (in)
$B1$ = displacement of LVDT B1 (in)
$B2$ = displacement of LVDT B2 (in)
$B3$ = displacement of LVDT B3 (in)
$B4$ = displacement of LVDT B4 (in)
L_H = measured head length (2 in. for steel or 2.75 in. for GFRP)
L_L = lead length (0.5 in.)
L_G = gage length (2 in)

2.7 TEST PROCEDURE

2.7.1 Bond Test

The specimen was aligned along the axis of the grip and then tightened against the main reaction beam. The back end of the specimen was supported by a hydraulic jack until load was applied.

During the test, the actuator was run in displacement control. The initial load was applied quickly at a rate of 1 in./min. so that the support at the back end of the specimen can be removed as soon as possible. This was important because to perform an inverted half-beam test, there should not be any support at the back end of the specimens that can create another reaction. The support was removed after reaching a load of approximately 3 kips. The specimen was then loaded at a rate of 0.05 in./min until failure, as specified in ASTM C234 for comparing concretes on the basis of the bond developed with reinforcing steel. As the specimen was loaded, the load and the displacements of the LVDT's were recorded at approximately 1 second intervals.

2.7.2 Mechanical Fatigue Test

Three No.6 steel specimens and three No.6 GFRP M1 specimens were subjected to mechanical fatigue before the bond test. These specimens were mechanically tension-tension cycled using the bond test set up mentioned above. A sinusoidal load was chosen, controlled by a function generator, with a load range of 4 to 10 kips. The lower limit was selected as the minimum load to keep the bar in tension and also to simulate dead load. The upper limit was selected to be 10 kips to represent service load in the real structure. Based on a reasonable flow capacity of the 77 kip actuator, a frequency of 0.5 Hz was used to apply the sinusoidal load cycles. Each specimen was subjected to 100,000 cycles in order to apply the equivalent of at least one year of traffic to the specimen and to test the specimens at similar age.

Free end and loaded end slip instrumentation was installed to monitor any degradation of the bond during the fatigue test. Load and LVDT readings were sampled

every 25,000 cycles. At the end of the mechanical fatigue test, the load was completely released. The bond test was then conducted with the procedure described in Section 2.7.1.

2.7.3 Thermal Fatigue Test

Twelve specimens were subjected to thermal cycles: three No.6 steel, three No.6 & No.4 GFRP M1, and three No.6 GFRP M2. These specimens were stored inside an enviromental chamber with a temperature controller. The temperature range of this chamber was cycled between -20 and 25 °C.

The temperature cycling was conducted over 3-1/2 months, with a total of 20 cycles. These cycles represent the cycles of temperature ranges over a life time of a bridge deck (20 years). A temperature probe was placed inside the room to monitor the temperature. To monitor the temperature inside the concrete, four type T thermocouples were embedded in four beams (one thermocouple per beam). They were positioned near the bonded region of the bar in order to monitor the temperature changes undergone by the concrete near the test bar. Readings from the thermocouples were sampled every 2 hours using a data logger. The data is presented in Figure 2.13 in which the readings from the temperature probe and the average of the four thermocouples inside the specimens were plotted versus time. The data from the four thermocouples agree with each other with a maximum deviation of 0.5 °C in cold peaks and 2°C in hot peaks.

During temperature cycling, the bar was also subjected to a constant load of 5%f_u to simulate dead load from self weight. Assuming 90 ksi for f_u of GFRP bars, this load equals 2 kips for No.6 GFRP and 1 kip for No.4 GFRP bars. The load for No.6 steel bars was chosen to be the same as that for No.6 GFRP bars, assuming a one-to-one

replacement of steel with GFRP bars in construction. A load frame, illustrated in Figure 2.14, was built based on a pulley concept to serve this purpose. The intention was to create a 2.4 kip load for the No.6 steel and GFRP bars and a 1.2 kip load for the No.4 GFRP bars by hanging 50 and 100 lb. weights respectively.

As can be seen in Figure 2.14, the weight was hung from a "magic box" (model 252940 manufactured by West Marine) which consisted of 4 pulleys that provided an 8:1 mechanical advantage. The magic box was then connected to a lever arm which provided a 3:1 mechanical advantage. Thus, the load carried to the bar was 24 times the weight hung below the "magic box".

A model was built to test this load system in which the load was carried to an actuator. The actual load measured was 23 times the load hung below the magic box due to friction in the system (mostly in the bearing of the pulley).

After finishing the temperature cycling, specimens were tested for bond according to the procedure described in Section 2.7.1.

2.7.4 Control Specimens

Control specimens were specimens that were not subjected to thermal or mechanical cycles before the bond test. They were twelve control specimens, consisted of three replicates for each bar type (i.e, No.6 steel, No.4 and No.6 GFRP M1, and No.6 GFRP M2). These specimens were subjected to a $5\%f_u$ constant loading in the same manner as that applied to the thermally cycled specimens. All of the control specimens were placed in the lab environment until they were tested.

Chapter 3: Experimental Results and Evaluation

This chapter presents the results and evaluation of the bond test experiments described in Chapter 2. General observations regarding bar load, specimen failure, and post failure are discussed in Section 3.1. The results of the mechanically and thermally cycled specimens are compared to those of the corresponding control specimens in Sections 3.2 and 3.3 respectively.

3.1 GENERAL

3.1.1 Bar Load

The maximum loads that were achieved in each specimen are tabulated in Table 3.1, along with the initial cracking load. The mean, standard deviation, and coefficient of variation values for the maximum load of each specimen group are presented in Table 3.2. Each group represents the results of three replicate specimens (i.e. A, B, and C).

From the values of coefficient of variation (COV) tabulated in Table 3.2, it can be seen that the scatter was relatively small (within 3 to 10% from the mean), with an exception for GFRP M2 control specimens with a COV of 12.4%. This may be due to the fact that GFRP M2 rebars were less uniform than the other bar types in terms of diameter, strand spacing and indentation.

The bar load was also tabulated based on the slip criteria for steel which is based on the critical bond stress at the lesser load associated with a free end slip of 0.002 in. or a loaded end slip of 0.01 in. [13]. This was done to compare the bond performance not only

by maximum load but also by slip. The loads are tabulated in Table 3.3 and will be used later in analyzing specimens with a relatively large slip at failure compared to the others in the same group.

3.1.2 Specimen Failure and Cracks

All of the specimens failed in bond by splitting of the concrete around the test bar. The initial cracking loads of the specimens are listed in Table 3.1 in kips and in fraction of the maximum load. As can be seen, some specimens started to crack at 80 to 99% of the maximum load while some did not exhibit any cracking up until failure. In the former type, the crack grew from an initial hair-line crack to a longer crack along the embedment length. The specimen failed when this crack reached the end of the embedment length. In most cases, the initial crack was first seen at the top surface of the beam at approximately 1 in. from the loaded end face. Only a few specimens had initial cracks near the bar circumference at the loaded end face. In the latter type, all of the cracks occurred simultaneously when the specimen experienced a sudden drop in load.

In general, specimens with the same bar type showed a similar crack patterns even though some variation was observed within the group. In No.6 GFRP M1 specimens (Figures 3.1 to 3.3), the crack extended along the embedment length and from below the bar at the loaded end face. The crack that extended along the embedment length was mostly straight until it split at the end, except for CG6AM1 in which case some cracks also existed in the direction perpendicular to the embedment. The crack at the loaded end face extended vertically below the bar before splitting in two directions.

In No.6 GFRP M2 specimens (Figures 3.4 to 3.5), the crack along the embedment length varied from a single line, as in TG6BM2 and CG6AM2, to a more diverse pattern as observed in CG6CM2 and TG6CM2. The crack at the loaded end face did not extend vertically except in TG6CM2.

In No.4 GFRP M1 specimens (Figure 3.6 to 3.7), the cracks at the top surface of the specimen did not follow any regular pattern along the embedment length and most specimens did not have cracks extending from below the bar at the loaded end face.

In most of the steel specimens, the crack formed a triangular shape near the bar both at the loaded end face and at the top surface of the beam (Figure 3.8 to 3.10). Cracks also extended from below the bar at the loaded end face of the specimen.

3.1.3 Post Failure Observation

For each specimen, the concrete along the embedment length of the bar was removed to inspect the bar condition and the concrete surface in contact with the bar. Table 3.4 summarizes the observation of the opened specimens in terms of the bar condition (e.g. helical strand and sand coating), the amount of concrete particles on the bar, and whether or not the helical strand was attached to concrete. Photographs of the opened specimens can be found in Appendix B.

In the steel specimens, a lot of concrete particles were found still adhered to the surface of the rebar, showing that the concrete had good adhesion with the steel bar. Most of the adhered concrete particles were found near the ribs (deformations) of the steel bar.

In GFRP M1 specimens, little or no concrete was found adhered to the surface of the bar. The helical strands that provided bar indentations were found broken and attached

to the concrete surface in contact with the rebar. In general, most of the sand coating was still in place with an exception of specimens MG6CM1 and TG6CM1 in which cases the coating was completely gone. In No.4 M1 control specimens, little pieces of the surface resin was found missing near the helical strands. These pieces were found attached to the concrete in contact with the rebar. This was the only specimen type that experienced the shearing of the surface resin. In CG6AM1, CG4AM1, and CG4CM1, longitudinal strands of glass fiber were also found attached to the concrete.

In GFRP M2 specimens, some concrete particles were found adhered to the bar upon removal. Most of the concrete was found near the helical deformations and the amount was less than that found in the steel specimens. All helical strands were intact but the bar coating was gone, leaving the bar with a dull color.

3.2 MECHANICAL FATIGUE

The bond performance of the mechanically cycled specimens was compared to that of the control specimens in terms of the maximum load that could be applied to the bar and the load-slip curve behavior. In the load-slip curves, the free and loaded end slip were plotted relative to the load up to the failure point (point of maximum load). Before discussing the results, a brief evaluation of the results from the LVDT readings taken during the mechanical cycles is presented.

3.2.1 Results From LVDT Readings During Mechanical Cycles

As mentioned in Chapter 2, LVDT readings were taken every 25,000 cycles to monitor any bond degradation during cycling. Each reading was taken over a 3-cycle period (6 seconds). The data was then plotted as free and loaded end slip versus time, as can be found in Appendix C. The slips amplitude (peak to peak slips) and slips average during the mechanical cycles were shown in Figures 3.11 to 3.12 for the GFRP specimens and Figures 3.13 to 3.14 for the steel specimens.

In the GFRP specimens, the slips amplitude and average were sligthly increasing with the number of cycles, showing that the bond was degraded progressively by the mechanical cycling. In the next section, it will be found that this degradation did not affect the overall bond strength because only the front end of the bond was being damaged.

The slips amplitude for the steel specimens were constant during the cycles (except for MS6A due to problem with data acquisition system). Even though no bond degradation was observed from the slips average, it will be found later that mechanical cycling had caused some bond reduction in the steel specimens. It is possible that all of the bond damage had taken place before the data for 0 cycle was taken, because the 0 cycle reading was taken within 5 minutes after the cycling begun.

3.2.2 Results from GFRP Specimens

The load-slip curves of the mechanically cycled GFRP specimens were compared to those of the control specimens as illustrated in Figure 3.15. Because the data for CG6AM1 was accidentally deleted, no slip information was available for this specimen (only the maximum load recorded). From the loaded end slip curves, it can be seen that

the slopes of the cycled specimens were flatter in the region between 4 to 10 kips (load range for mechanical cycles) compared to the region above the 10 k load. This indicates that the mechanical cycles lowered the stiffness of the specimen in this load range, but above this range the stiffness has not been degraded, therefore the slope starts to increase again.

The free end slip of MG6BM1 was the largest of the specimens in the group. From Table 3.3, the load at a free end slip of 0.002 in. for MG6BM1 was about 5 k lower than that of the other two replicate specimens. This lower performance could be due to lack of compaction at the time of pouring because no unsual damage on the bar was found in the opened specimen.

From Table 3.2, the mean maximum load of the mechanically cycled GFRP specimens was 23.7 k with 0.6 k standard deviation. The mean maximum load for the control specimens was 22.6 k with 0.8 k standard deviation. To compare the bond performance, the maximum tensile stress (P_{max}/A_{bar}) developed in the cycled specimens was divided by the maximum tensile stress in the control specimens. Because A_{bar} is the same, the ratio can be obtained only by dividing the load, to yield a range of stress ratio.

The lower limit of this ratio was calculated by dividing the minimum of the three loads from the cycled specimens by the maximum of the three loads from the control specimens. Likewise, the upper limit was obtained by dividing the maximum of the three loads from the cycled specimens by the minimum of the three loads from the control specimens. The average ratio was calculated by dividing the average load from the three cycled specimens by that of the control specimens.

The range obtained for the GFRP specimens was 0.99 to 1.11, with an average of 1.05. This implies that the cycled specimens developed larger stress than the control specimens. In this case, 100,000 mechanical cycles did not lower the bond strength in the GFRP specimens. The 5% increase of bond strength in the mechanically cycled specimens may be due to statistical variation in the results. The percentage is too small to have statistical significance as a real increase in bond strength.

Mechanical cycling did not lower the bond strength of the GFRP specimens (as will be mentioned for steel specimens) because GFRP bars have less surface deformations than steel bars. Thus, concrete near the indentation of a GFRP bar was not subjected to as much crushing as concrete near the rib of a steel bar. The difference in the height of deformation between steel and GFRP bars can be found in Section 2.3.1 which listed a rib height of 0.1 in. for steel and only 0.03 in. indentation for No.6 GFRP M1. In addition to the greater deformation height, the rib of a steel bar also crushes more concrete because steel is a harder material than GFRP.

3.2.3 Results from Steel Specimens

The load-slip curves of the mechanically cycled steel specimens were compared to those of the control specimens in Figure 3.16. The curves for MS6A were noisy due to problems with the data acquisition system and therefore were not included in the graphs. The curves for CS6B were not smooth near the maximum load because the specimen readjusted itself at the concrete block support (at the front end) by translating and rotating, therefore creating a load fluctuation. This adjustment occurred when the specimen overcame the friction built up in the system as load was applied. A change in

stiffness (slope) was observed in LES curve of MS6C above the 10 k load, which indicates that mechanical cycling only affect the stiffness of the specimen within the load range of the mechanical cycles (4 to 10 kips) as observed in the GFRP specimens.

The mean maximum load for the mechanically cycled steel specimens was 18.27 k with 1.14 k standard deviation (STD). The mean maximum load for the control specimens was 20.9 k with 0.9 k STD. By calculating the range of maximum stress ratio in the same way as for the steel specimens, a range of 0.79 to 0.97 was found with an average of 0.87. This implies that the maximum stress developed in the cycled specimens was less than that developed in the control specimens. In this case, 100,000 mechanical cycles reduced the bond strength by 13% in No.6 steel specimens. The reduction was caused by crushing (pulverizing) of the concrete by the ribs of the steel bar as the specimen underwent mechanical cycling. The pulverizing action rounded the concrete area near the ribs, thus loosening the bond between the bar and the concrete.

3.3 THERMAL FATIGUE

The bond performance of the thermally cycled specimens was compared to that of the control specimens in the same manner as was done for the mechanically cycled specimens.

3.3.1 No.6 GFRP M1 Specimens

The load-slip curves comparison between thermally cycled and control No.6 M1 specimens is presented in Figure 3.17. From the free end slip curves, it can be seen that the stiffness (slope) of the cycled specimens was much less than that of the control specimens.

The loaded end slip curves show a lot of variability, which is common in GFRP bond test results due to the non-uniform property of the composite rebar.

It can be seen that the failure point in TG6AM1 was reached at a lower LES compared to the other two replicate specimens. This was due to the elimination of the rubber pad between the concrete specimen and the steel reaction beam because the test bar was not long enough to reach the grip. This elimination caused the load to increase at a faster rate, even though the actuator displacement rate was the same, resulting in failure at less slip. The load at failure was also lower compared to the other two replicates, which contradicts the expectation of a higher failure load associated with a faster loading rate. The low performance of TG6AM1 might also due to lack of compaction, because when the specimen was opened, all helical strands and sand coating were still intact.

From the free end slip curves, it can be seen that the stiffness of TG6CM1 was much lower than the other two replicates. This may be caused by rebar defect, because the sand coating was no longer observable upon opening the specimen and no concrete was attached to the bar. In the other two replicate specimens, the sand coating was still on the bar and some concrete particles were found attached to the bar.

The mean maximum load for the GFRP M1 cycled specimens was 20.0 k with 1.3 k standard deviation. The control specimens had a mean maximum load of 22.6 k with 0.8 k standard deviation. The range of maximum stress ratio calculated was 0.80 to 0.97 with an average of 0.89. This implies that the stress developed in the thermally cycled specimens was lower than that in the control specimens. In this case, 20 temperature cycles had lowered the bond strength of No.6 M1 specimens by approximately 11% .

3.3.2 No.6 GFRP M2 Specimens

Figure 3.18 shows the load-slip curves comparison between the thermally cycled GFRP M2 specimens and the control specimens. The free end slip curves also show that the thermally cycled specimens had a lower stiffness than the control specimens, although the difference in stiffness was less than that observed in GFRP M1 specimens. This means that thermal cycling had less effect on GFRP M2 than on M1 specimens. The amount of loaded end slip in GFRP M1 and M2 specimens were similar but the variability observed in the loaded end slip curves was less for M2 than that for M1.

Comparing the maximum free end slip in Figures 3.17 and 3.18, it was found that the free end slip in GFRP M2 was 3.5 times less than those of M1, which may be due to the larger modulus of elasticity for M2 (8625 psi) than for M1 (7375 psi).*(Preliminary values calculated from the load and LVDT data).* According to the Poisson effect, the stiffer the bar, the less change in bar diameter is experienced by the bar under loading. The less change in bar diameter will in turn lessen the slip. Therefore, a bar with a higher longitudinal modulus of elasticity will have less slip than bar with a lower longitudinal modulus if the transverse Poisson ratio of the two bars is the same.

The mean maximum load for the thermally cycled and control GFRP M2 was 19.1 k and 21.8 k respectively, with standard deviations of 1.5 k and 2.7 k respectively. The standard deviations were larger than those of M1. This may be due to the fact that the bar diameter and the helical strand spacing in the GFRP M2 bar were less uniform than those of GFRP M1.

The range of maximum stress obtained was 0.71 to 1.06 with an average of 0.87, which implies that the stress developed in the cycled specimens was lower than that in the control specimens. Thus, 20 temperature cycles had lowered the bond strength of GFRP M2 specimens by 13%. This is only slightly greater than M1, in which the bond strength was reduced by 11% due to thermal fatigue. This small difference was probably a result of statistical variation in the data. Therefore, it was concluded that thermal cycling had the same detrimental effect on the bond between GFRP M1 and M2 bars and concrete.

3.3.3 No.4 GFRP M1 Specimens

The load-slip curves for the thermally cycled and control No.4 GFRP M1 specimens are presented in Figure 3.19. A lot of variability was seen in both free and loaded end slip curves. This might be due to a production problem of No.4 M1 bars which had caused a large variability in the product (as informed by the manufacturer). The amount of free and loaded end slips of No.4 M1 specimens were four times and twice as large as those of No.6 M1 specimens respectively. Thus, more slip was developed in specimens with smaller bar size.

The large amount of slip in the No.4 M1 specimens may be explained from the opened specimens, where some of the surface resin and coating was found missing near the helical strands. The shearing of the bar surface occurred because the outside of the bar stayed intact with the concrete as the bar was pulled, therefore creating a large slip. This shearing action was only found in No.4 control specimens. Inferior product quality of the No.4 M1 bars was the suspected reason.

The mean maximum load of the cycled and control specimens from Table 3.2 were 11.9 k and 11.7 k respectively, with standard deviations of 0.5 k and 1.2 k respectively. The range of maximum stress ratio obtained was 0.88 to 1.17 with an average of 1.02. The average was only slightly higher than one, and might be the result of statistical variation in the data.

Even though the stress ratio shows that the bond strength of No.4 M1 bars was unaffected by thermal fatigue, both thermal and control specimens had very large free and loaded end slips as a result of shearing of the bar surface. The free end slip at failure was 50 times the allowable FES (0.002 in.) while the loaded end slip was 13 times the allowable LES (0.01 in.). Therefore, for this product, No.4 M1 bars, the bond performance was poor regardless of the thermal fatigue effect.

3.3.4 No.6 Steel Specimens

The load-slip curves for thermally cycled and control steel specimens are presented in Figure 3.20. The curves for TS6B, TS6C, and CS6B were not smooth near the maximum load because the specimens readjusted themselves by translating and rotating (as explained in Section 3.2.2), thus creating a load fluctuation. From the free-end slip curves, it is seen that the stiffnesses of the thermally cycled specimens were less than those of the control specimens.

The mean maximum load of the cycled and control specimens were 20.2 k and 20.9 k respectively, with standard deviations of 1.0 k and 0.9 k respectively. The range of maximum stress ratio obtained was 0.87 to 1.05 with an average of 0.97. Therefore, the thermal cycling reduced the bond strength by 3% in No.6 steel specimens. This reduction

was much less compared to those of the No.6 GFRP specimens, in which the reductions were 11 and 13 % for M1 and M2, respectively. The lower bond reduction in steel specimens was due to the similar thermal expansion coefficient between steel and concrete that enabled them to expand and contract together. The thermal expansion coefficient of GFRP bars in the transverse direction is about five times that of concrete, which caused a discrepancy in expansion and contraction of the two materials, that in turn loosened the bond.

Thus, it can be concluded that thermal fatigue has less effect on the steel specimens than on GFRP specimens. Despite of this, GFRP bars are still acceptable for reinforcement in concrete structure because the percentage of bond reduction in GFRP specimens due to thermal fatigue (12%) was similar to that of steel specimens due to mechanical fatigue (13%), which has not been a concern.

3.4 SUMMARY

Table 3.6 summarizes the range of maximum stress ratios along with the average ratios for each group of specimens. A ratio greater than 1 (such as in mechanically cycled No.6 M1 and thermally cycled No.4 M1 specimens) indicates that the bond strength increased in the cycled specimens compared to that of the control ones. But as discussed earlier, this increase was negligible if less than 5% to be considered. Results in this range of bond ratio were attributed to the statistical variation in the results. The conclusions of the bond experiment can be found in the next chapter.

Chapter 4: Conclusions

It was found in the investigation that mechanical and thermal fatigue have different effects on steel and GFRP specimens. Before stating the conclusions, a short discussion on the variability among the test results from the GFRP specimens is presented. The conclusions were based on the evaluation of experimental results discussed in Chapter 3.

4.1 Variability Among GFRP Test Results

Variability in the results was a common observation in GFRP bond studies due to the non-uniform property of the composite rebars. The variability in this investigation can be seen from the free and loaded end slip curves of the specimens. For No.4 GFRP M1 specimens, the suspected reason was inferior product quality.

4.2 Conclusion from Experimental Results

The conclusions from this investigation are as follows:

1. The effect of mechanical fatigue on bond was observed more in the steel specimens than in the GFRP specimens. This was attributed to the greater rib deformations of the steel bars that pulverized more concrete near the ribs as the mechanical cycles were applied. The crushing of concrete was also more for the steel bar because steel is a harder material than GFRP. The reduction in bond strength for the mechanically cycled steel specimens was 13% while no reduction was found in the GFRP specimens.
2. The effect of thermal fatigue was seen more in the GFRP specimens than in the steel specimens. This was due to the dissimilarity of thermal expansion coefficient of GFRP bar in the transverse direction with that of concrete. This difference caused a discrepancy in the expansion and contraction between the two materials that in turn

loosened the bond. The reduction in bond strength due to thermal fatigue was about 12% for GFRP specimens and only 3% for steel specimens.

3. The reduction in bond strength due to thermal fatigue between GFRP bar and concrete need not be a concern because the percent reduction was similar to that observed between steel and concrete due to mechanical fatigue, which has not been a concern.

4. The difference in stiffness between the control and thermally cycled specimens showed that thermal fatigue had more of an effect on GFRP M1 than on GFRP M2, even though the bond reduction was similar. This may be due to the fact that GFRP M2 had greater bar indentations and closer helical strand spacings compared to GFRP M1.

5. The difference in bond performance under thermal fatigue between No.6 and No.4 GFRP bars cannot be determined from this study due to the variability in the quality of No.4 GFRP bars received from the manufacturer (resulting from production problems).

4.3 Summary

GFRP bars are acceptable as reinforcement in concrete structures because the bond performance of the GFRP specimens under thermal fatigue was similar to that of the steel specimens under mechanical fatigue. GFRP bars are also suitable for structures subjected to mechanical cycles (such as bridges or highways) because it was proven in this study that bond to GFRP bars is even better than bond to steel bars under mechanical fatigue.

REFERENCES

1. Saadatmanesh H., and Ehsani M., "Fiber Composite Bar for R/C Constr.," J.of Composite Materials, Vol.25, Feb 1991, pp.188-203.

2. Ehsani, M.R., Saadatmanesh, H., and Tao, S., "Experimental Study of Bond of Deformed Composite Rebars to Concrete," Draft for publication in ACI Structural Journal - February 1994.

3. Chaallal, O. and Benmokrane, B., "Physical and mechanical performance of an innovative glass-fiber-reinforced plastic rod for concrete and grouted anchorages,"Canadian Journal of Civil Engineering, Vol. 20, 1993, pp.254-268.

4. Brown V. and Bartholomew C., "FRP Reinforcing Bars in R/C Members," ACI Material J., Vol.90, No.1, Jan-Feb 1993, pp.34-39.

5. Plecnik, J., Azar, W., and Kabbara, B., "Composite Applications in Highway Bridges," Construction Materials Serviceability/Durability,"

6. Rinaldi, G. and Maura, G., "Durable Glass-Epoxy Composites Cured at Low Temperatures - Effects of Thermal Cycling, UV Irradiation and Wet Environment," Polymer International, 1993, pp.339-345.

7. Faza,S. and GangaRao H., "Composite Materials as Concrete Reinforcement in the Next Decade," Plastics Composites for 21st Century Construction, 1993, pp.15-22.

8. Ehsani, M.R., Saadatmanesh, H., and Tao, S., "Bond of GFRP Rebars to Ordinary Strength Concrete," FRP Reinforcement for Concrete Structures - International Symposium, 1993, pp.333-345.

9. Sen, R., Mariscal, D., and Shahawy, M., "Investigation of S-2 Glass/Epoxy Strands in Concrete," FRP Reinforcement for Concrete Structures - Internatinal Symposium, 1993, pp.15-33.

10. Daniali, S., "Bond Strength of FRP Bars in Concrete," Construction Materials Serviceability/Durability, pp.1182-1191.

11. Faza S. and GangaRao H., "Bending and Bond Behavior of Concrete Beams Reinforced with Plastic Rebars," Transportation Research Record, No.1290, V.2, pp.185-193.

12. Larralde and Silva, "Bond and Slip of FRP Rebars in Concrete," Journal of Materials in Civil Engineering, Vol. 5, No. 1, February 1993, pp. 30-40.

13. Grundhoffer T., "Bond Behavior of Uncoated and Epoxy-Coated Reinforcement in Concrete," University of Minnesota, May 1992.

14. Pleimann L.G, "Strength, Modulus of Elasticity, and Bond of Deformed FRP Rods," Advanced Composites Materials in Civil Engineering Structures, 1990 , pp.99-110.

15. Chaallal, O. and Benmokrane, B., "Pullout and Bond of Glass-Fibre Rods embedded in Concrete and Cement Grout,"Materials and Structures, Vol.26, 1993, pp.167-175.

16. Budelmann, H., Kepp, B., and Rostasy, F.S., "Fatigue Behavior of Bond-Anchored Unidirectional Glass-FRP's," Construction Materials Serviceability/Durability,

17. Orangun, Jirsa, and Breen, "A reevaluation of Test Data on Development Length and Splices," ACI Journal, March 1977.

18. Holte, L.E., Dolan, C.W., and Schmidt, R.J.,"Epoxy Socketed Anchors for Non-Metallic Prestressing Tendons," FRP Reinforcement for Concrete Structures - Internatinal Symposium, 1993, pp.381-400.

Table 1.1
Bond Test Results From Previous Research
a) Pullout Test

Cylinder Specimens

Reference	Bar Size	l_d/d_b	$f'c$ (psi)	P_{max} (kip)	$\%f_u$	Failure	k
4	No.3	16	4200	8.46[a]	49	Splitting	21.8
4	No.3	11	4200	4.67[a]	27	Splitting	18.0
4	No.3	16	1930	5.84[a]	34	Pullout	22.2
4	No.3	11	1160	2.71[a]	16	Pullout	19.9
12	No.3	8	4000	5.06	58	Pullout	26.7
12	No.3	8	4000	4.74	54	Pullout	25.0
12	No.3	8	4000	5.52	63	Pullout	29.1
12	No.3	16	4000	9.45	107	Pullout	24.9
12	No.3	16	4000	9.65	110	Pullout	25.4
12	No.3	16	4000	-[d]	-[d]	-[d]	-[d]
3	No.4	5	4500	8.4[b]	77	-[c]	50.1
3	No.4	10	4500	12.4[b]	114	-[c]	37.0
12	No.5	5	4000	6	24	Pullout	31.6
12	No.5	5	4000	4.8	20	Pullout	25.3
12	No.5	5	4000	6.34	26	Pullout	33.4
12	No.5	10	4000	-[d]	-[d]	-[d]	-[d]
12	No.5	10	4000	11.1	45	Pullout	29.3
12	No.5	10	4000	9.1	37	Pullout	24.0
3	No.5	5	4500	10.5[b]	35	-[c]	52.2
3	No.5	10	4500	19.1[b]	63	-[c]	47.5
3	No.6	5	4500	18.3[b]	40	-[c]	77.9
3	No.6	10	4500	29.5[b]	64	-[c]	62.8

[a] Average of six tests [b] Average of four tests [c] Not mentioned in the paper
[d] Indicates delamination of rebar during test

Block Specimens [12]

Concrete below bar (in.)	Bar Size	l_d/d_b	$f'c$ (psi)	P_{max} (kip)	$\%f_u$	Failure	k
8	No.3	4	4670	7.39	50	Pullout	72.1
24	No.3	4	4670	7.09	48	Pullout	69.2
40	No.3	4	4670	7	47	Pullout	68.3
8	No.3	16	6640	10.76	72	Tensile	22.0
24	No.3	16	6640	9.47	64	Tensile	19.4
40	No.3	16	6640	8.98	61	Tensile	18.4
8	No.6	8	4670	23.45	57	Pullout	57.2
24	No.6	8	4670	19.71	48	Pullout	48.1
40	No.6	8	4670	19.02	47	Pullout	46.4
8	No.6	16	6640	26.74	65	Pullout	27.4
24	No.6	16	6640	24.57	60	Pullout	25.1
40	No.6	16	6640	23.58	58	Pullout	24.1
8	No.9	7	4670	47.2	61	Pullout	86.3
24	No.9	7	4670	41.58	54	Pullout	76.1
40	No.9	7	4670	41.19	54	Pullout	75.3
8	No.9	20	6640	48.65	63	Pullout	27.1
24	No.9	20	6640	45.19	59	Pullout	25.2
40	No.9	20	6640	44.4	58	Pullout	24.8

Table 1.1 cont.

b) Inverted Half-Beam Test

Bottom bar specimens with stirrups [a]

Reference	Bar Size	l_d/d_b	$f'c$ (psi)	Cover ($\#d_b$)	P_{max} (kip)	Failure	k
11	No.3	43	4200	2.67	-	In the grip	-
11	No.3	43	4200	2.67	-	In the grip	-
11	No.3	64	4200	2.67	11	Tensile	7.1
11	No.3	64	4200	2.67	10.9	Tensile	7.0
11	No.3	32	4200	2.67	8.2	Tensile	10.5
11	No.3	32	4200	2.67	8.1	Tensile	10.4
11	No.3	21	4200	2.67	9.4	Tensile	18.1
11	No.3	21	4200	2.67	8	Tensile	15.4
11	No.8	16	4200	1	22.46	Splitting	21.7
11	No.8	16	4200	1	24	Splitting	23.1
11	No.8	24	4200	1	29	Splitting	18.6
11	No.8	24	4200	1	30	Splitting	19.3

[a] No f_u information was available

Bottom bar specimens without stirrups

Reference	Bar Size	l_d/d_b	$f'c$ (psi)	Cover ($\#d_b$)	P_{max} (kip)	$\%f_u$	Failure	k
2	No.3	11	4330	2	7.7	52	Tensile	29.2
2	No.3	16	5080	4	10.0	67	Tensile	23.3
2	No.3	21	5080	6	10.5	71	Tensile	18.4
2	No.3	11	7100	2	8.4	56	Tensile	24.8
2	No.3	16	7100	4	9.7	65	Tensile	19.2
2	No.3	21	7100	6	8.6	58	Tensile	12.7
2	No.6	4	4010	1	13.7	33	Splitting	72.1
2	No.6	4	4010	2	17.5	43	Pullout	92.3
2	No.6	8	4010	2	19.0	46	Pullout	50.0
2	No.6	16	5680	2	23.0	56	Pullout	25.5
2	No.6	21	5680	4	29.8	73	Pullout	24.7
2	No.6	24	5680	6	31.4	77	Tensile	23.2
2	No.6	16	6920	2	23.3	57	Pullout	23.3
2	No.6	21	6920	4	28.4	69	Pullout	21.3
2	No.6	24	6920	6	30.3	74	Tensile	20.2
2	No.9	4	4010	1	22.5	29	Splitting	88.7
2	No.9	4	4010	2	32.0	42	Pullout	126.2
2	No.9	7	4010	2	35.6	46	Pullout	70.3
2	No.9	20	5760	2	48.3	63	Pullout	28.9
2	No.9	23	5760	4	52.6	68	Pullout	26.7
2	No.9	27	5760	6	56.0	73	Tensile	24.6
2	No.9	20	6490	2	44.9	58	Pullout	25.3
2	No.9	23	6490	4	48.5	63	Pullout	23.1
2	No.9	27	6490	6	50.6	66	Tensile	20.9

Table 1.1 cont.

Top bar specimens without stirrups

Reference	Bar Size	l_d/d_b	$f'c$ (psi)	Cover ($\#d_b$)	P_{max} (kip)	$\%f_u$	Failure	k
2	No.3	4	4010	1	5.1	34	Splitting	53.8
2	No.3	4	4010	2	6.4	43	Pullout	67.3
2	No.3	8	4010	2	6.9	47	Pullout	36.5
2	No.3	11	4330	2	8.3	56	Tensile	31.7
2	No.3	16	5080	4	8.9	60	Tensile	20.9
2	No.3	21	5080	6	8.8	60	Tensile	15.5
2	No.3	11	7100	2	9.0	60	Tensile	26.6
2	No.3	16	7100	4	8.5	57	Tensile	16.8
2	No.3	21	7100	6	9.7	65	Tensile	14.4
2	No.6	4	4010	1	11	27	Splitting	57.7
2	No.6	4	4010	2	14.6	36	Pullout	76.9
2	No.6	8	4010	2	15.5	38	Pullout	40.9
2	No.6	21	5680	2	21.5	53	Pullout	23.8
2	No.6	21	5680	4	28.0	69	Pullout	23.3
2	No.6	24	5680	6	31.9	78	Tensile	23.6
2	No.6	16	6920	2	22.6	55	Pullout	22.6
2	No.6	21	6920	4	27.2	66	Pullout	20.4
2	No.6	24	6920	6	29.6	72	Tensile	19.8
2	No.9	20	5760	2	47.3	61	Pullout	28.3
2	No.9	23	5760	4	50.4	66	Pullout	25.6
2	No.9	27	5760	6	56.7	74	Tensile	24.9
2	No.9	20	6490	2	43.0	56	Pullout	24.3
2	No.9	23	6490	4	46.7	61	Pullout	22.3
2	No.9	27	6490	6	52.7	68	Tensile	21.8

c) Beam Test

Specimens with stirrups

Reference	Bar Size	l_d/d_b	$f'c$ (psi)	Cover ($\#d_b$)	P_{max} (kip)	$\%f_u$	Failure	k
10	No.4	16	4500	3	19.7[a]	100	Tensile	36.7
10	No.4	24	4500	3	19.7[a]	100	Tensile	24.5
10	No.4	32	4500	3	19.7[a]	100	Tensile	18.4
10	No.6	16	4500	2	27.6[a]	90	Pullout	34.3
10	No.6	24	4500	2	27.6[a]	90	Splitting	22.9
10	No.6	32	4500	2	30.6[a]	100	Tensile	19.0
10	No.8	20	4500	1.75	44.1[b]	85	Pullout	32.9
10	No.8	20	4500	1.75	36.3	70	Pullout	27.1
10	No.8	25	4500	1.75	46.6[b]	90	Pullout	27.8
10	No.8	25	4500	1.75	41.4	80	Pullout	24.7
10	No.8	30	4500	1.75	36.3	70	Pullout	18.0
10	No.8	30	4500	1.75	41.4[b]	80	Splitting	20.6

[a] Same for three replicate specimens

[b] Same for two replicate specimens

Table 2.1 Development Length Table for Steel

Stress ratio (f_s/f_y) No.6 Bars	f'_c (ksi)		
l_d/d_b	4.5	6	8
8	0.70	0.81	0.93
9.33	0.75	0.87	1
10.67	0.80	0.92	1.07
11.87	0.85	0.98	1.13

Table 2.2 Development Length Table for GFRP

Stress Ratio: Left Column = f/f_u, Right column = $f/(0.7f_u)$

No.6 Bars	f'_c (ksi)					
l_d/d_b	4.5		6		8	
12	0.46	0.65	0.53	0.75	0.61	0.87
13.33	0.51	0.73	0.59	0.84	0.68	0.97
14.67	0.56	0.80	0.65	0.92	0.75	1.06
16	0.61	0.87	0.70	1.01	0.81	1.16

No.4 Bars	f'_c (ksi)					
l_d/d_b	4.5		6		8	
8	0.37	0.53	0.43	0.61	0.50	0.71
10	0.47	0.67	0.54	0.77	0.62	0.89
12	0.56	0.80	0.65	0.92	0.75	1.06

Table 2.3 Results of Pilot Specimens

Bar Type	l_d/d_b	f'_c at age of testing (psi)	P_{max} (kips)	Resulted Stress Ratio (f_s/f_y or f/f_u)	Expected Stress Ratio (f_s/f_y or f/f_u)
No.6 GFRP M1	13.33	4200	18.1	0.46	0.48
No.6 GFRP M2	13.33	3940	18.3	0.46	0.48
No.6 GFRP M1	16	4200	17.5	0.44	0.57
No.6 GFRP M2	16	3940	17.3	0.44	0.57
No.4 GFRP M1	12	3770	10.2	0.51	0.53
No.6 Steel	8	4430	13.0	0.49	0.66
No.6 Steel	10.67	4430	19.1	0.72	0.76

Table 2.4 Mechanical Properties of the Test Bars

Bar Type	Ultimate Strength (ksi)	Modulus of Elasticity (ksi)
No.6 GFRP M1	68.3	5500
No.6 GFRP M2	86.6	5500

Table 3.1 Test Results

Specimen Label	P_{max} (k)	$P_{first\ crack}$ (k)	$P_{first\ crack}/P_{max}$
MS6A	17.12	-	-
MS6B	18.31	17.43	0.95
MS6C	19.39	At failure	1
MG6AM1	23.07	At failure	1
MG6BM1	24.27	At failure	1
MG6CM1	23.71	-	-
TG6AM1	18.56	18	0.97
TG6BM1	21.20	At failure	1
TG6CM1	20.26	At failure	1
TG6AM2	18.76	18	0.96
TG6BM2	20.70	18.36	0.89
TG6CM2	17.69	16.66	0.94
TG4AM1	12.10	11.65	0.96
TG4BM1	12.34	At failure	1
TG4CM1	11.40	9.2	0.81
TS6A	19.05	16.4	0.86
TS6B	20.6	At failure	1
TS6C	21	16.8	0.80
CS6A	19.96	19.81	0.99
CS6B	20.92	At failure	1
CS6C	21.82	At failure	1
CG6AM1	23.36	23.16	0.99
CG6BM1	22.40	At failure	1
CG6CM1	21.88	20.9	0.96
CG6AM2	24.76	17.3	0.70
CG6BM2	19.47	16.65	0.86
CG6CM2	21.16	16.3	0.77
CG4AM1	11.54	At failure	1
CG4BM1	12.93	12.8	0.99
CG4CM1	10.53	9.6	0.91

- indicates that data was not taken

Table 3.2 Mean, STD, and COV Values of Maximum Load

Specimen Group	Mean (k)	Standard Deviation (k)	Coefficient of Variation
Mech. Fatigue Steel No.6	18.27	1.14	0.062
Mech. Fatigue Glass No.6 M1	23.68	0.60	0.025
Thermal Fatigue Steel No.6	20.22	1.03	0.051
Thermal Fatigue Glass No.6 M1	20	1.34	0.067
Thermal Fatigue Glass No.6 M2	19.05	1.53	0.080
Thermal Fatigue Glass No.4 M1	11.95	0.49	0.041
Control Steel No.6	20.90	0.93	0.045
Control Glass No.6 M1	22.55	0.75	0.033
Control Glass No.6 M2	21.80	2.70	0.124
Control Glass No.4 M1	11.67	1.21	0.103

Table 3.3 Load Based on Slip Criteria

Specimen Label	P at FES=0.002 in. (k)	P at LES=0.01 in. (k)
MS6A	-	-
MS6B	17.23	-
MS6C	18.50	-
MG6AM1	20.80	3.85
MG6BM1	15.97	3.54
MG6CM1	21.52	6.32
TG6AM1	12.62	10.38
TG6BM1	16.99	8.34
TG6CM1	7.06	4.49
TG6AM2	18.54	9.32
TG6BM2	20.35	10.48
TG6CM2	17.14	11.51
TG4AM1	7.90	3.20
TG4BM1	0.21	2.73
TG4CM1	4.76	4.02
TS6A	17.34	19.02
TS6B	17.99	20.6
TS6C	18.96	-
CS6A	16.10	18.15
CS6B	19.52	-
CS6C	19.06	-
CG6AM1	-	-
CG6BM1	17.92	5.27
CG6CM1	20.94	10.82
CG6AM2	22.12	7.96
CG6BM2	19.12	9.64
CG6CM2	21.08	9.15
CG4AM1	4.38	2.24
CG4BM1	4.63	3.49
CG4CM1	1.12	2.01

- indicates that data was not taken

Table 3.4 Summary of Observations on Opened Specimens

Specimen label	Helical strands broken	Sand coating remaining on bar	Concrete particles adhered to bar	Helical strands adhered to concrete	Other remarks
MS6A	N.A	N.A	Some	N.A	
MS6B	N.A	N.A	Some	N.A	
MS6C	N.A	N.A	A lot, in ribs	N.A	
MG6AM1	All	Yes	Some	Yes	
MG6BM1	All	Some	A lot	Little, almost none	
MG6CM1	All	Most is gone, almost smooth	A little	Yes	
TG6AM1	No	Yes	Very little	No	
TG6BM1	All	Yes	Very little	Yes	
TG6CM1	All	No	No	Yes	
TG6AM2	No	No	Very little, some in deformations	No	
TG6BM2	No	No, smooth surface	Very little, some in deformations	No	
TG6CM2	No	No, dull color	Very little, some in deformations	No	Only $1/3l_d$ opened
TG4AM1	All	Yes	No	Yes	Easy to remove concrete
TG4BM1	All	Yes	No	No	
TG4CM1	All	Yes	No	Yes	Opened 3.5 in.
TS6A	N.A	N.A	-	N.A	Not Opened
TS6B	N.A	N.A	-	N.A	Not Opened
TS6C	N.A	N.A	A lot, at surface	N.A	Only $3/4l_d$ opened
CS6A	N.A	N.A	A lot, in ribs	N.A	
CS6B	N.A	N.A	-	N.A	Not opened
CS6C	N.A	N.A	A lot, in ribs	N.A	
CG6AM1	2nd strand from loaded end	All	A little	Only the longitudinal strand	Helical strands are thick and closely spaced
CG6BM1	All	Some	Very little (almost none)	Some	
CG6CM1	All	All	A little on surface	Yes	
CG6AM2	No	No, dull color	A lot on surface	No	
CG6BM2	No	No, but surface still rough	Some, on deformations	No	
CG6CM2	No	No, dull color	A lot on surface	No	Opened 3 in.
CG4AM1	All	Some	No	Yes (plus longitudinal strands)	Surface resin gone in 3 places near deformation
CG4BM1	All	Yes, other than the 3 places	No	No	Surface resin gone in 3 places near deformation
CG4CM1	All	Yes, other than the 3 places	No	Yes (plus longitudinal strands)	Surface resin gone in 3 places near deformation

Table 3.5 Summary of Maximum Stress Ratio

Specimen Group	Range of Maximum Stress Ratio	Average of Maximum Stress Ratio
Mechanical Fatigue No.6 M1	0.99 - 1.11	1.05
Mechanical Fatigue No.6 Steel	0.79 - 0.97	0.87
Thermal Fatigue No.6 M1	0.80 - 0.97	0.89
Thermal Fatigue No.6 M2	0.71 - 1.06	0.87
Thermal Fatigue No.4 M1	0.88 - 1.17	1.02
Thermal Fatigue No.6 Steel	0.87 - 1.05	0.97

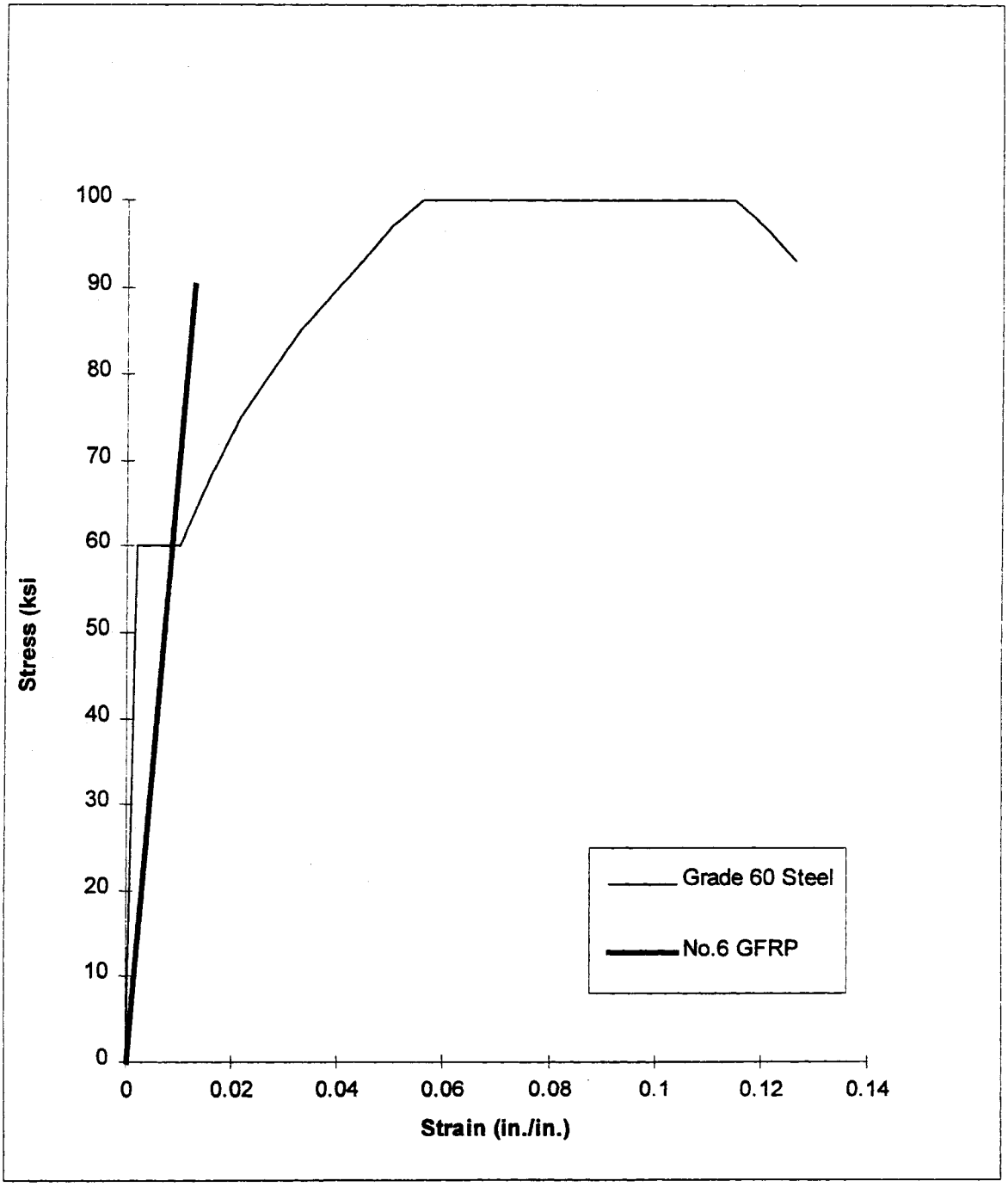

Figure 1.1 Stress-Strain Curve Comparison for Steel and GFRP Bars

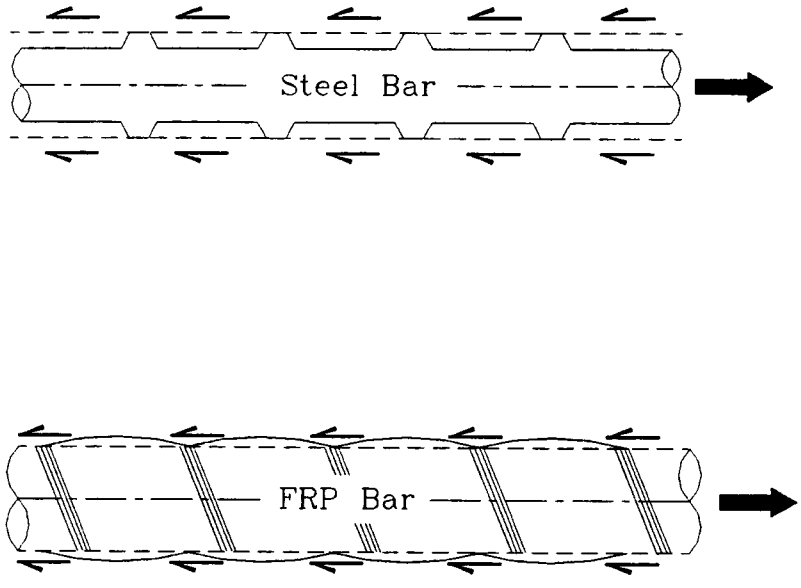

Figure 1.2 Pullout failure comparison for steel and FRP Bars

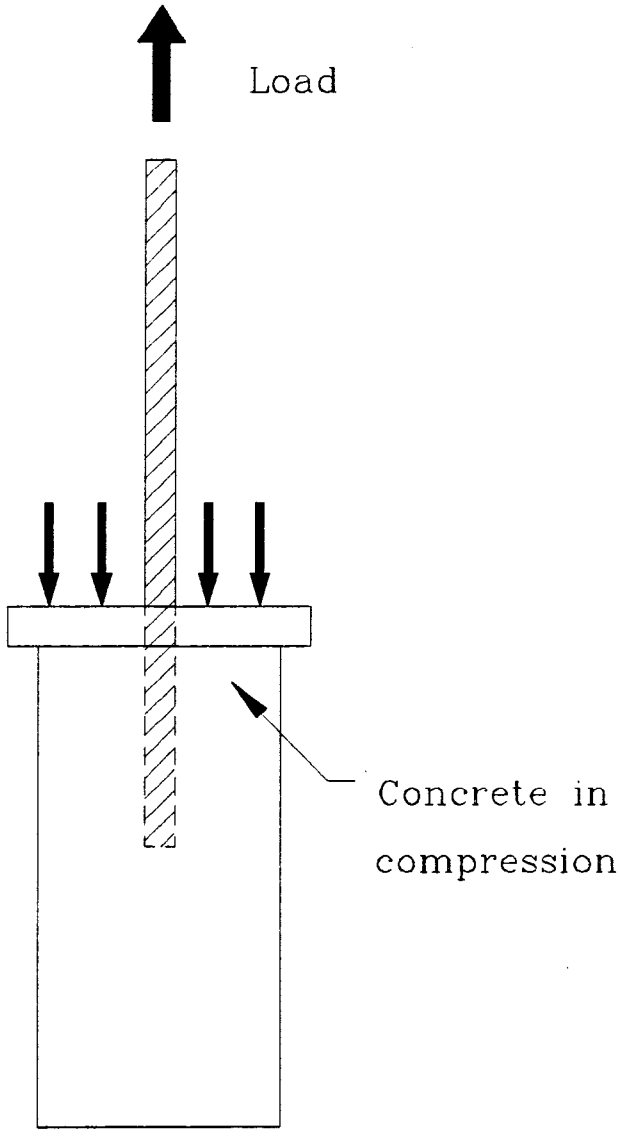

Figure 1.3 Pullout Type Bond Specimen

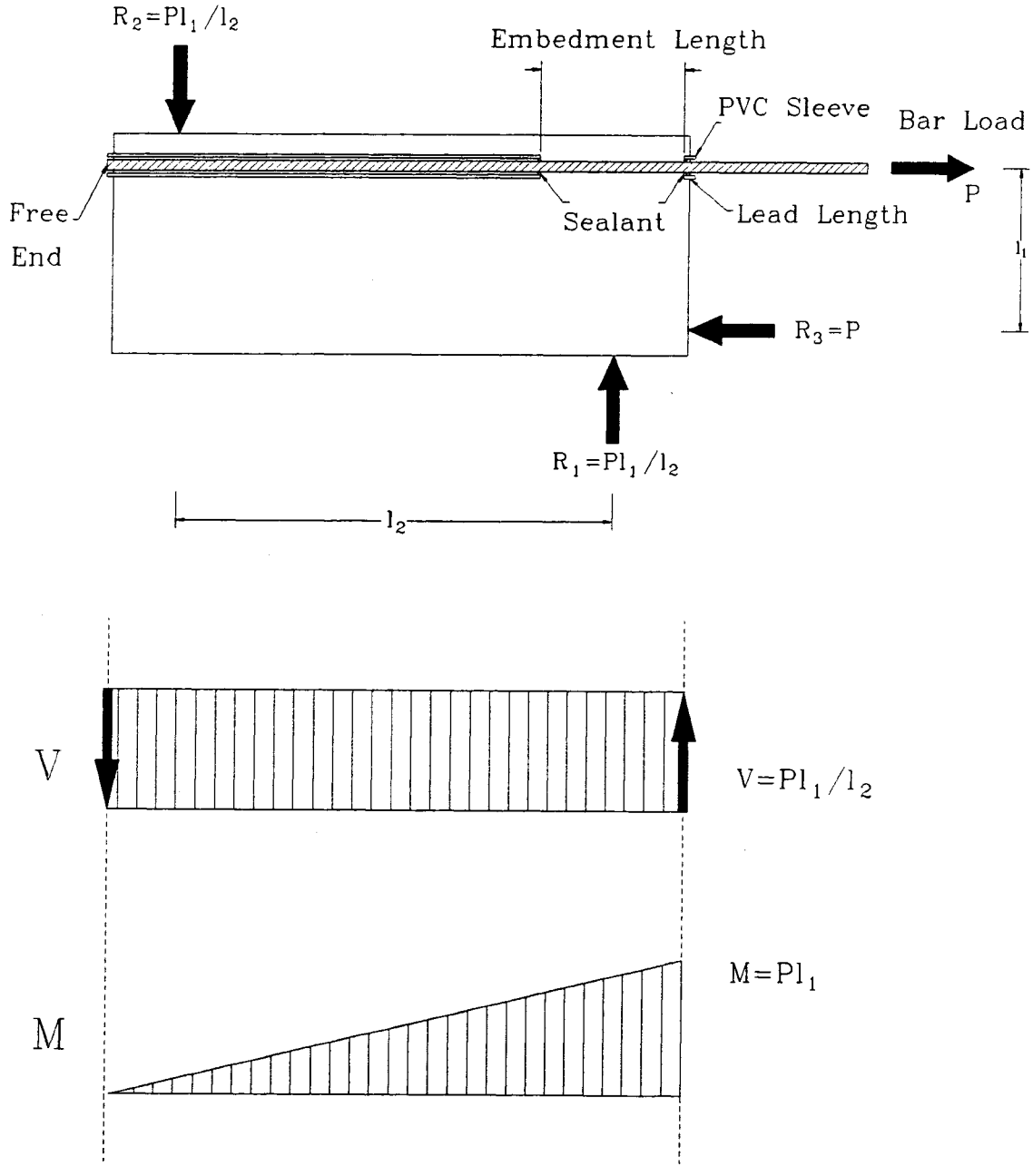

Figure 1.4 Inverted Half-Beam Bond Specimen

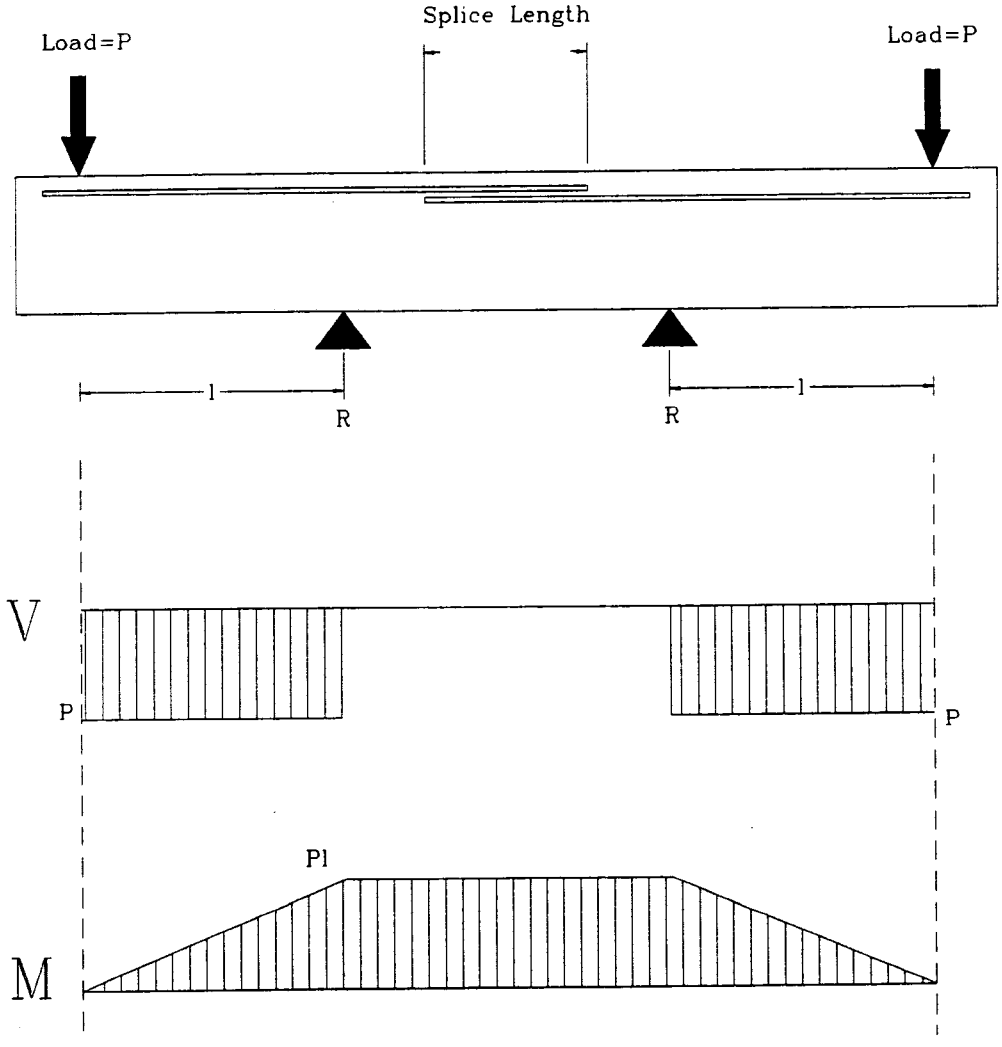

Figure 1.5 Splice Type Bond Specimen

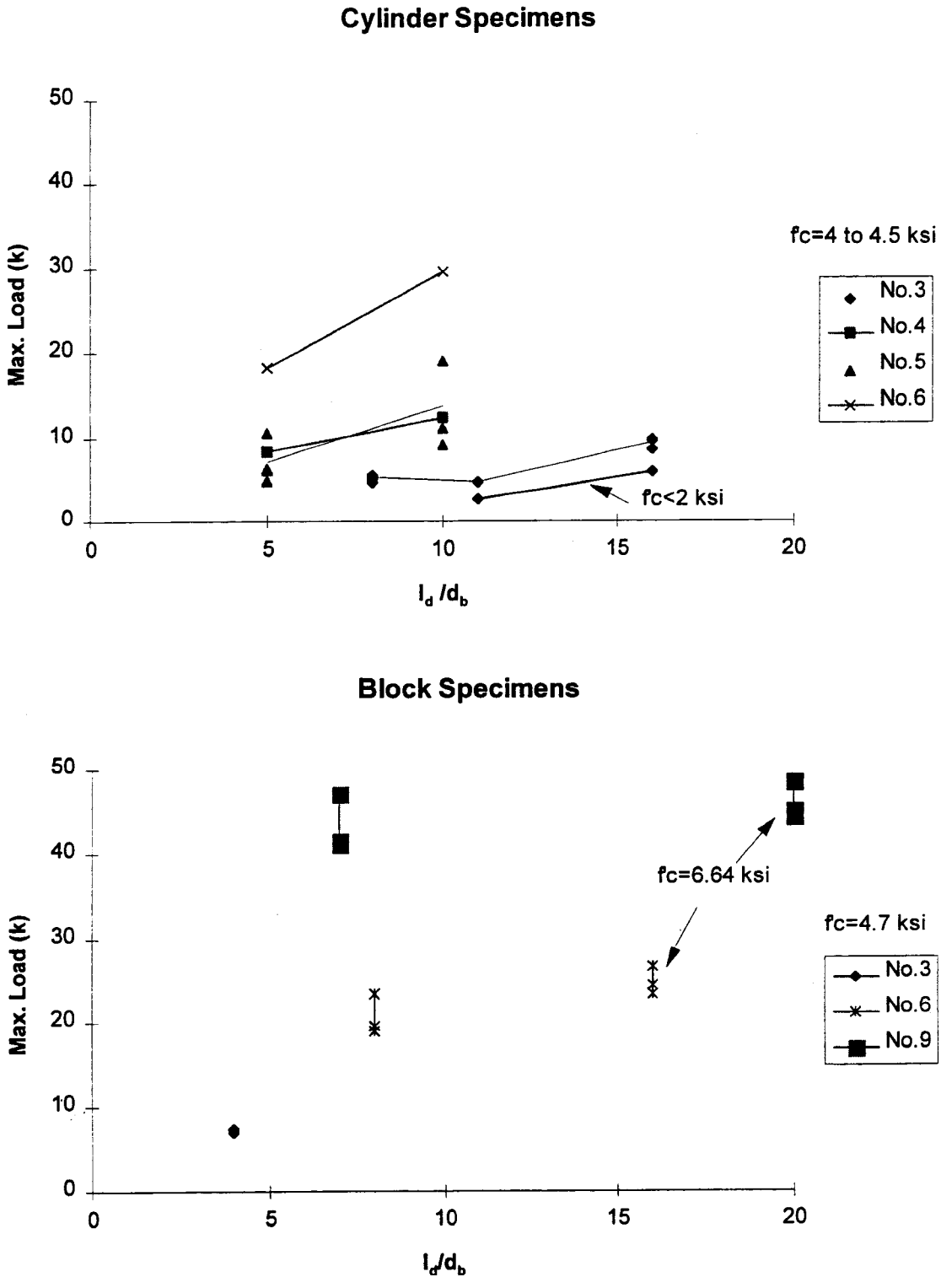

Figure 1.6 Maximum Load vs Development Length
a) Pullout Test

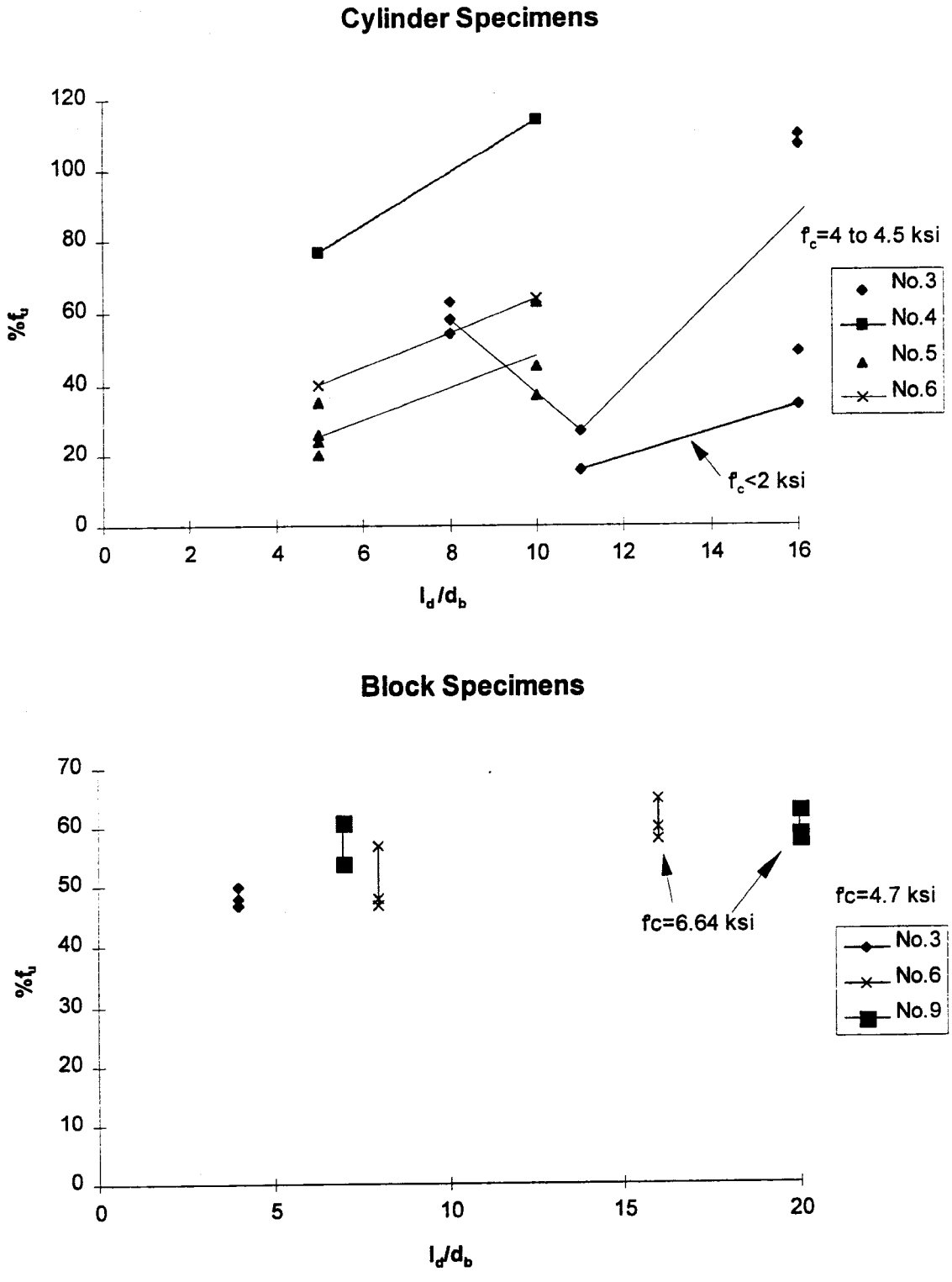

Figure 1.6 cont.: a) Pullout Test

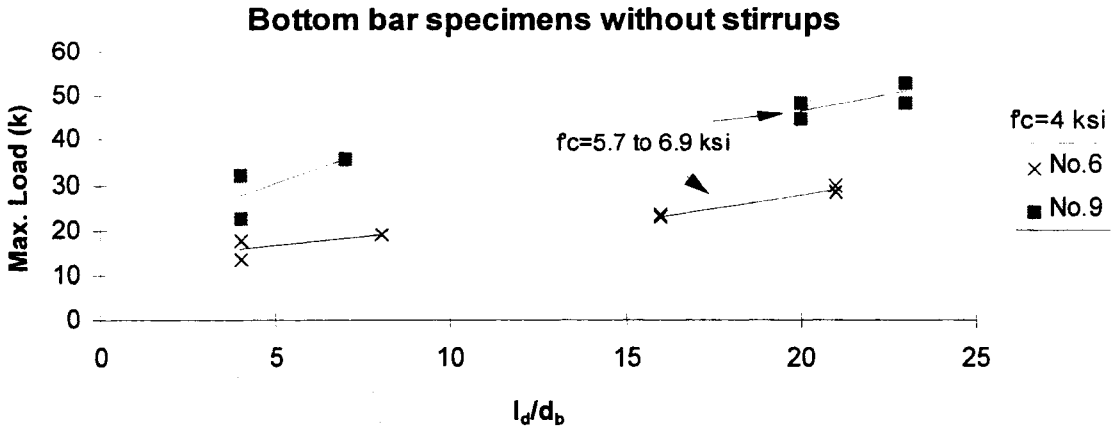

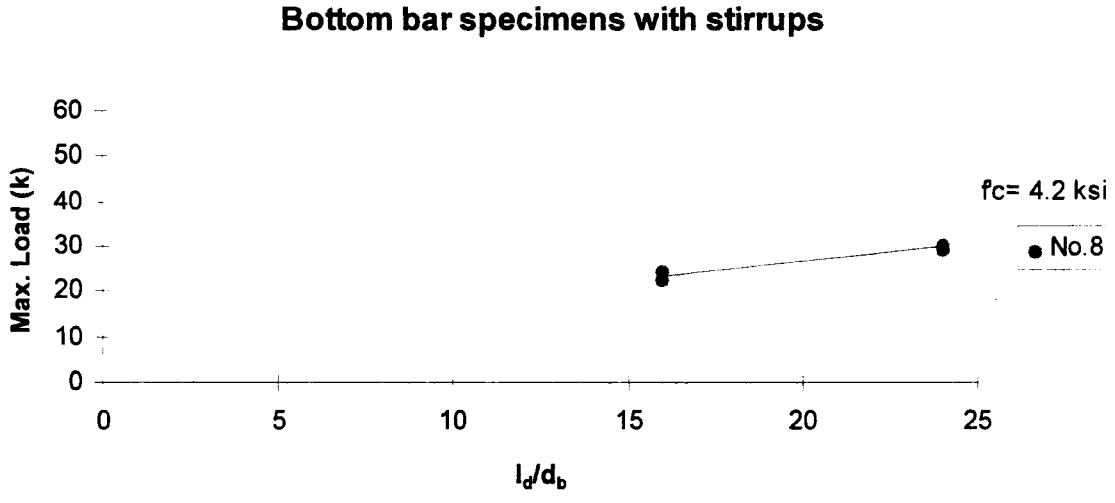

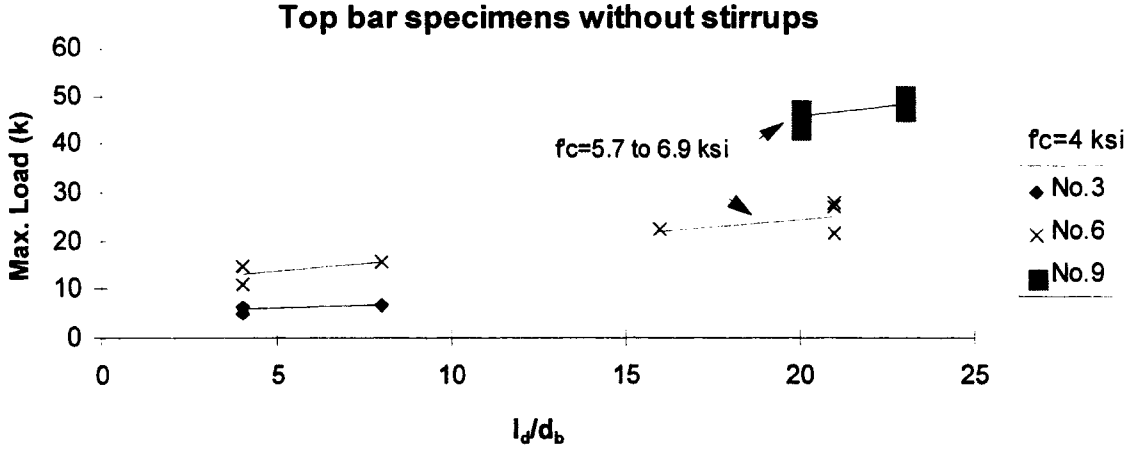

Figure 1.6 cont.: b) Inverted Half Beam Test

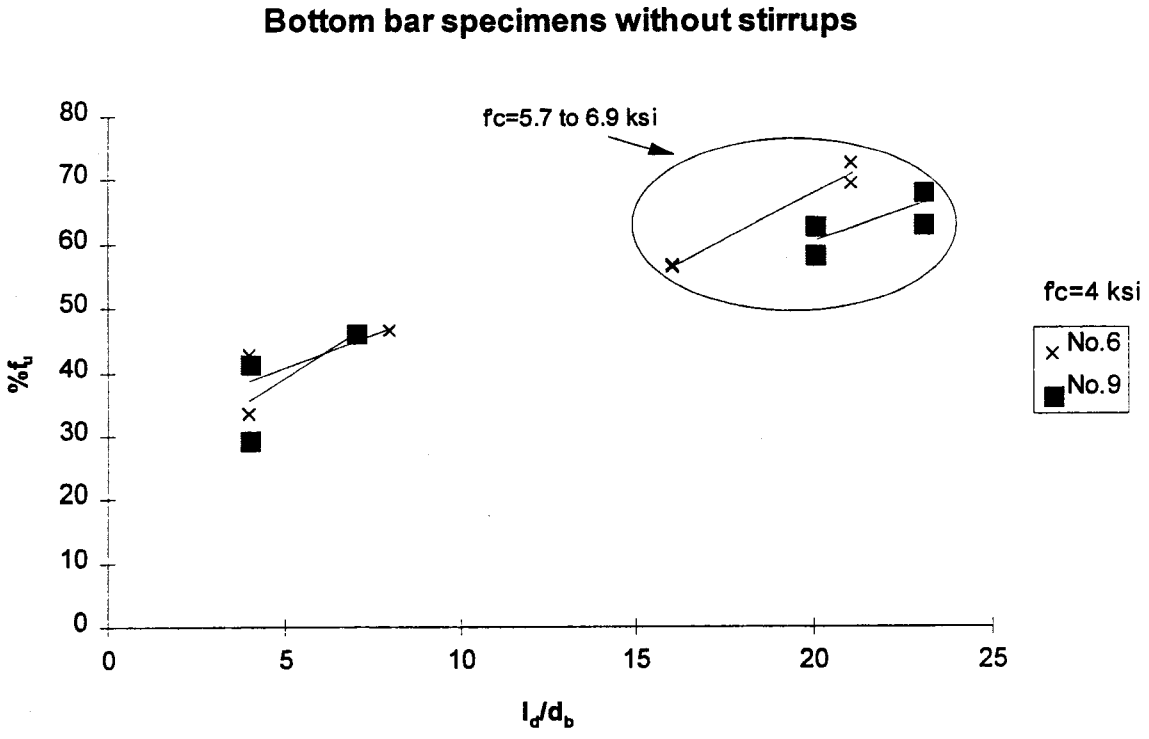

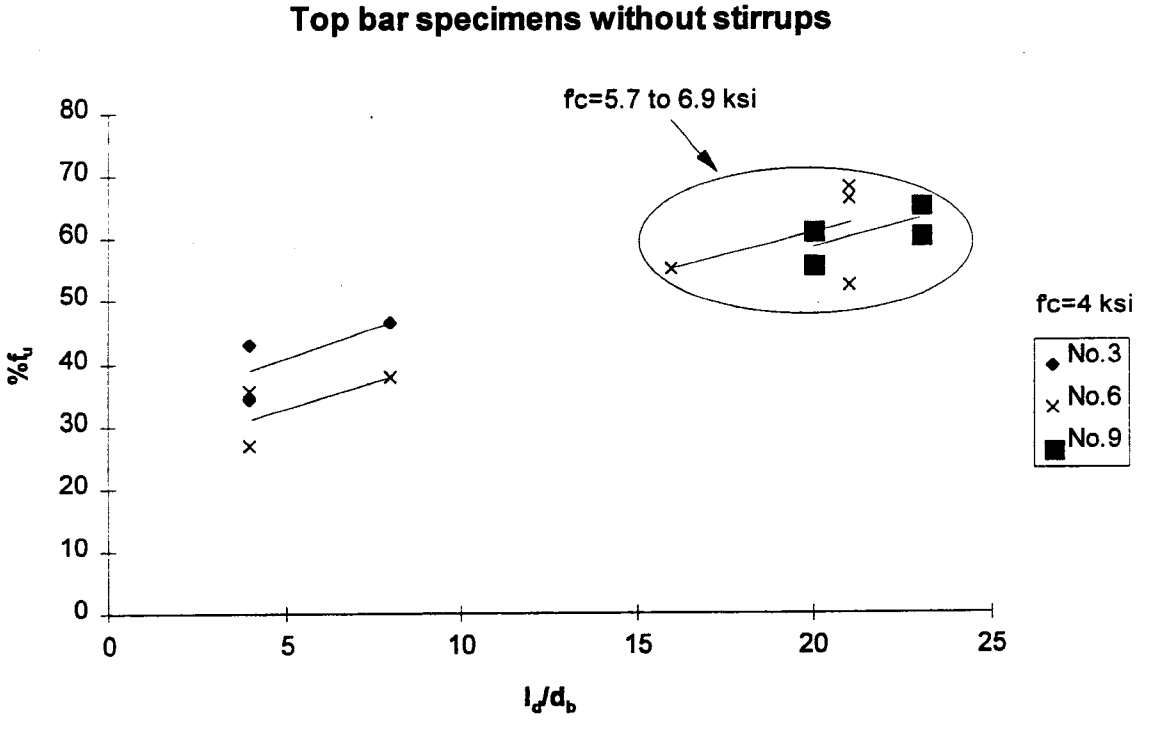

Figure 1.6 cont.: b) Inverted Half Beam Test

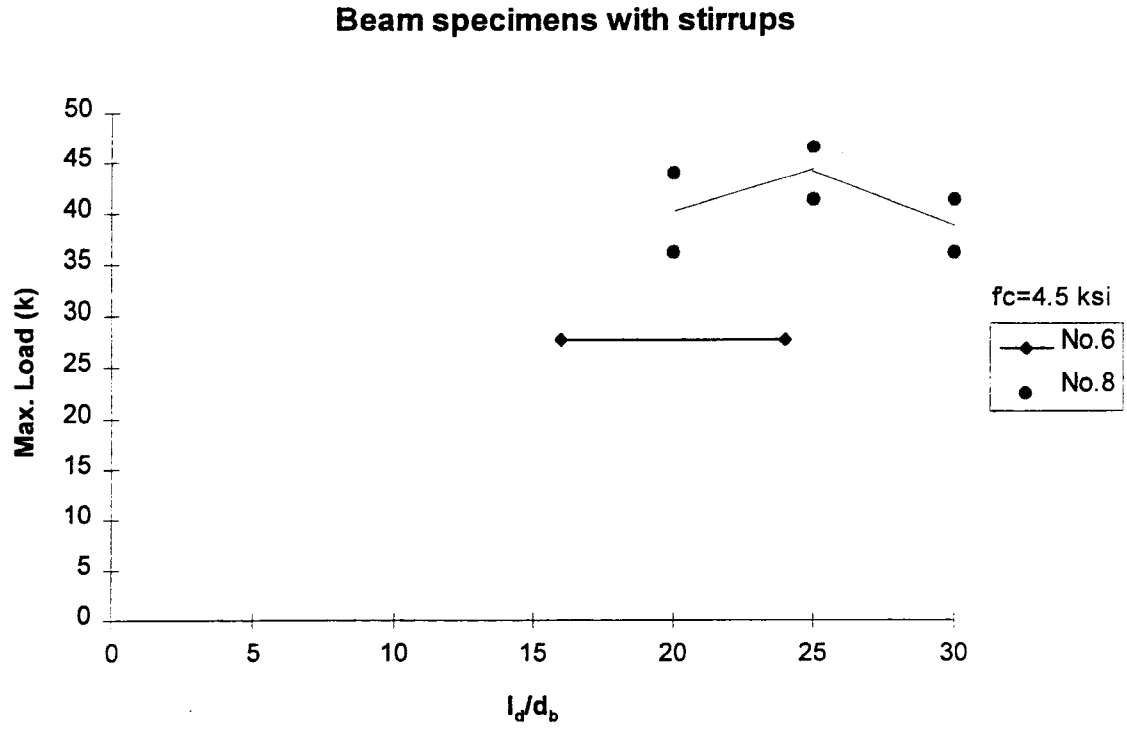

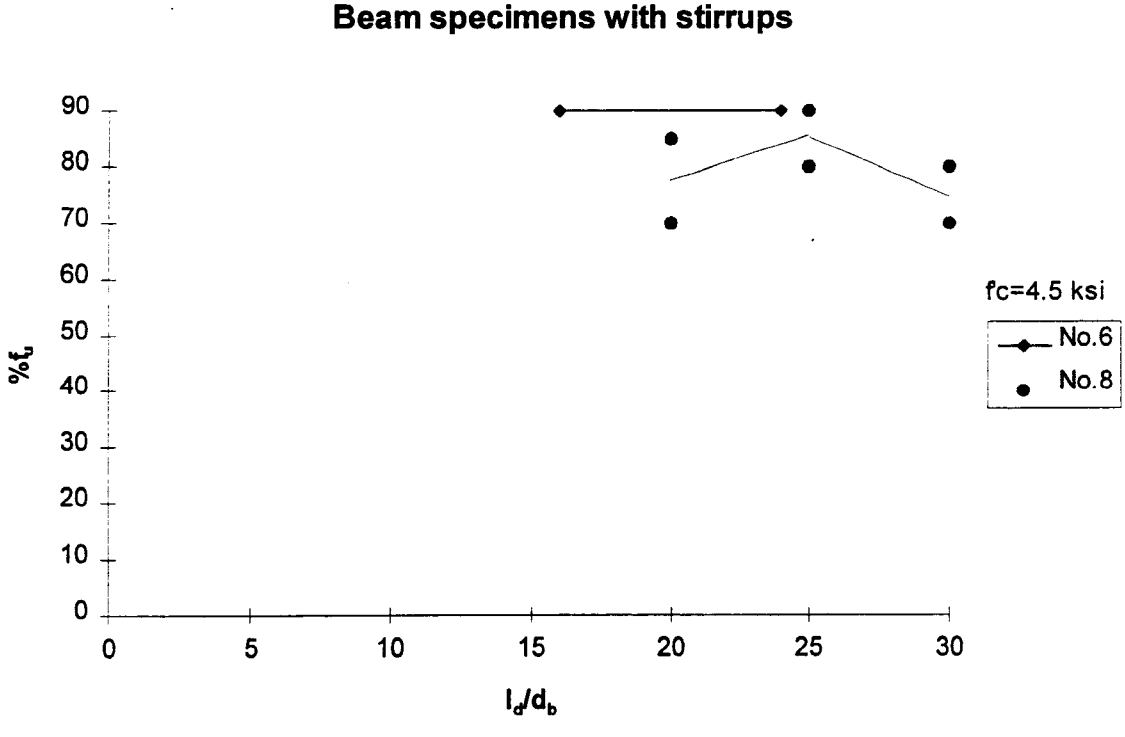

Figure 1.6 cont.: c) Beam Test

Figure 2.1 Picture of Test Bars

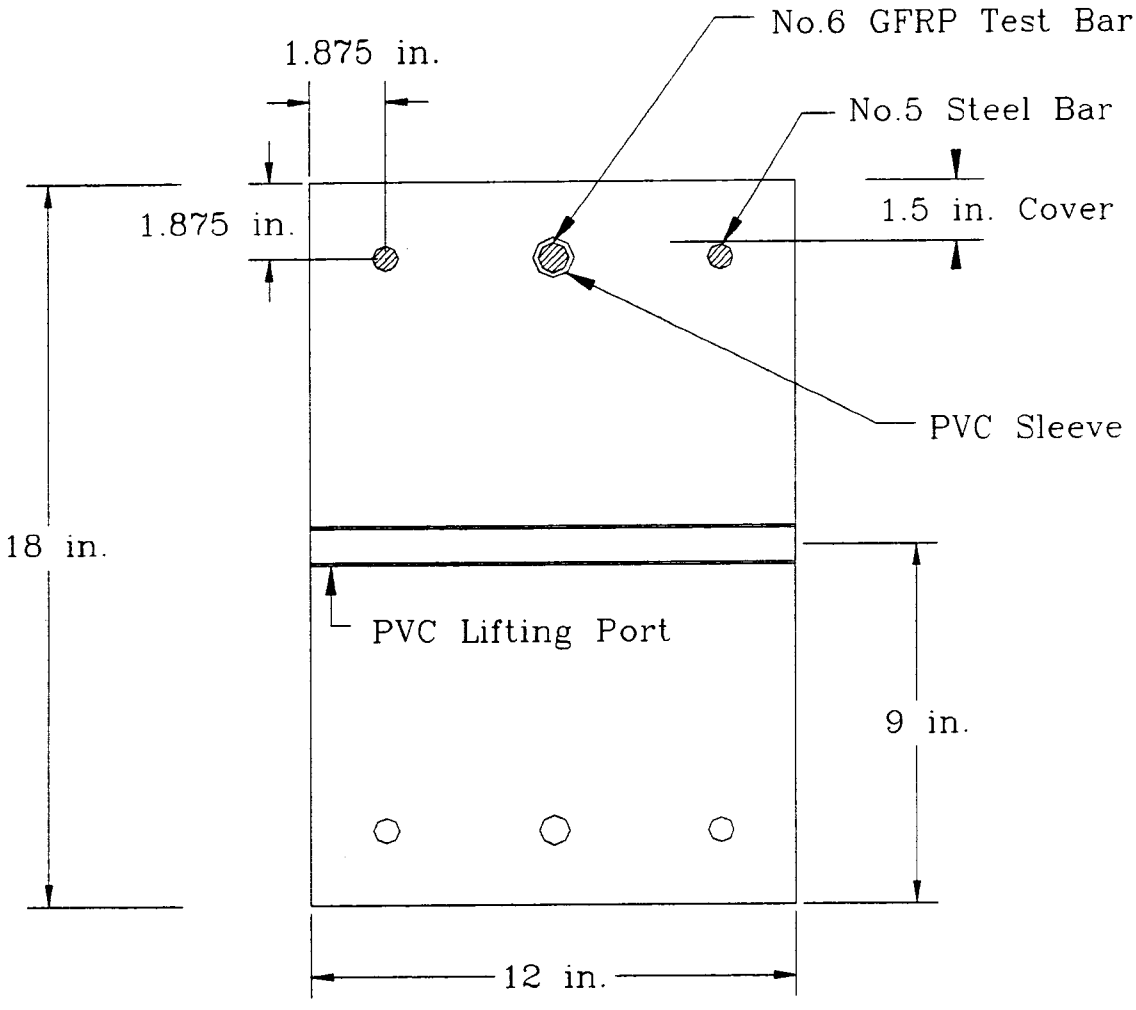

Figure 2.2 Cross Section of No.6 GFRP Specimen

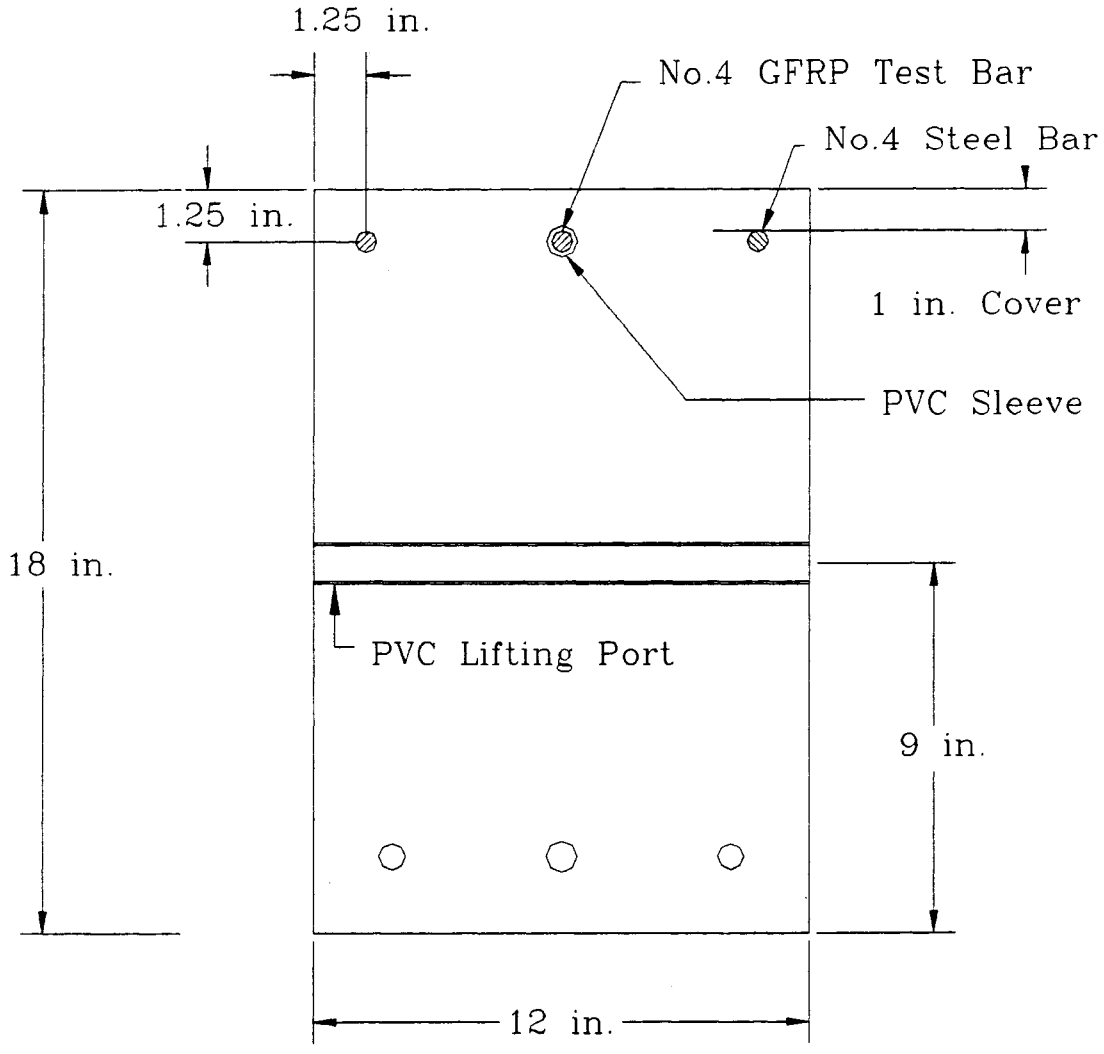

Figure 2.3 Cross Section of No.4 GFRP Specimen

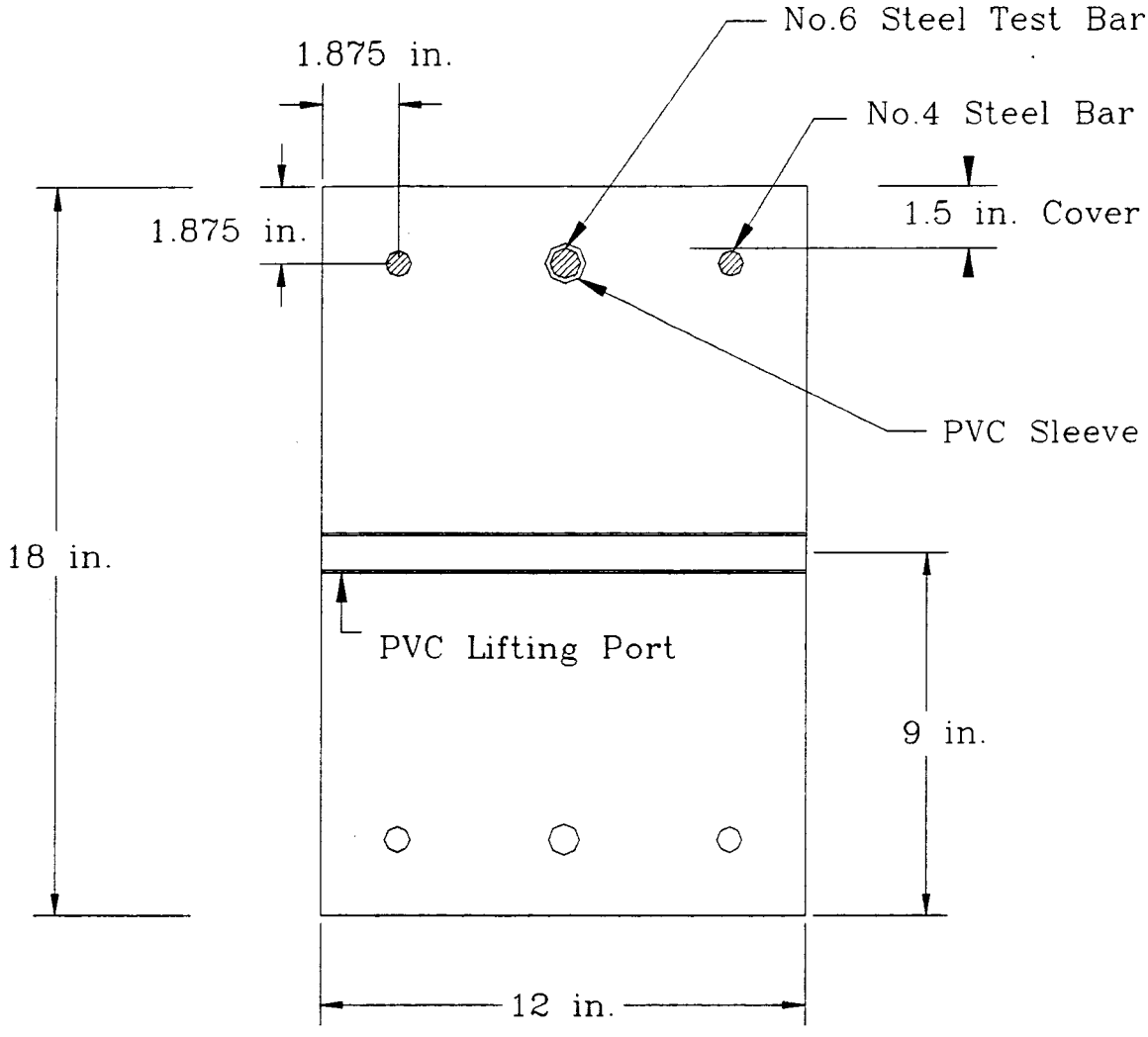

Figure 2.4 Cross Section of No.6 Steel Specimen

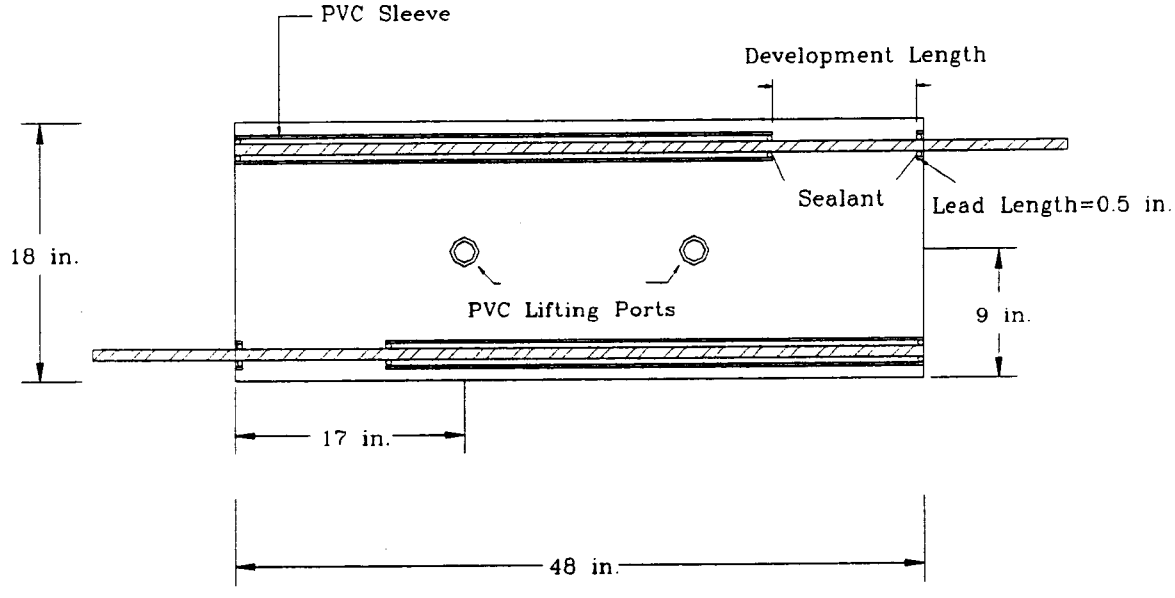

Figure 2.5 Typical Specimen Elevation

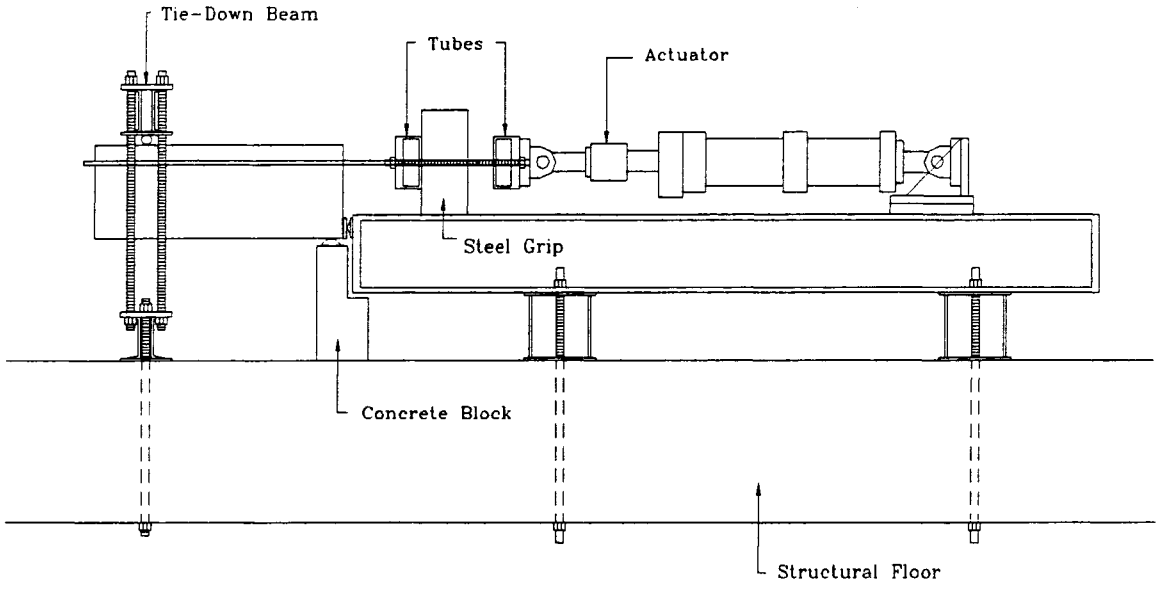

ELEVATION VIEW

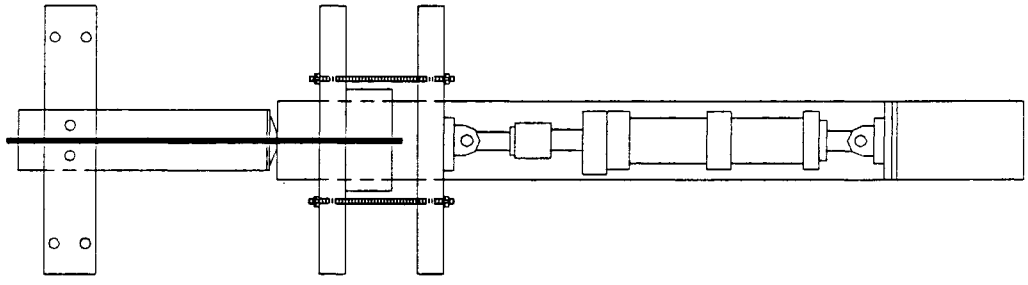

PLAN VIEW

Figure 2.6 Bond Test Frame, Plan and Elevation Views

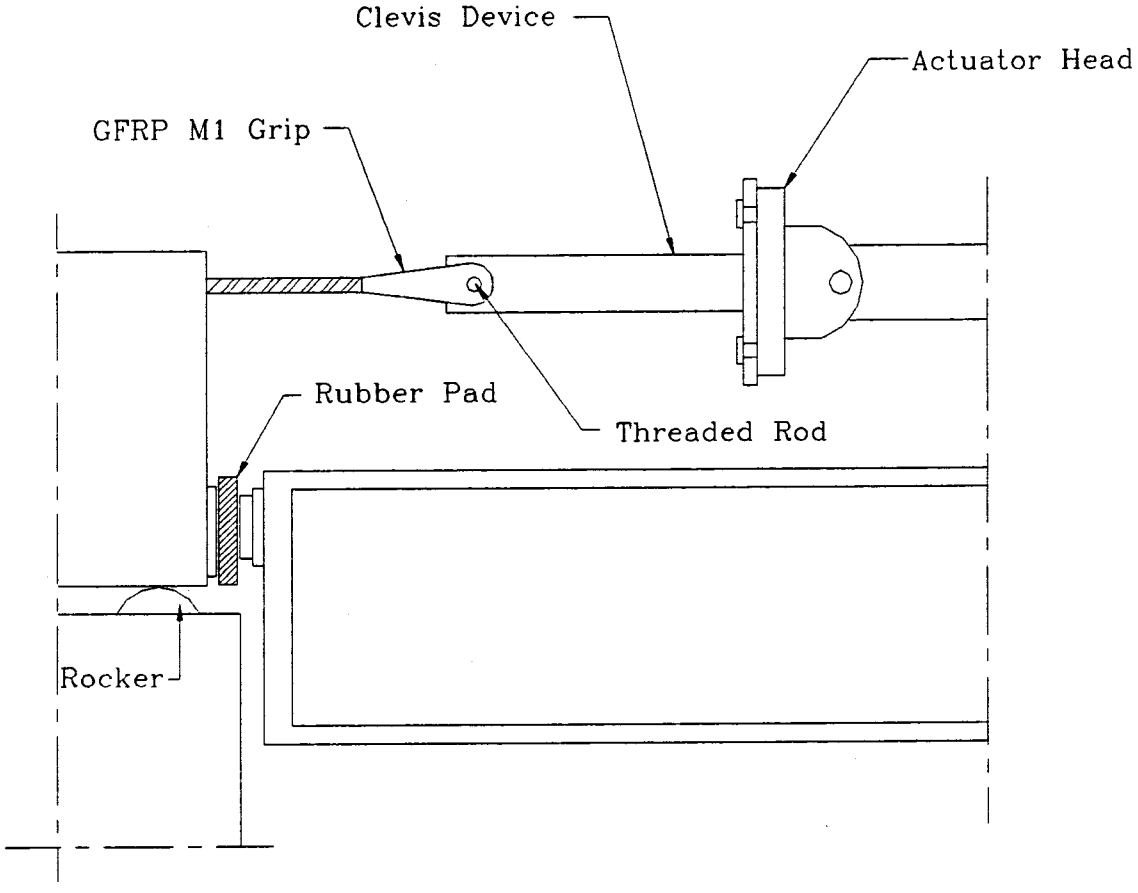

Figure 2.7 Grip System for GFRP M1

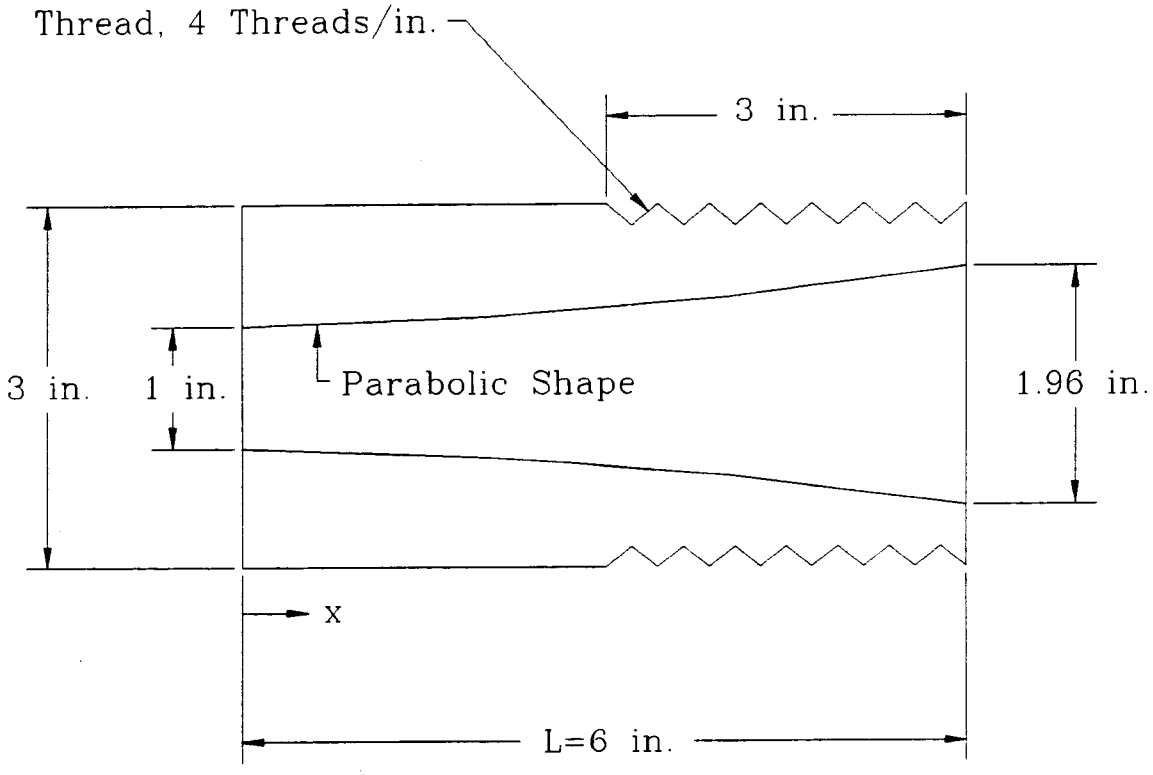

Figure 2.8 GFRP M2 Grip

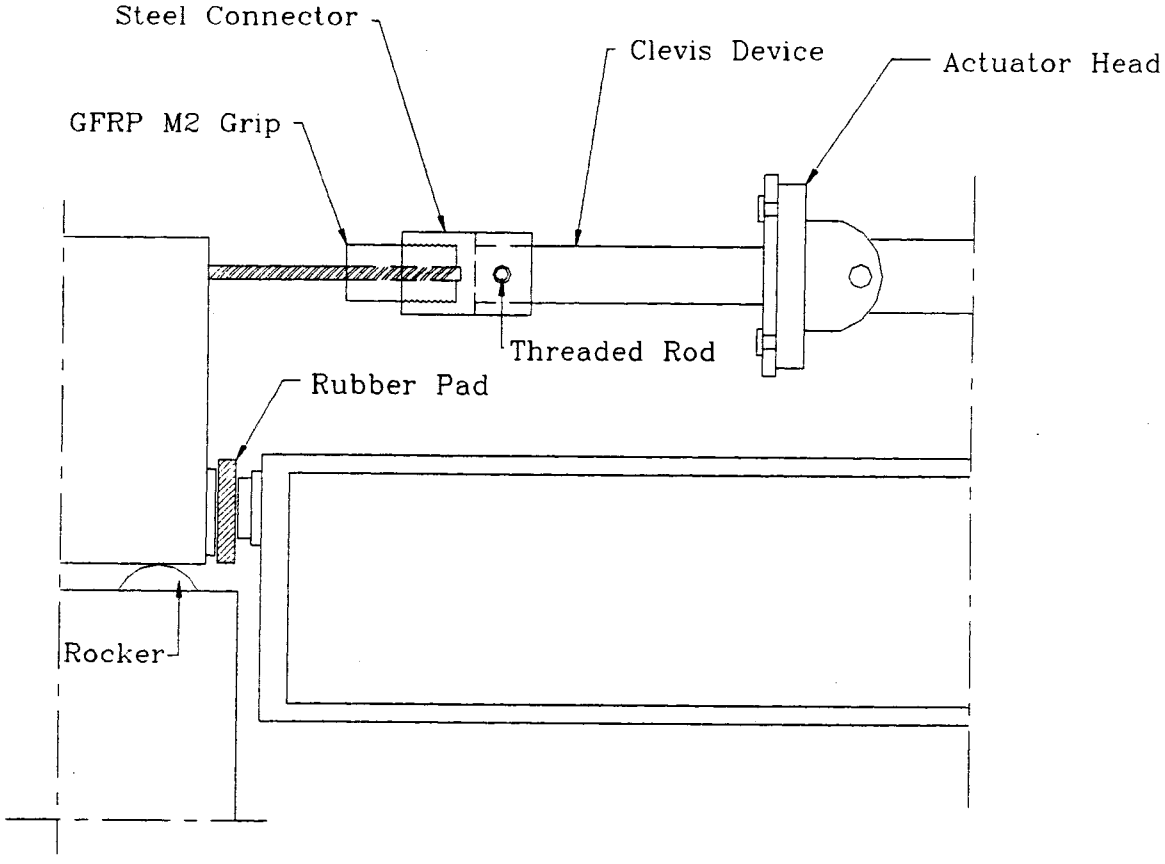

Figure 2.9 Grip System for GFRP M2

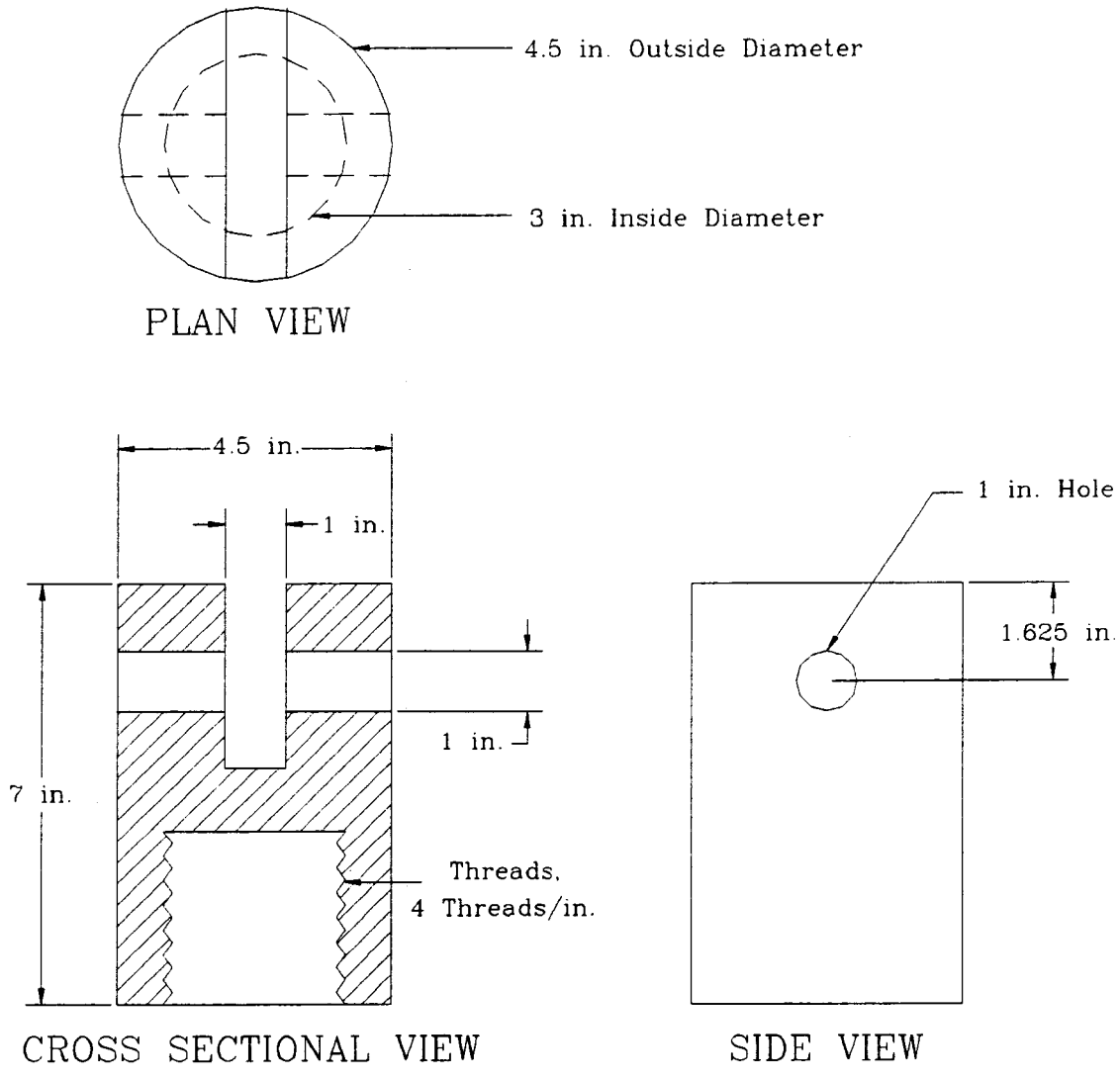

Figure 2.10 Steel Fixture for GFRP M2 Grip

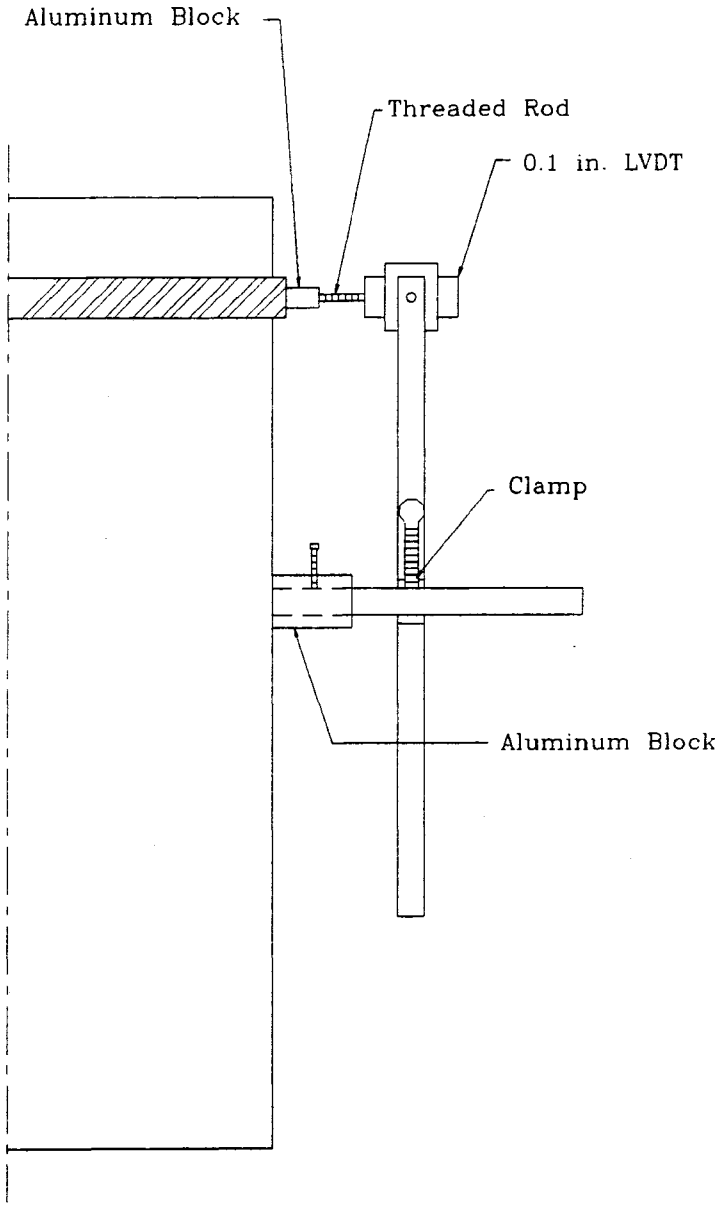

Figure 2.11 Free-end Slip Instrumentation

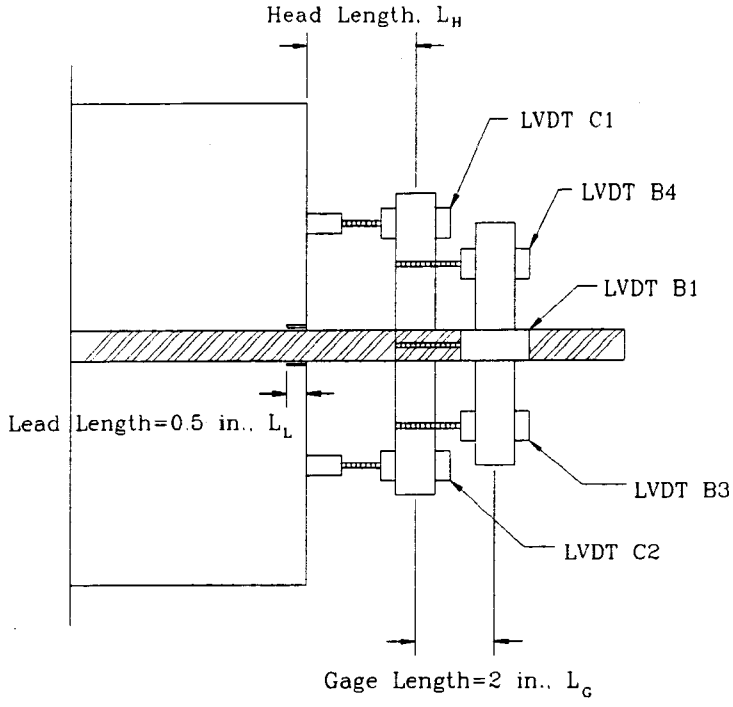

PLAN VIEW

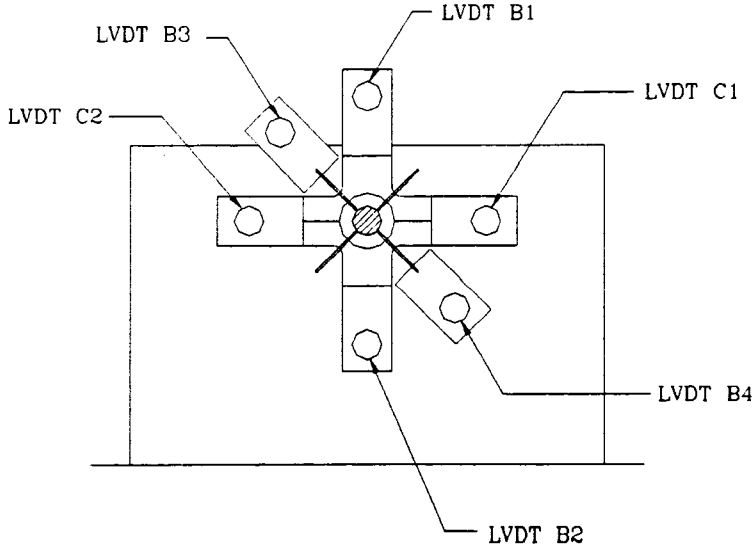

SIDE VIEW

Figure 2.12 Loaded-end Slip Instrumentation

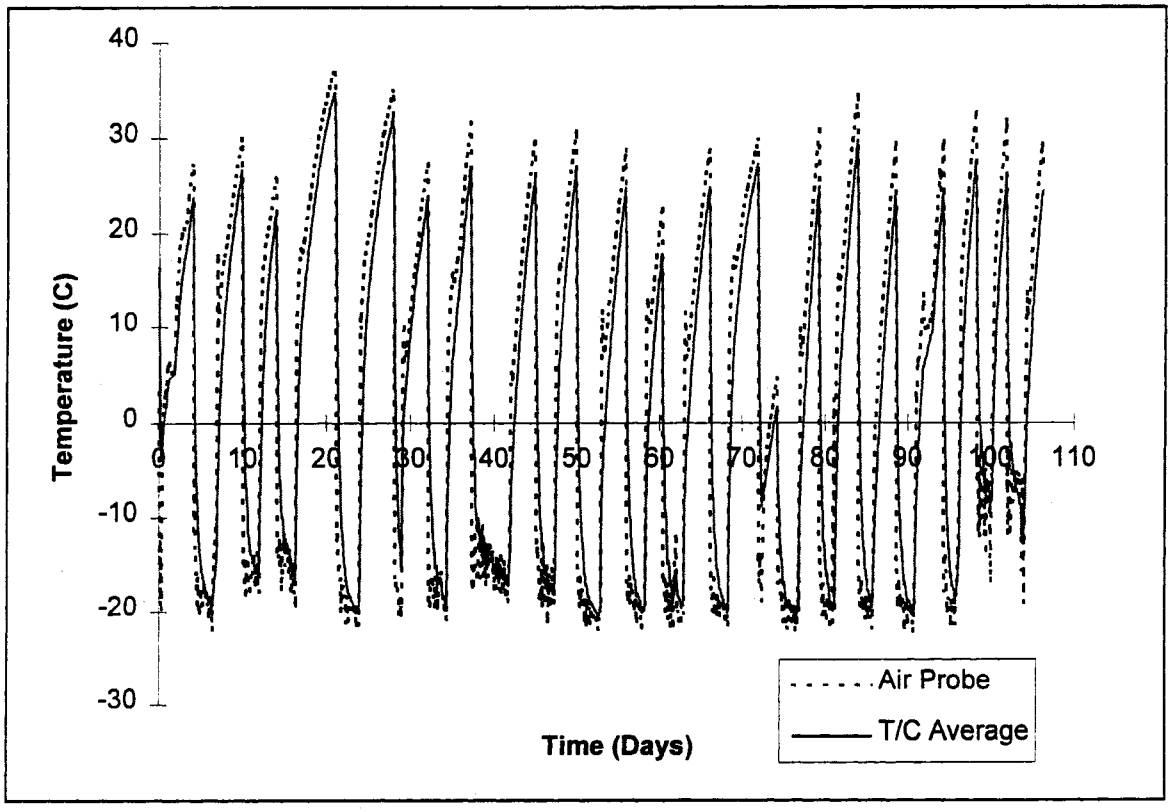

Figure 2.13 Temperature Data for Thermal Fatigue

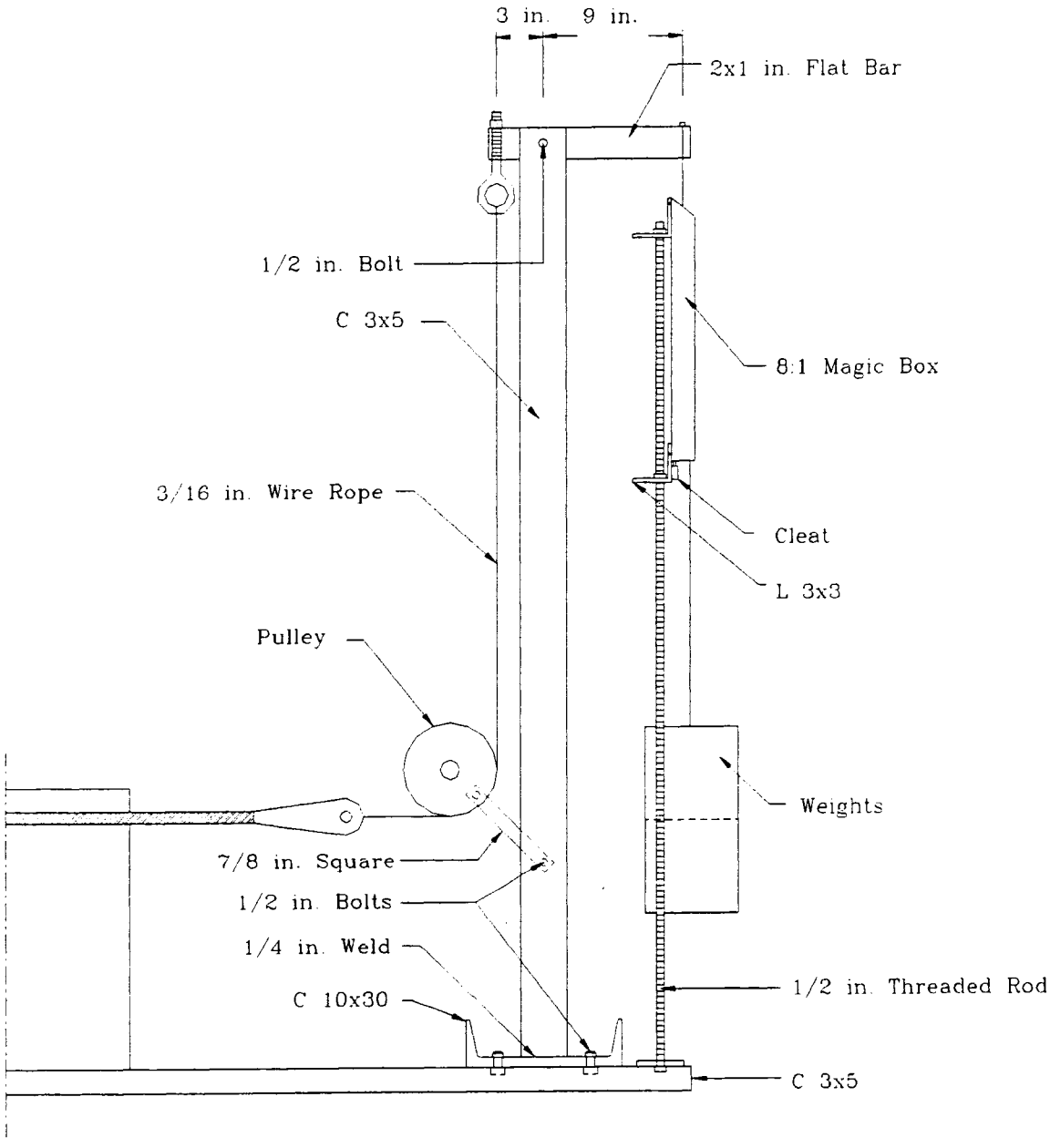

Figure 2.14 Load Frame for Thermal and Control Specimens

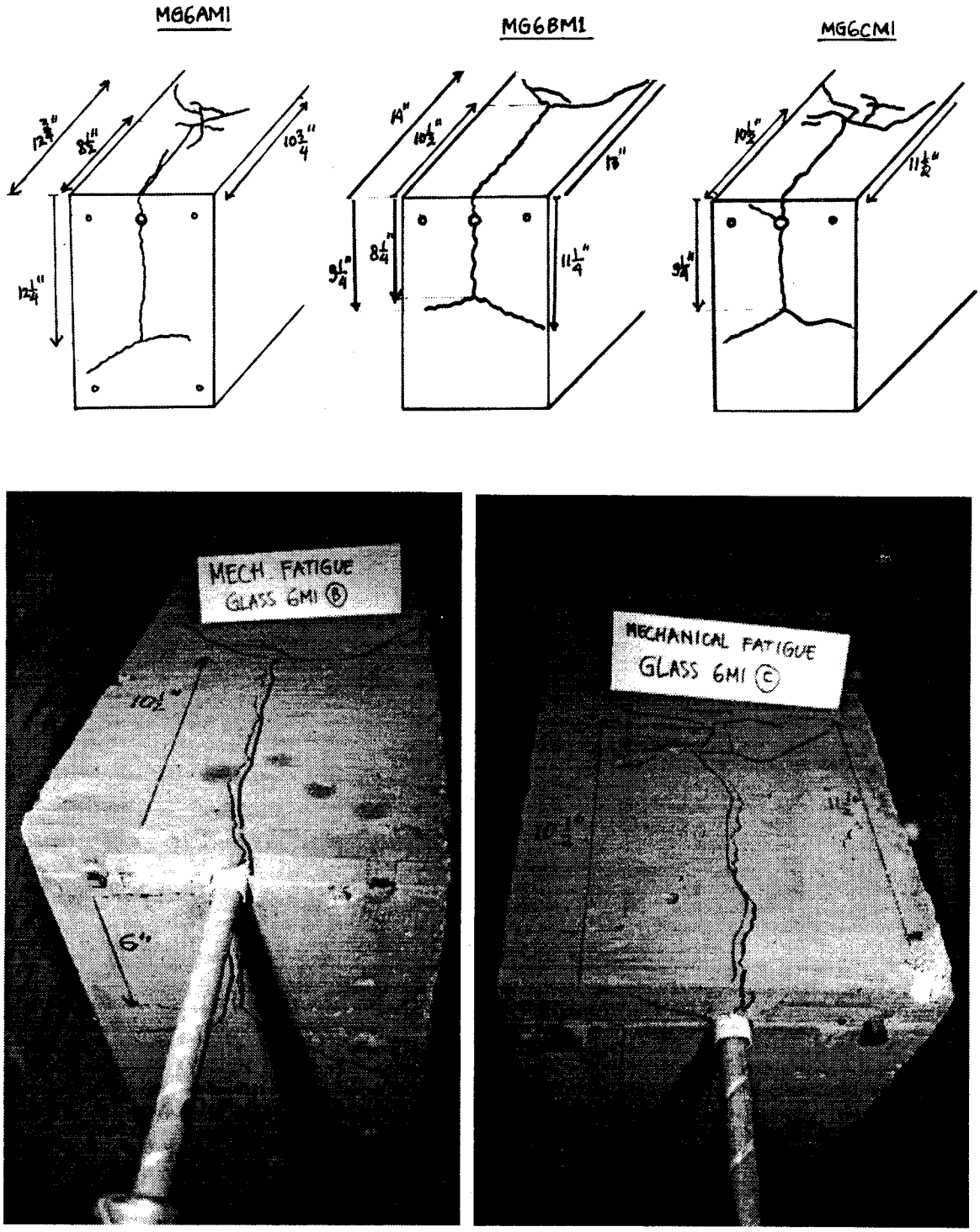

Figure 3.1 MG6AM1, MG6BM1 and MG6CM1 Specimens

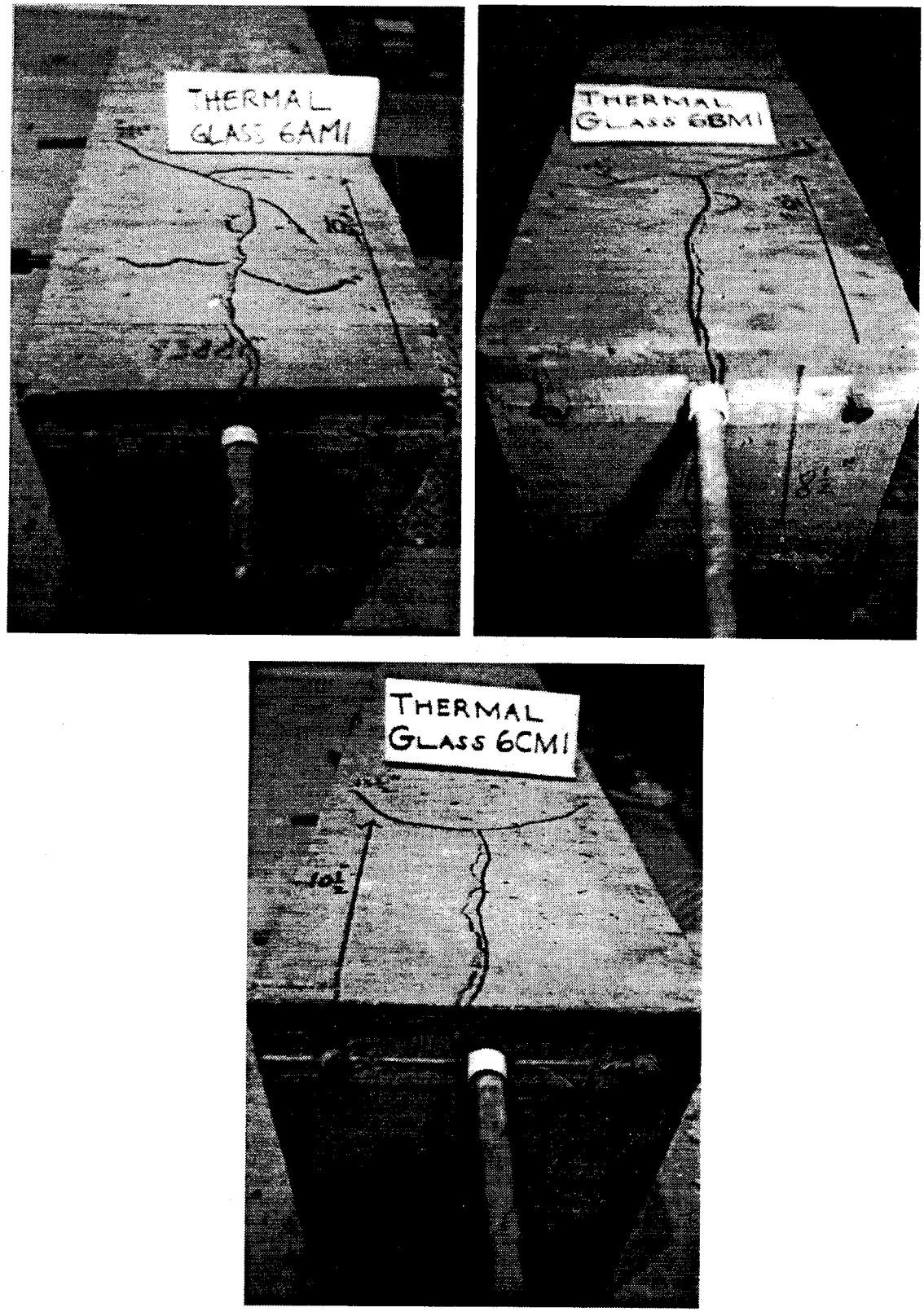

Figure 3.2 TG6AM1, TG6BM1, and TG6CM1 Specimens

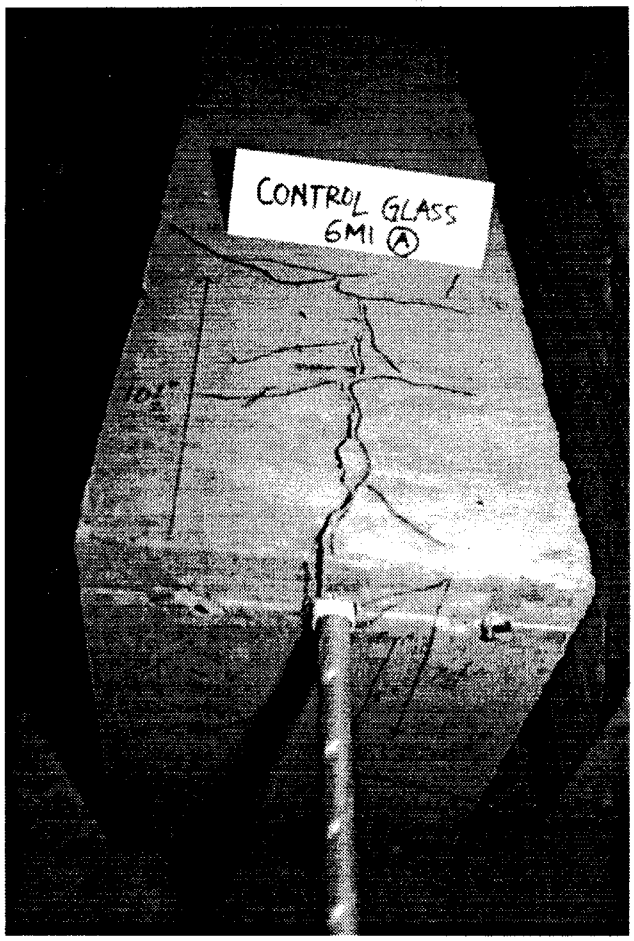

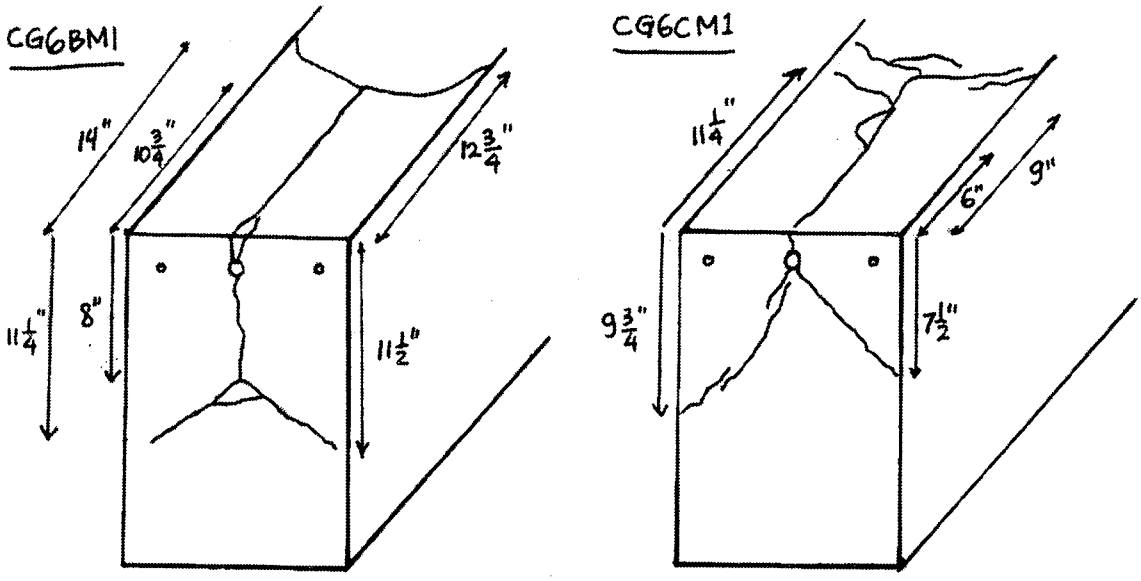

Figure 3.3 CG6AM1, CG6BM1, and CG6CM1 Specimens

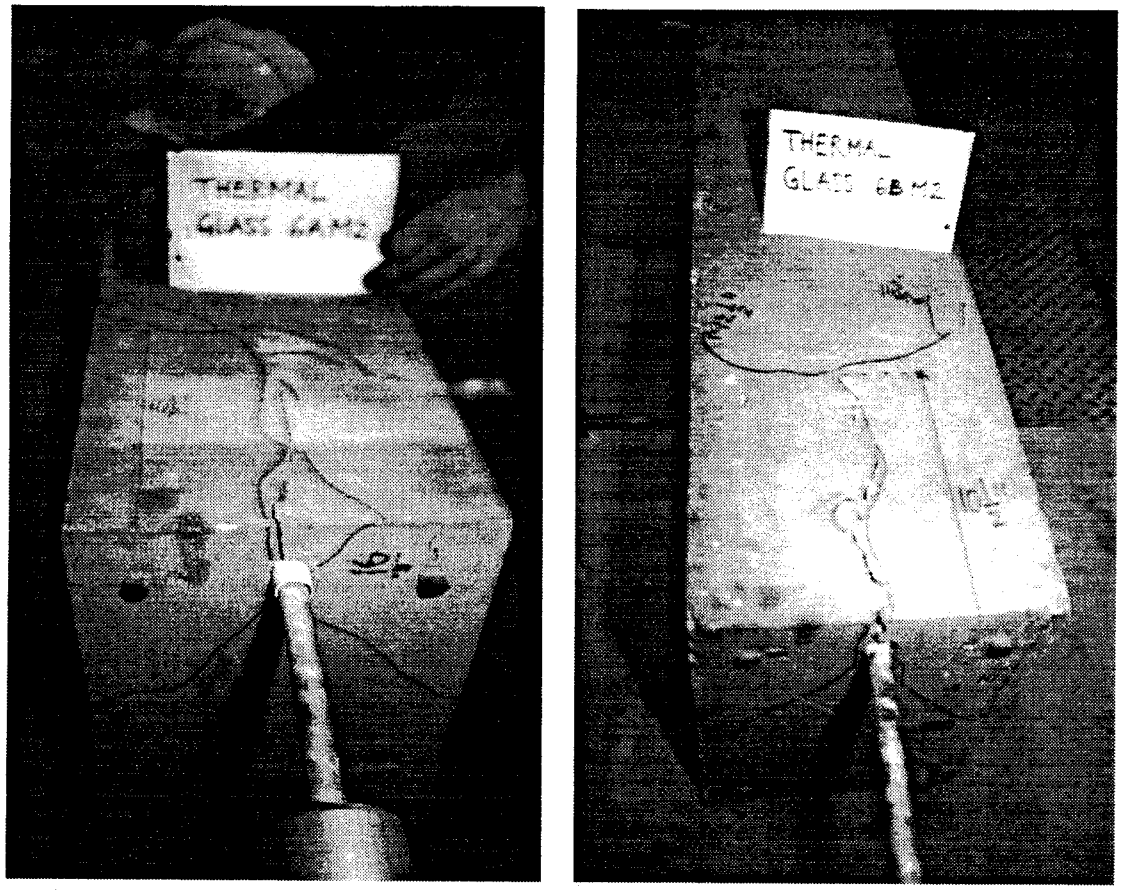

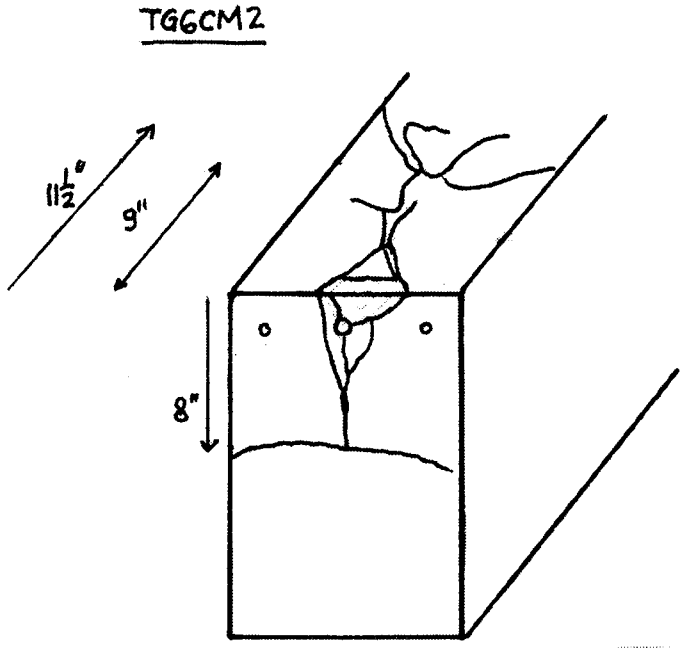

Figure 3.4 TG6AM2, TG6BM2, and TG6CM2 Specimens

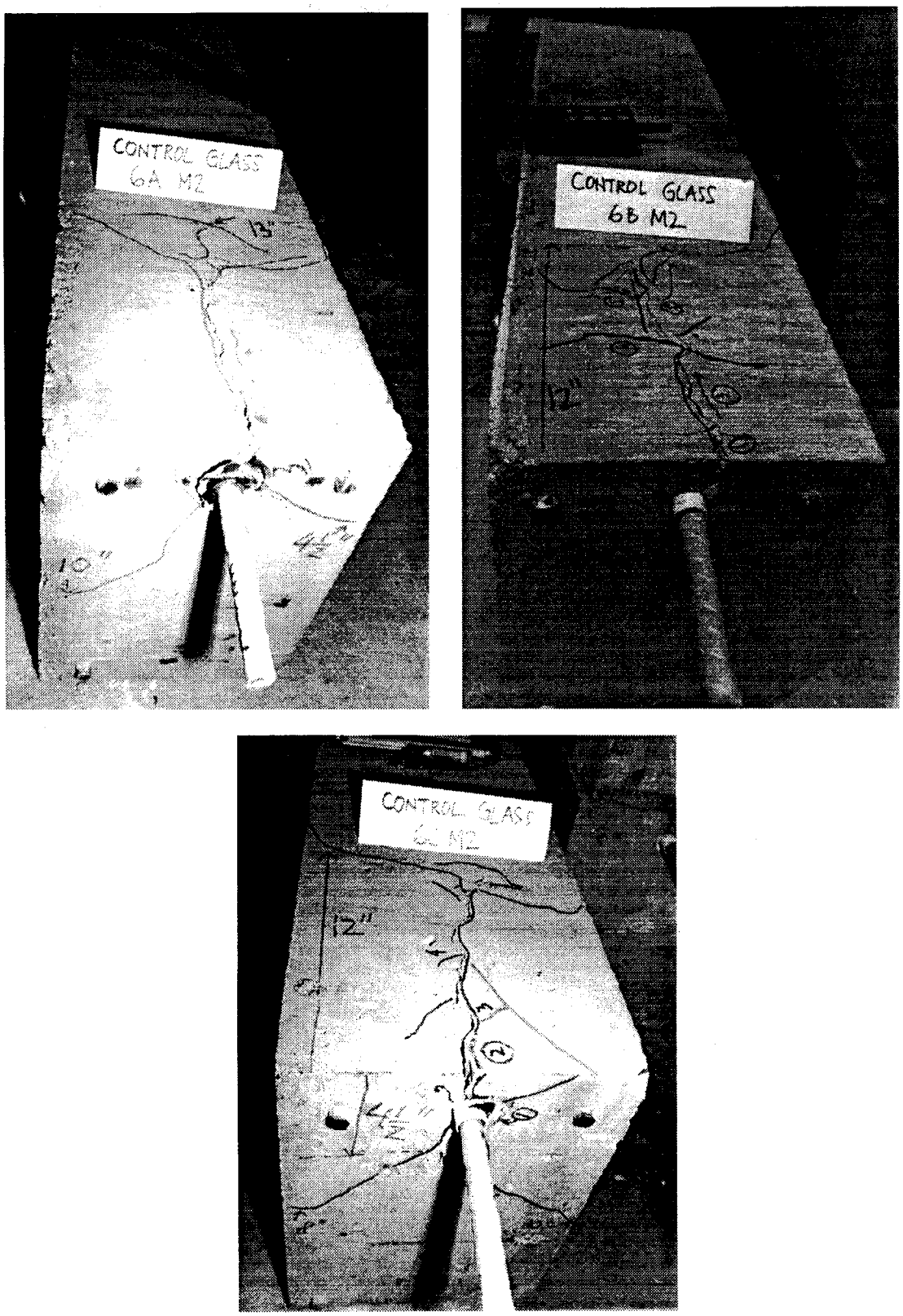

Figure 3.5 CG6AM2, CG6BM2, and CG6CM2 Specimens

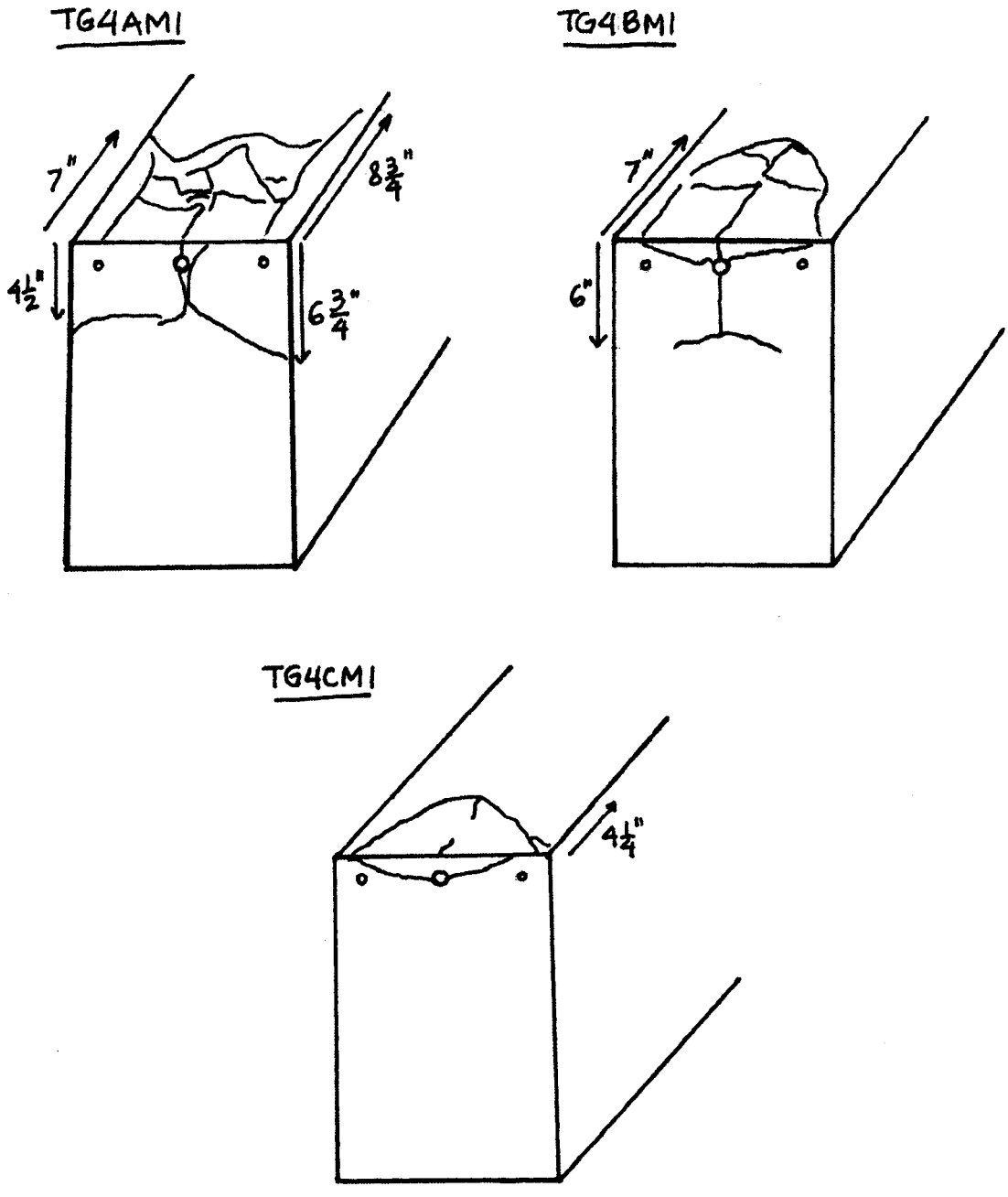

Figure 3.6 TG4AM1, TG4BM1, and TG4CM1 Specimens

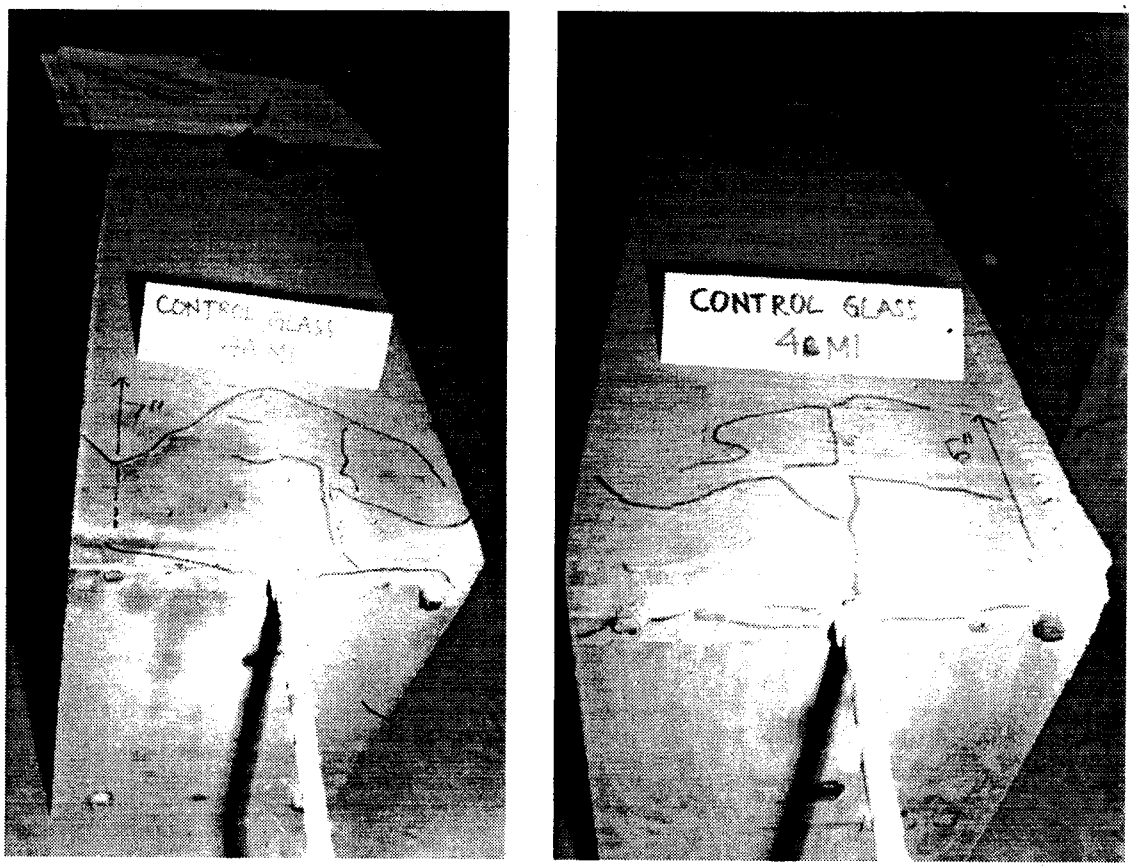

CG4CM1

Figure 3.7 CG4AM1, CG4BM1, and CG4CM1 Specimens

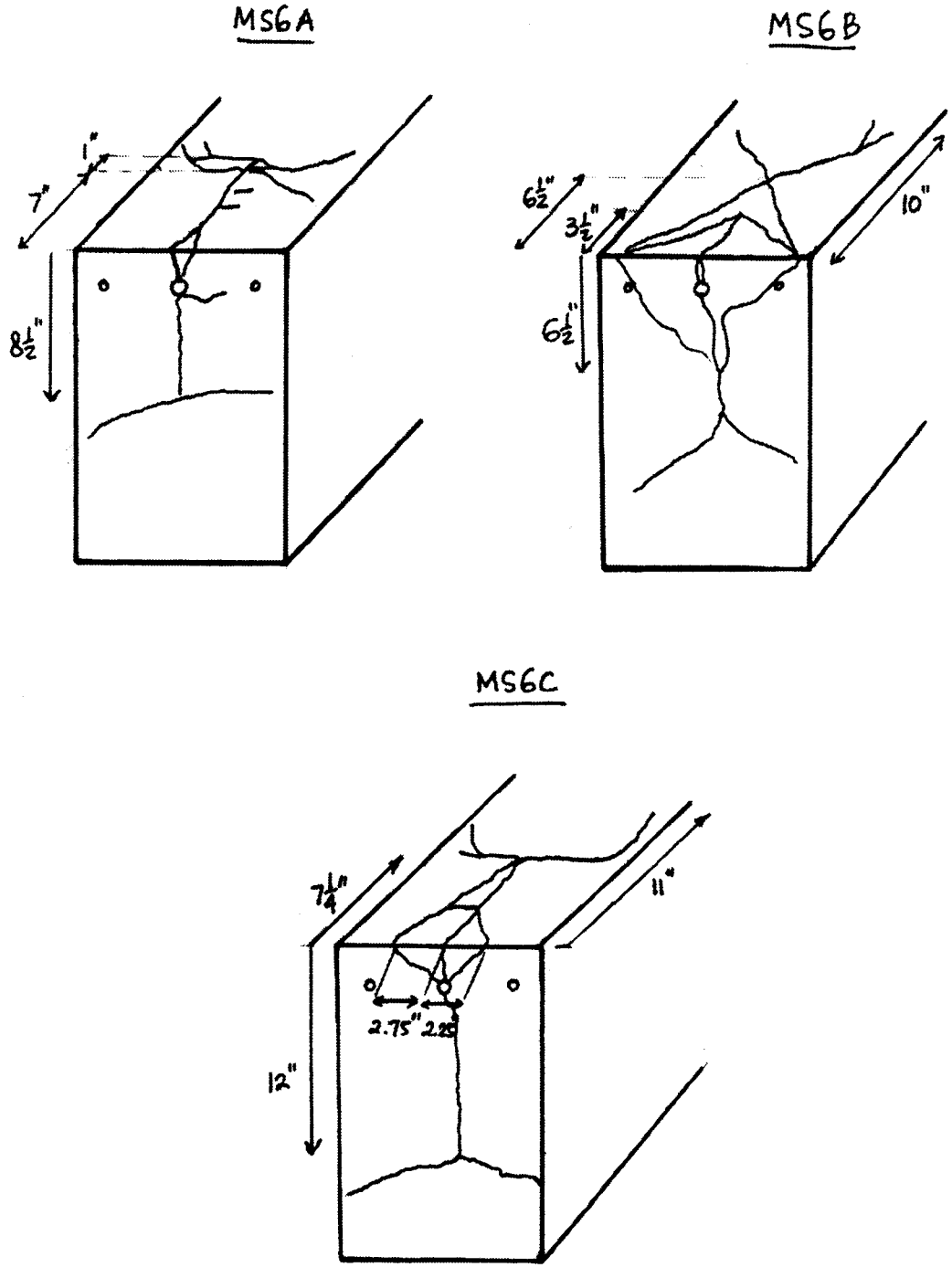

Figure 3.8 MS6A, MS6B, and MS6C Specimens

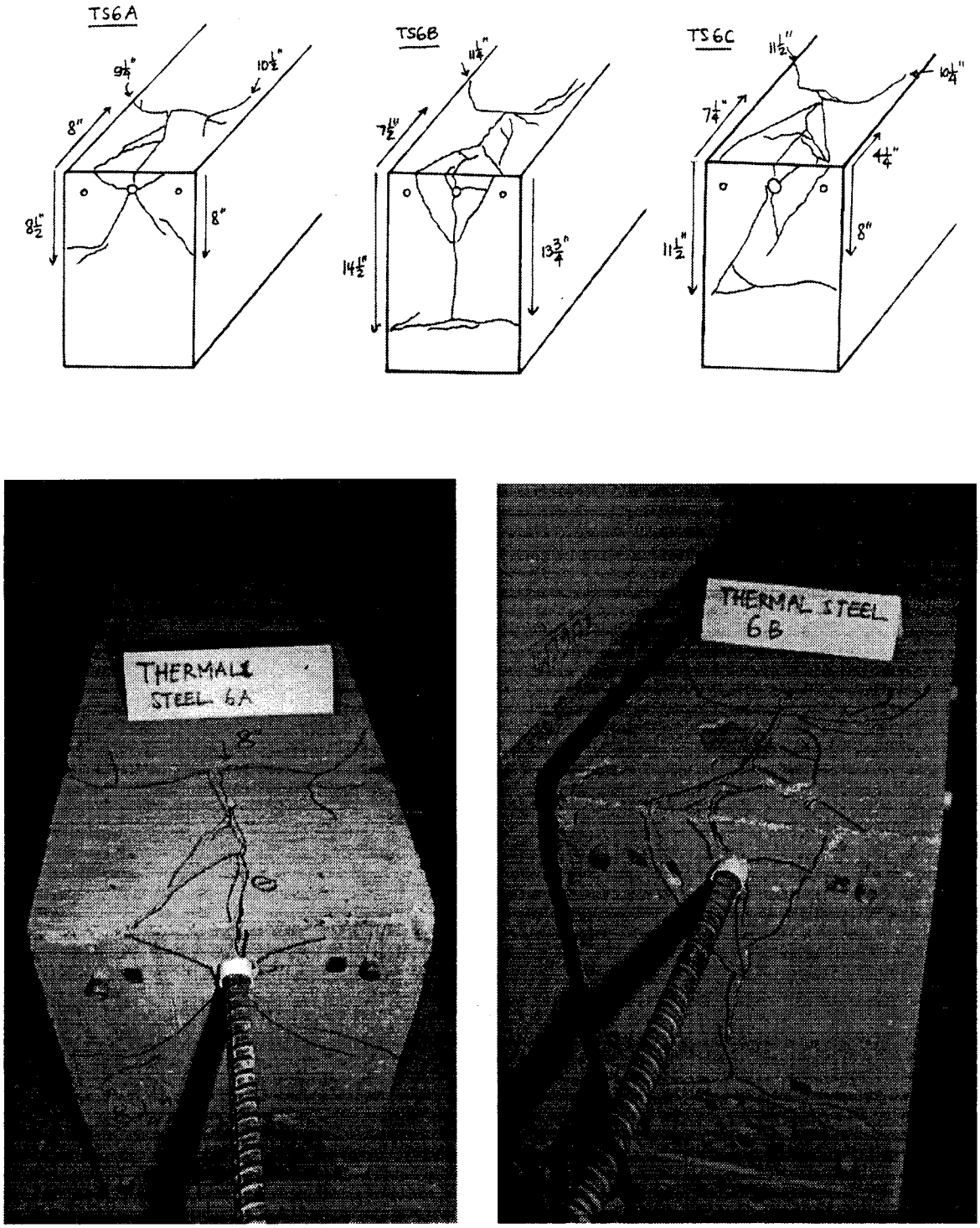

Figure 3.9 TS6A, TS6B, and TS6C Specimens

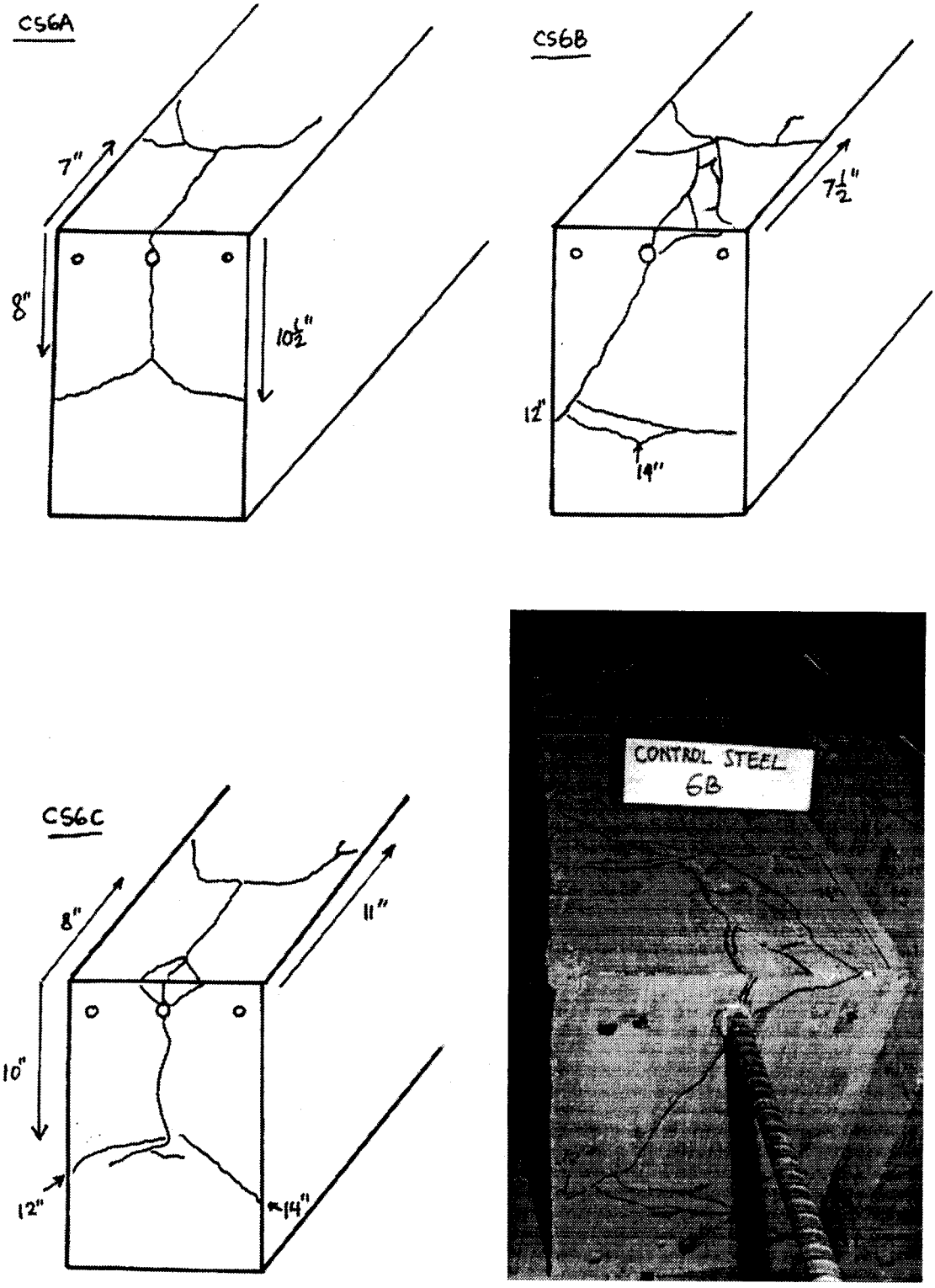

Figure 3.10 CS6A, CS6B, and CS6C Specimens

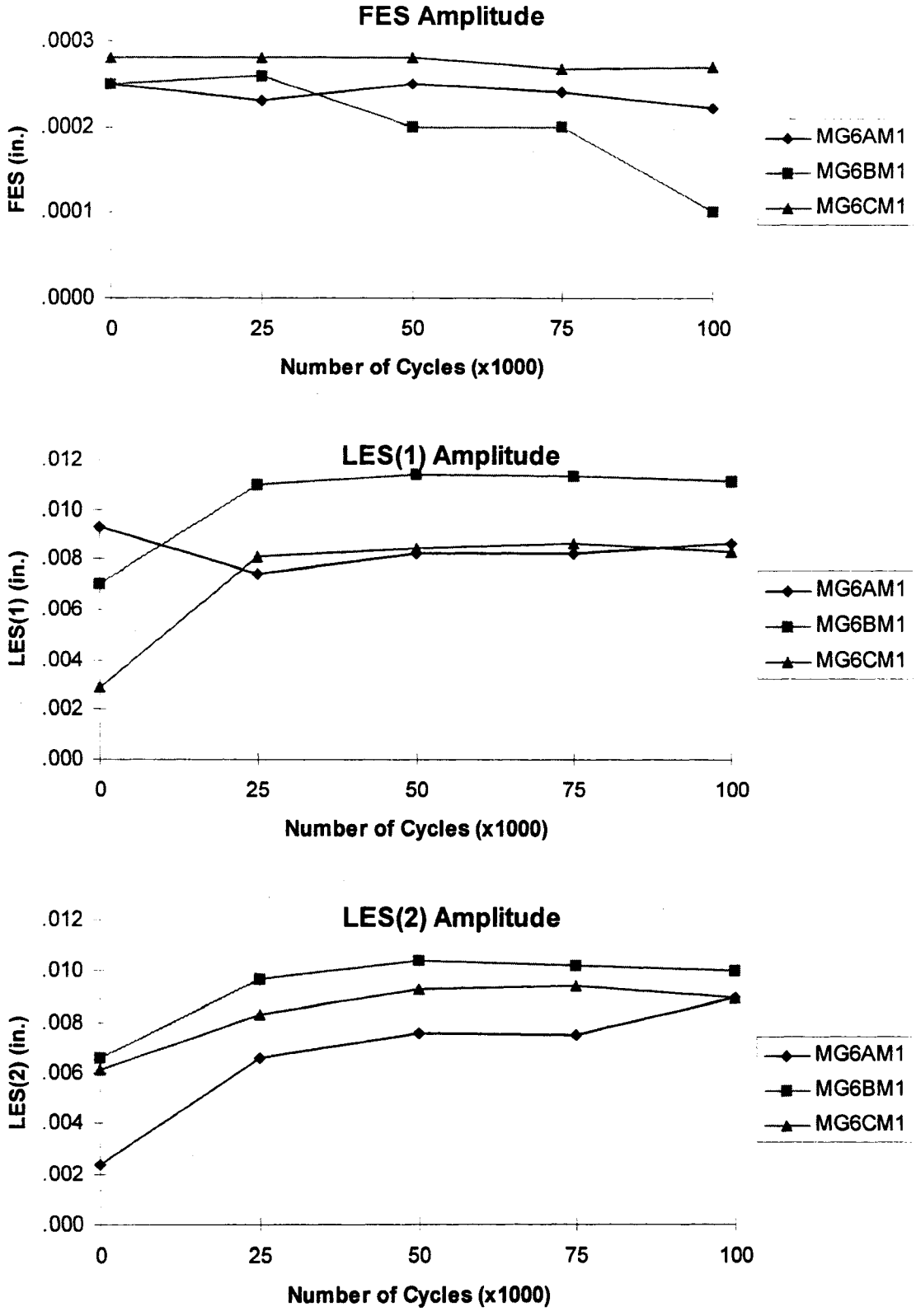

Figure 3.11 Slips Amplitude of Mechanically Cyled GFRP Specimens

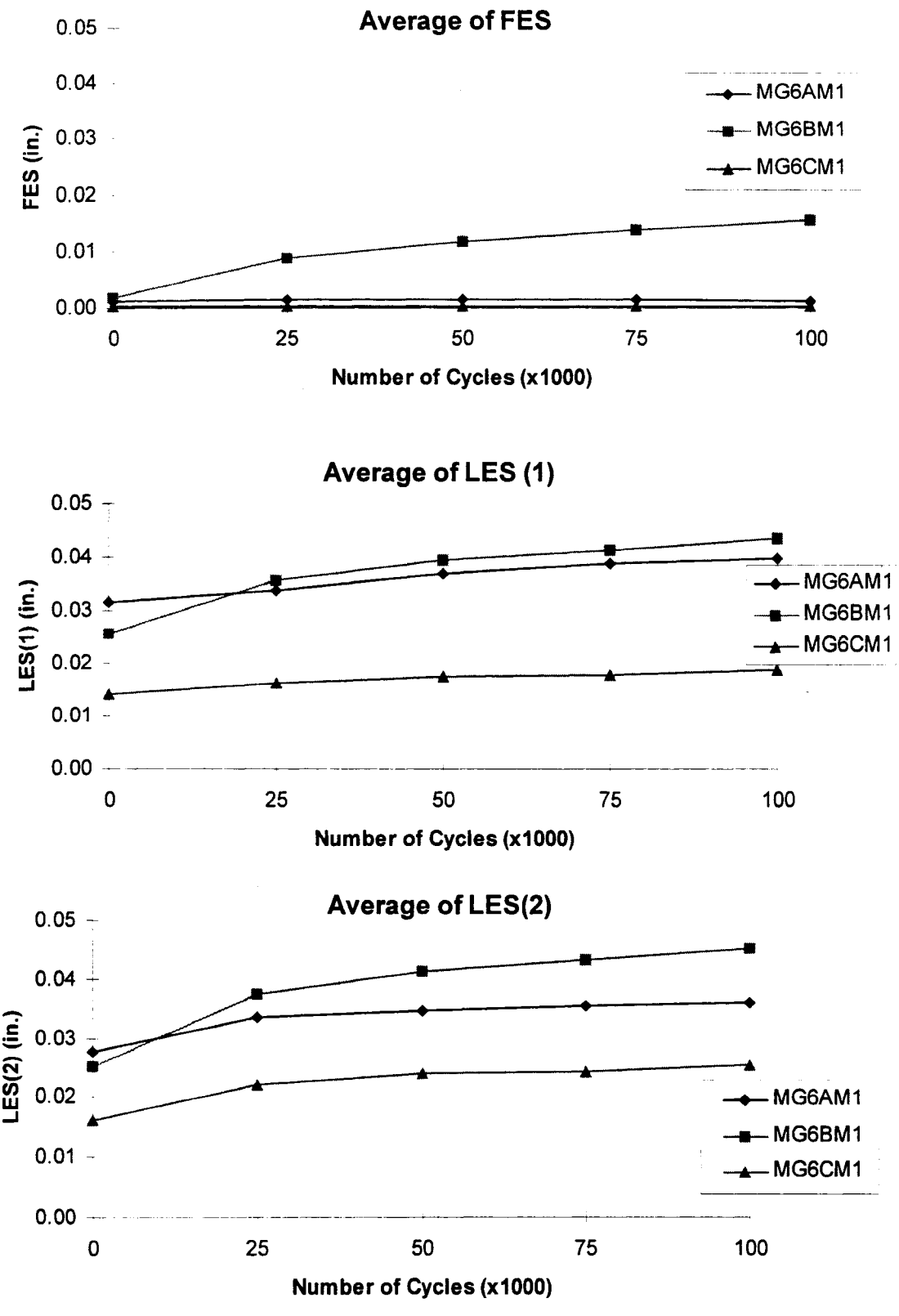

Figure 3.12 Slips Average of Mechanically Cycled GFRP Specimens

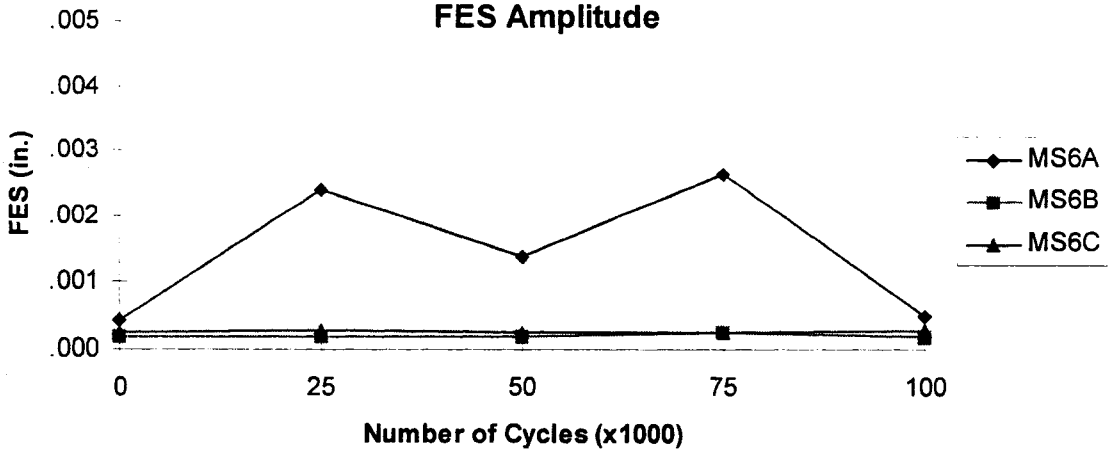

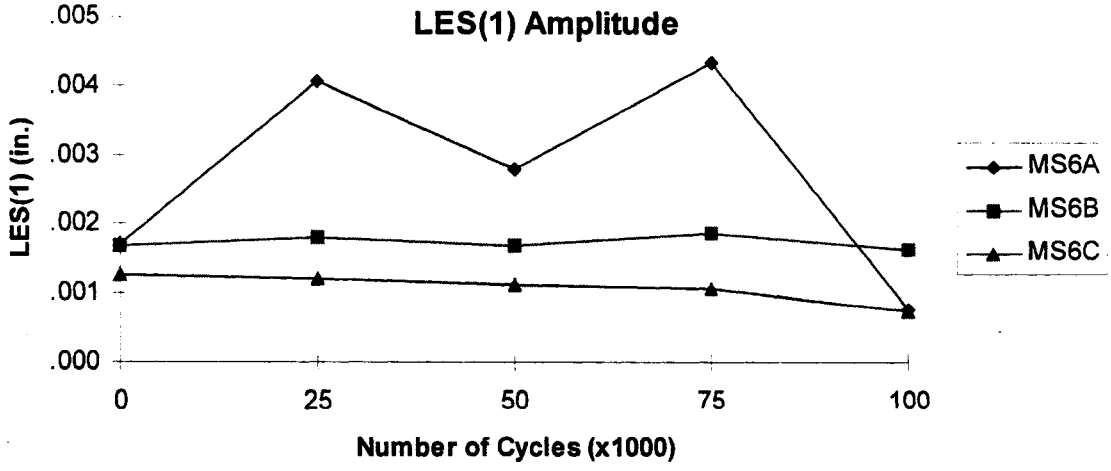

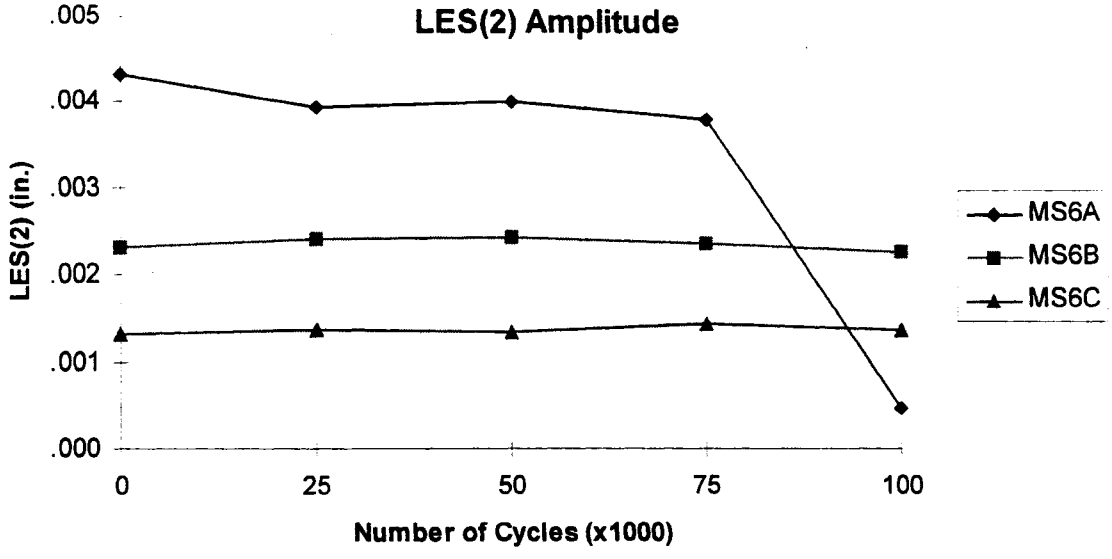

Figure 3.13 Slips Amplitude of Mechanically Cycled Steel Specimens

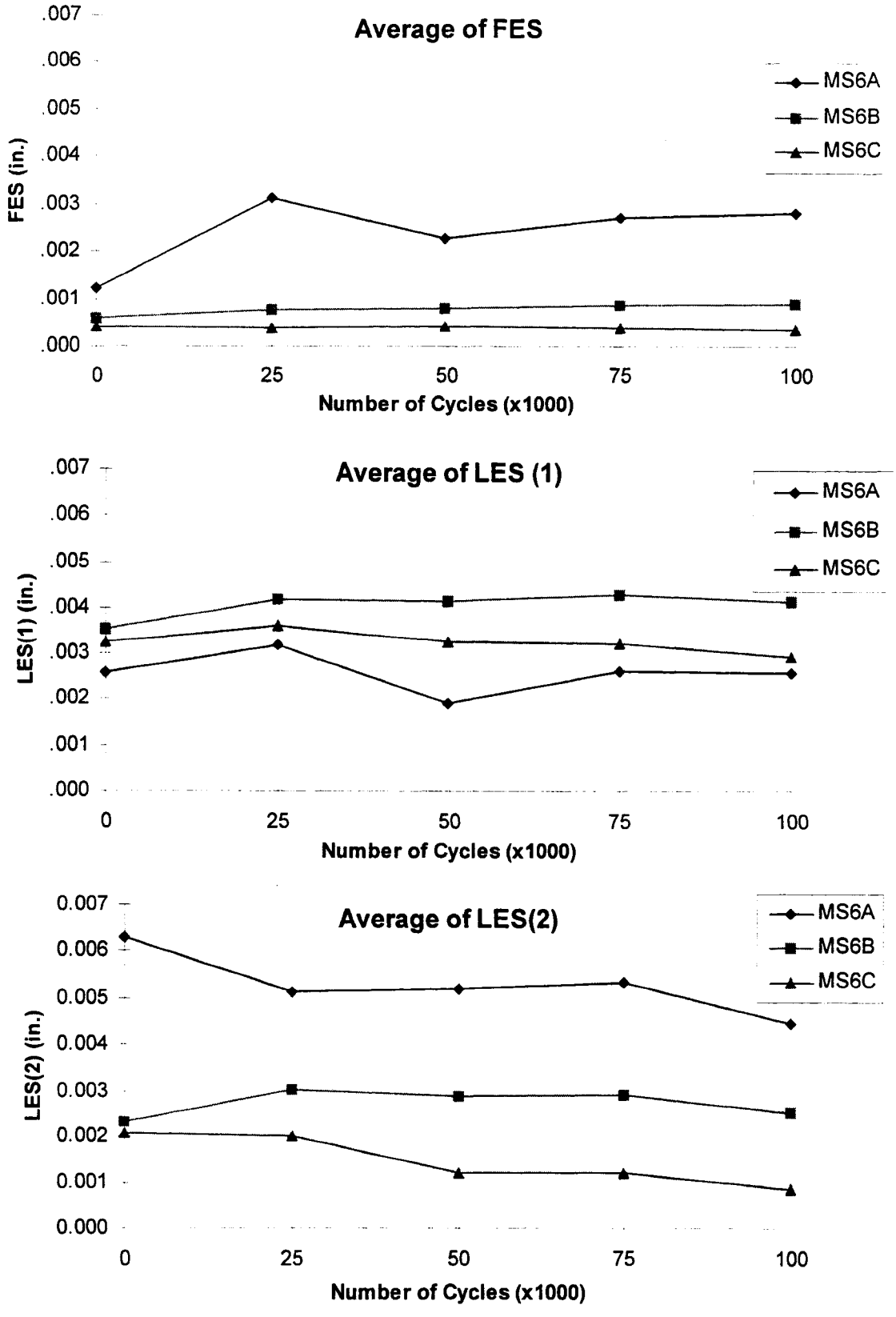

Figure 3.14 Slips Average of Mechanically Cycled Steel Specimens

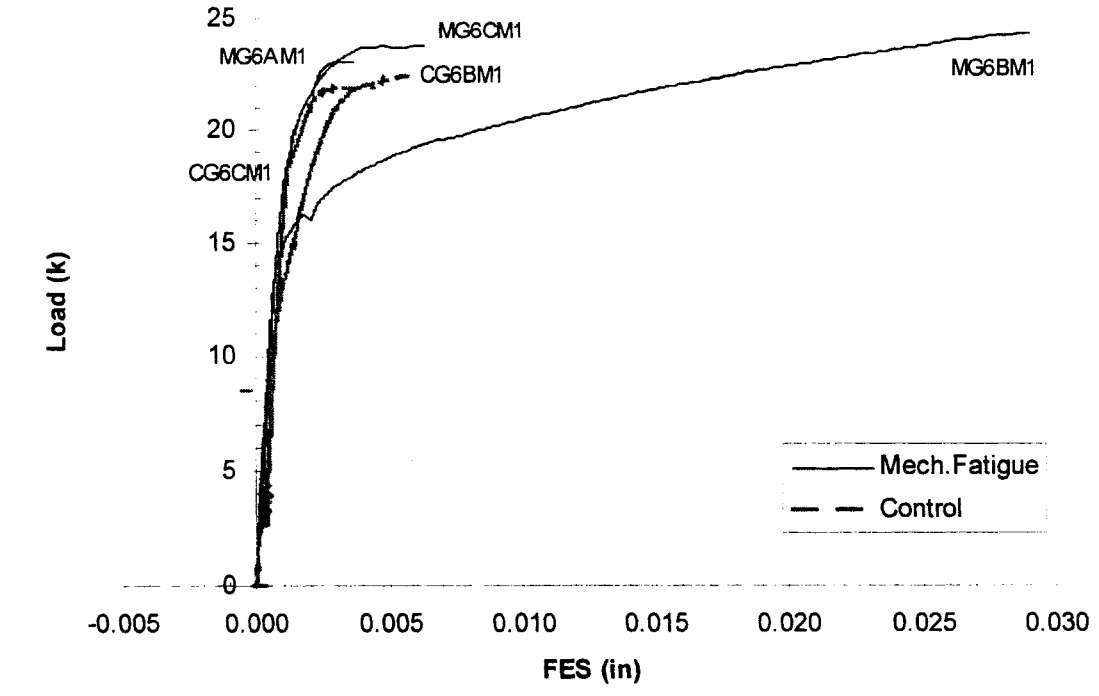

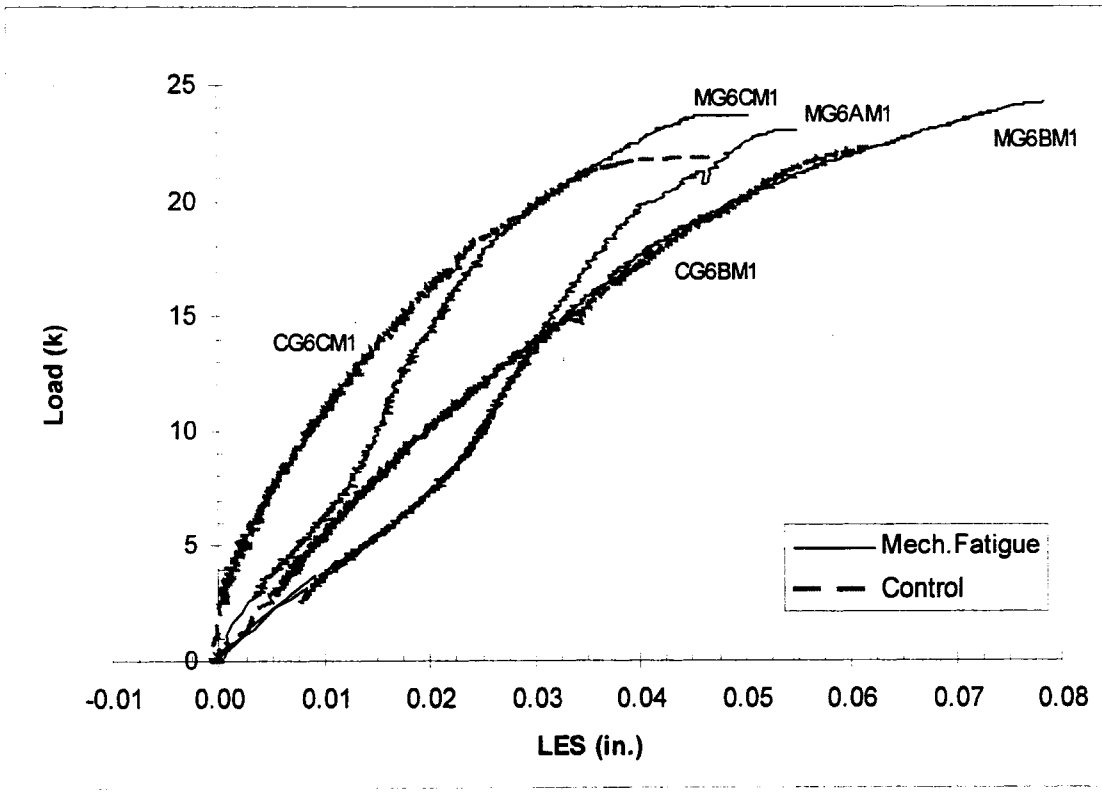

Figure 3.15 Load-Slip Curves for Mechanically Cycled and Control GFRP M1 Specimens

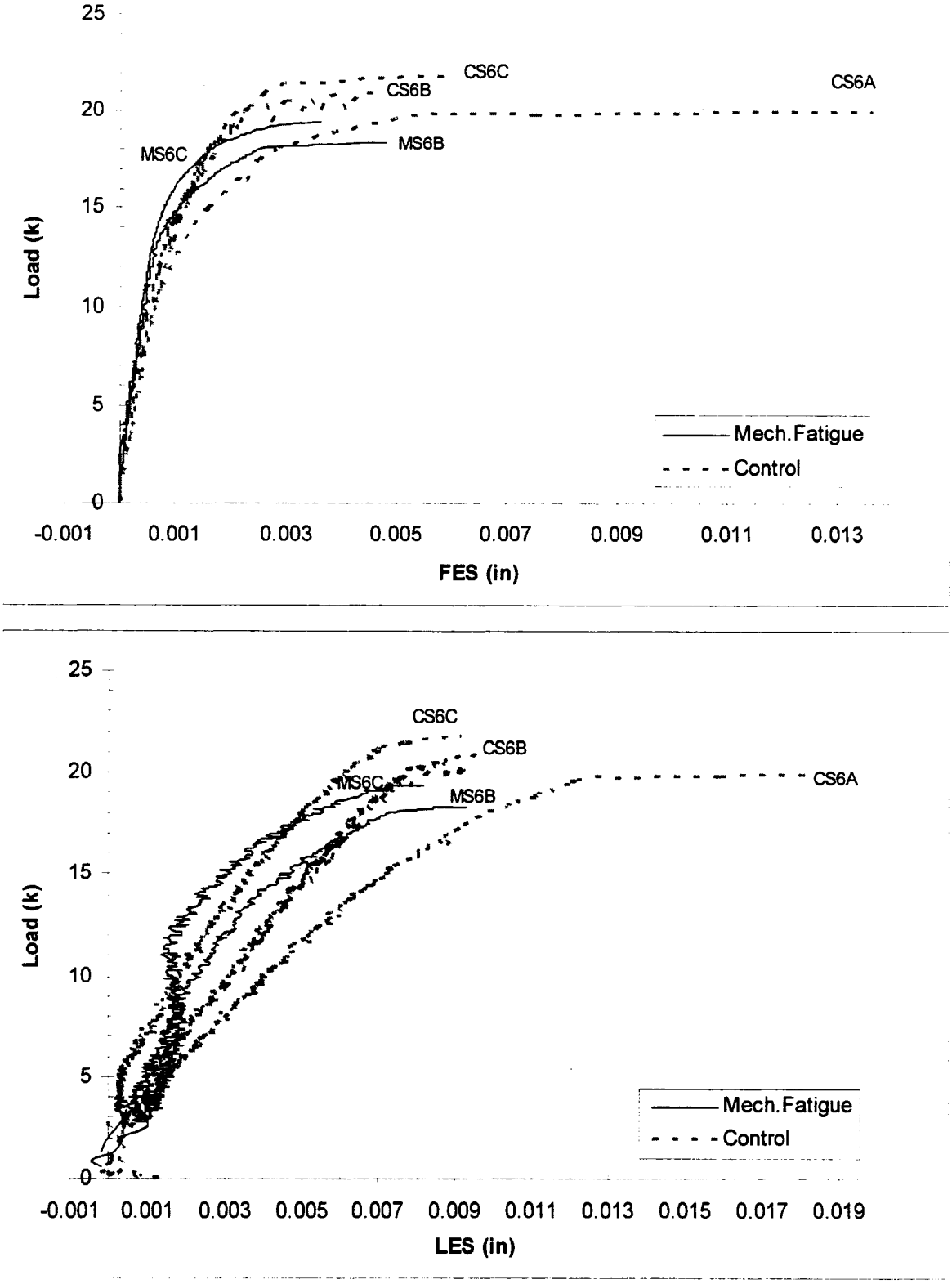

Figure 3.16 Load Slip Curve for Mechanically Cycled and Control Steel Specimens

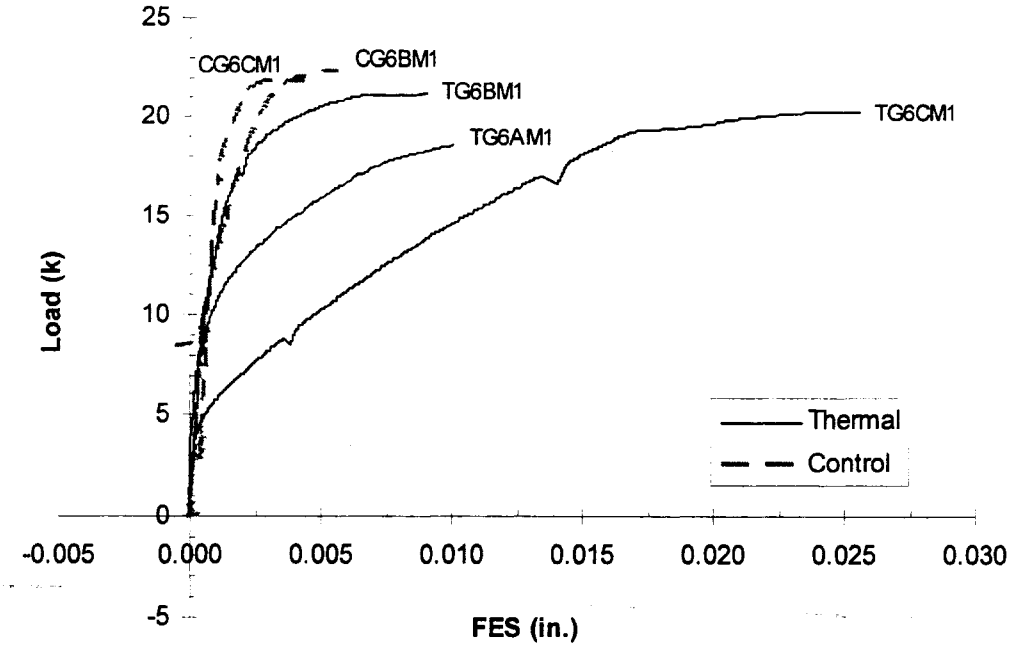

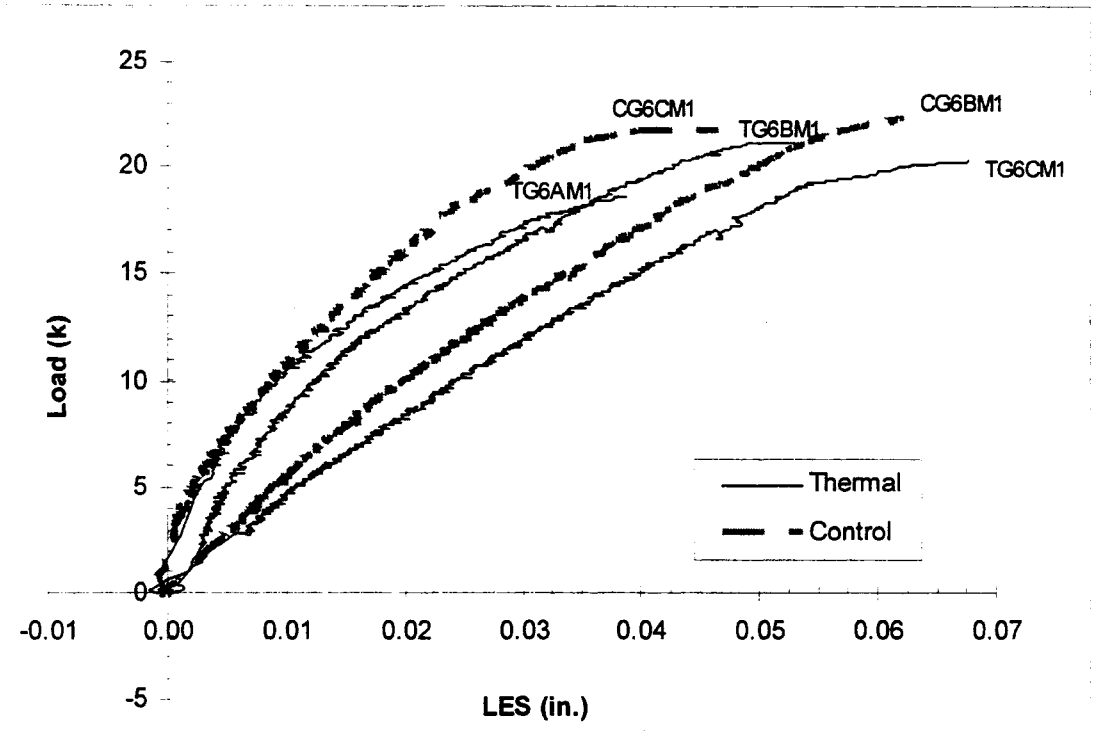

Figure 3.17 Load-Slip Curves for Thermally Cycled and Control No.6 GFRP M1 Specimens

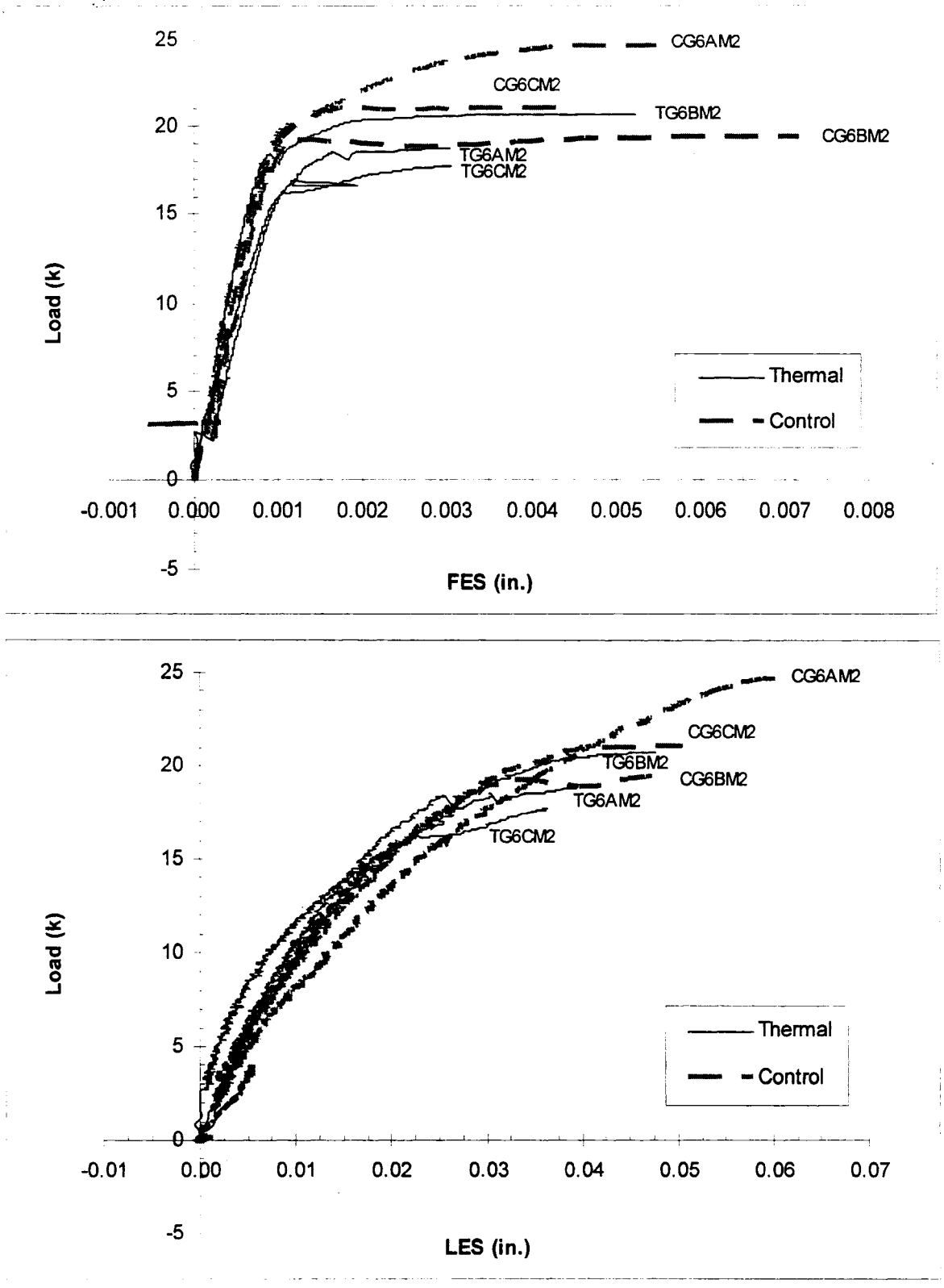

Figure 3.18 Load-Slip Curves for Thermally Cycled and Control No.6 GFRP M2 Specimens

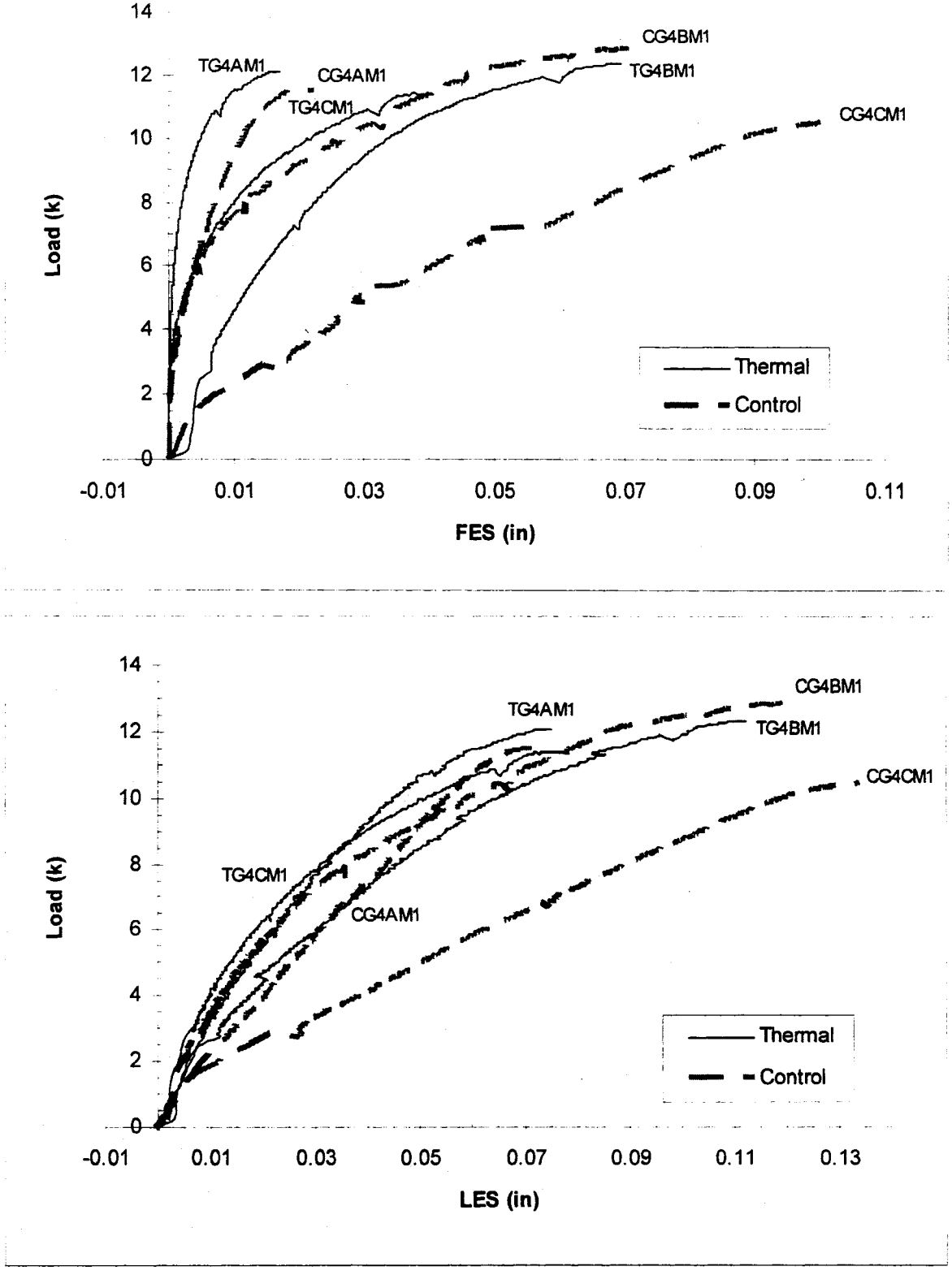

Figure 3.19 Load-Slip Curves for Thermally Cycled and Control No.4 GFRP M1 Specimens

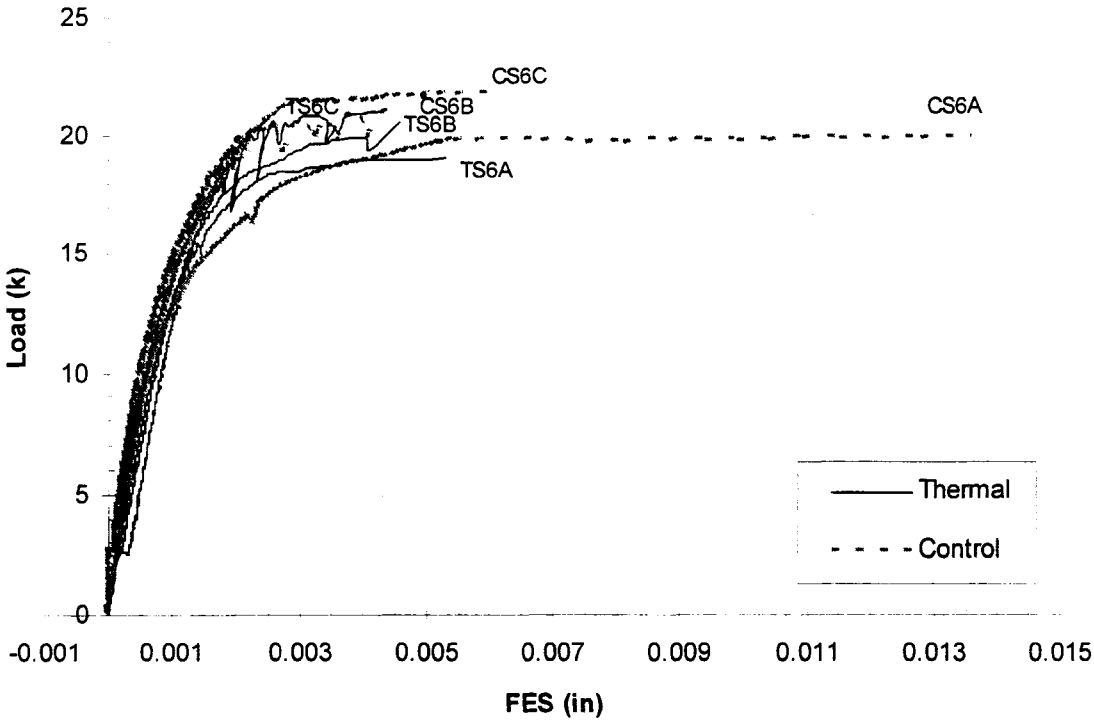

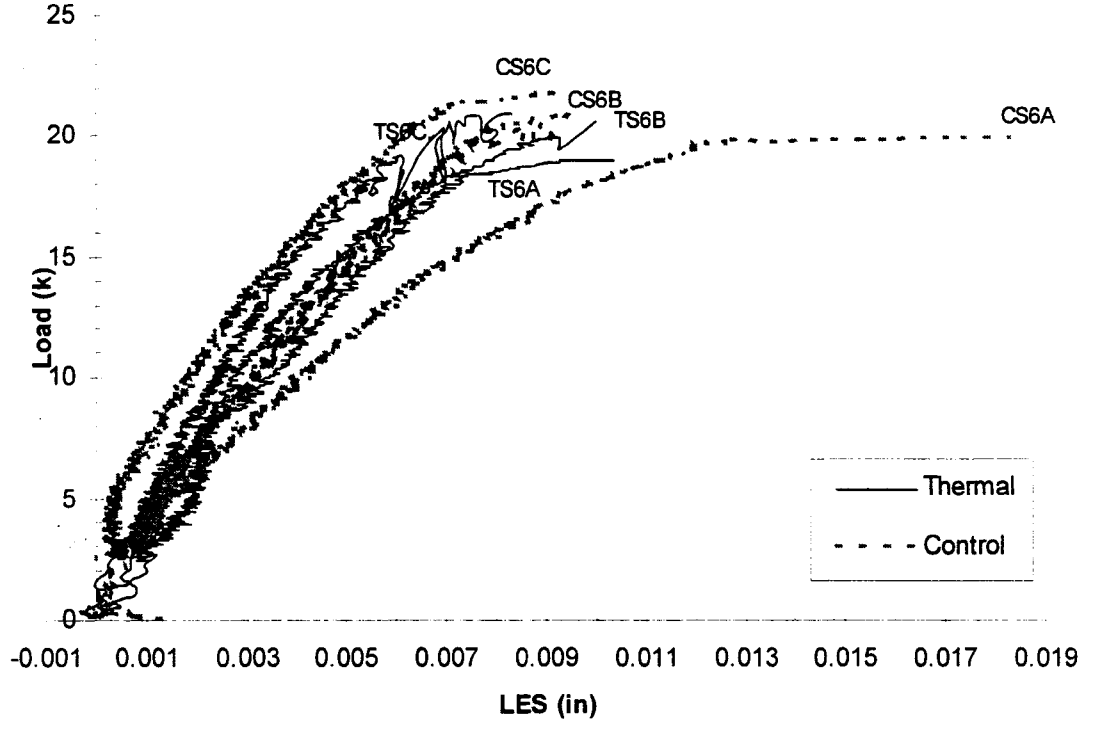

Figure 3.20 Load-Slip Curves for Thermally Cycled No.6 Steel Specimens

APPENDIX A

Procedure for Tesion Test
and
Thermal Expansion Coefficient Test

I. Tension Test

To determine the ultimate strength capacity of the GFRP rebars, six tension tests were conducted using a 600 kip MTS universal testing machine using ASTM D 638-95 (Standard Test Method for Tensile Properties of Plastics) as a guideline. Two samples were tested for each type of the GFRP rebars using the parabolic grip described in Section 2.6.2.3. Each bar had a length of approximately 34 in. The strain was measured by an extensometer over a gage length of 3 in. The testing speed chosen was 0.01 in./min. to produce rupture in 5 minutes (assuming a strain at rupture of 1.8% from previous tension tests on GFRP rebars [3]).

The results are tabulated in Table 2.4 in terms of ultimate strength, percent elongation over a 3 in. gage length, and modulus of elasticity.

II. Thermal Expansion Coefficient Test for Concrete

Three 4x8 in. concrete cylinders were used to determine the coefficient of thermal expansion according to CRD-C 39-81 (Test Method for Coefficient of Linear Thermal Expansion of Concrete). The procedure used in the test was based on the calibrations of the equipment used in the laboratory at the University of Minnesota. The average coefficient of thermal expansion was found to be 6.61×10^{-6}/°C with 1.63×10^{-6}/°C standard deviation.

APPENDIX B

Photographs of Opened Specimens

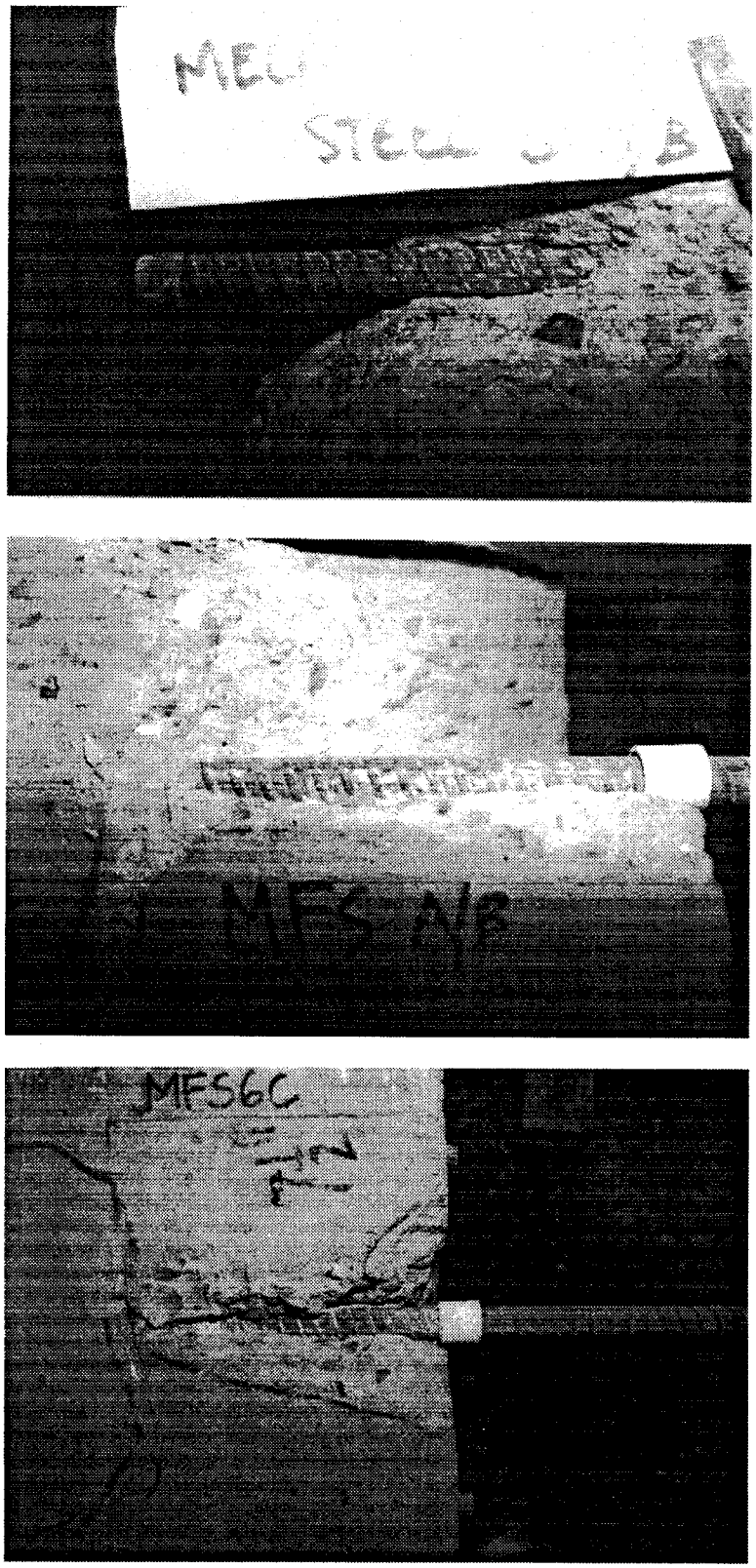

MS6A, MS6B, and MS6C Specimens

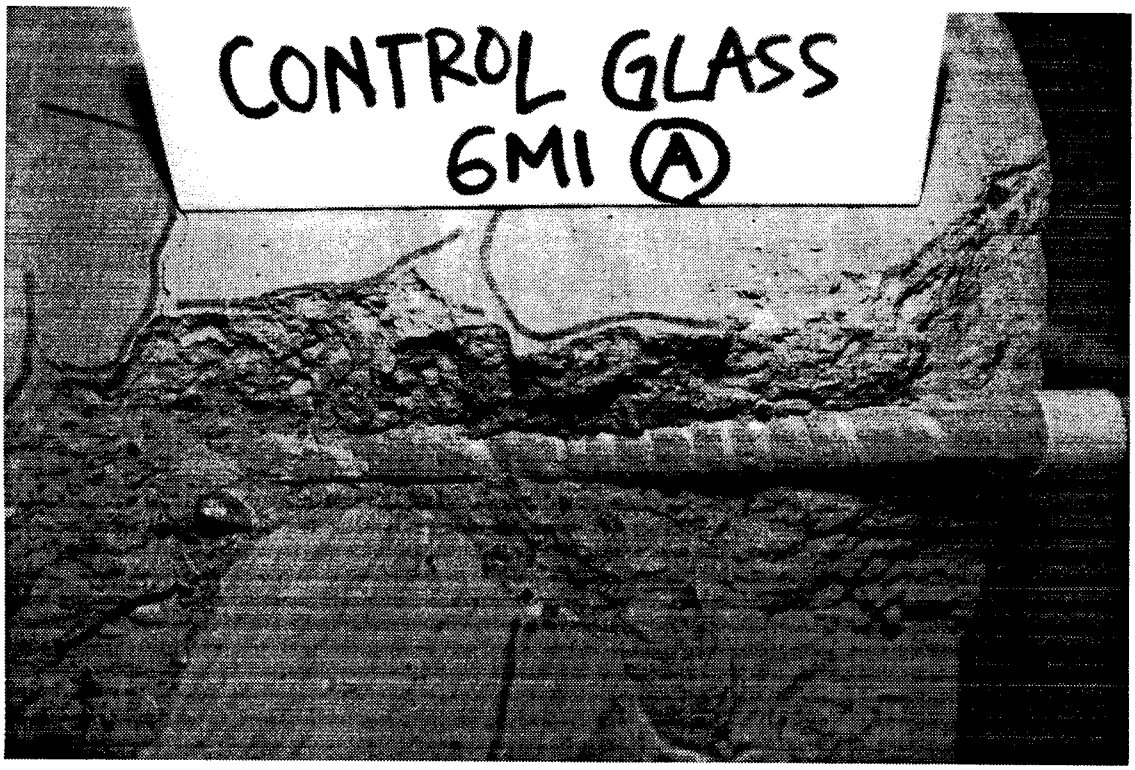

CS6A and CG6AM1 Specimens

MG6AM1, MG6BM1, and MG6CM1 Specimens

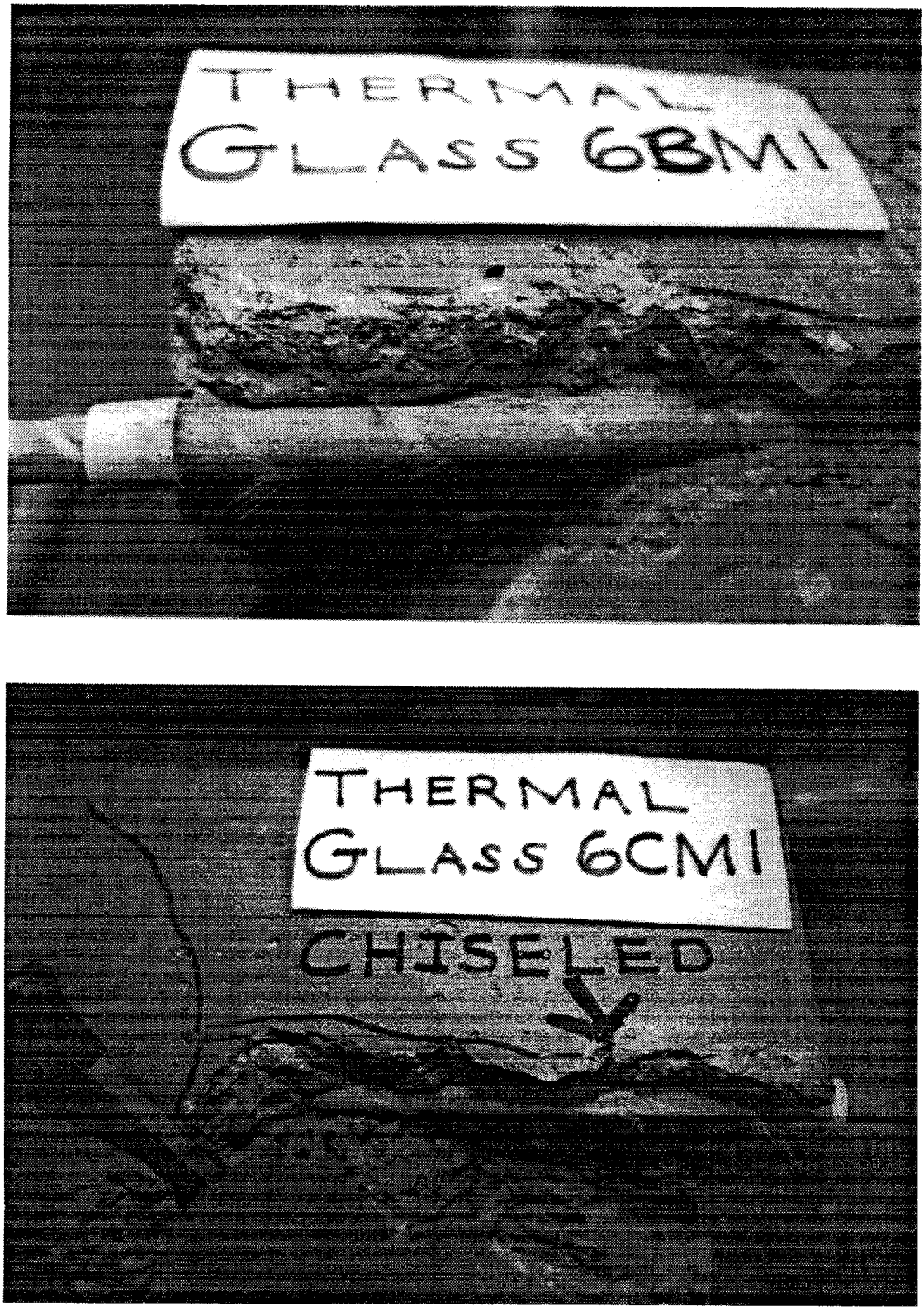

TG6BM1 and TG6CM1 Specimens

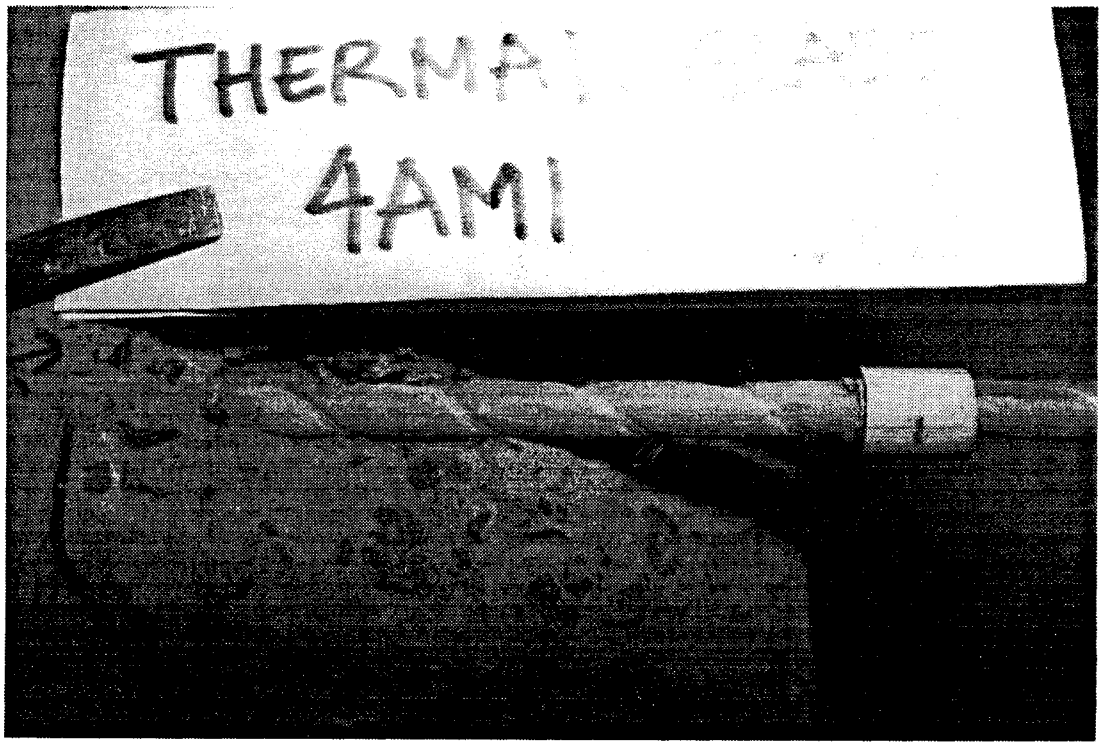

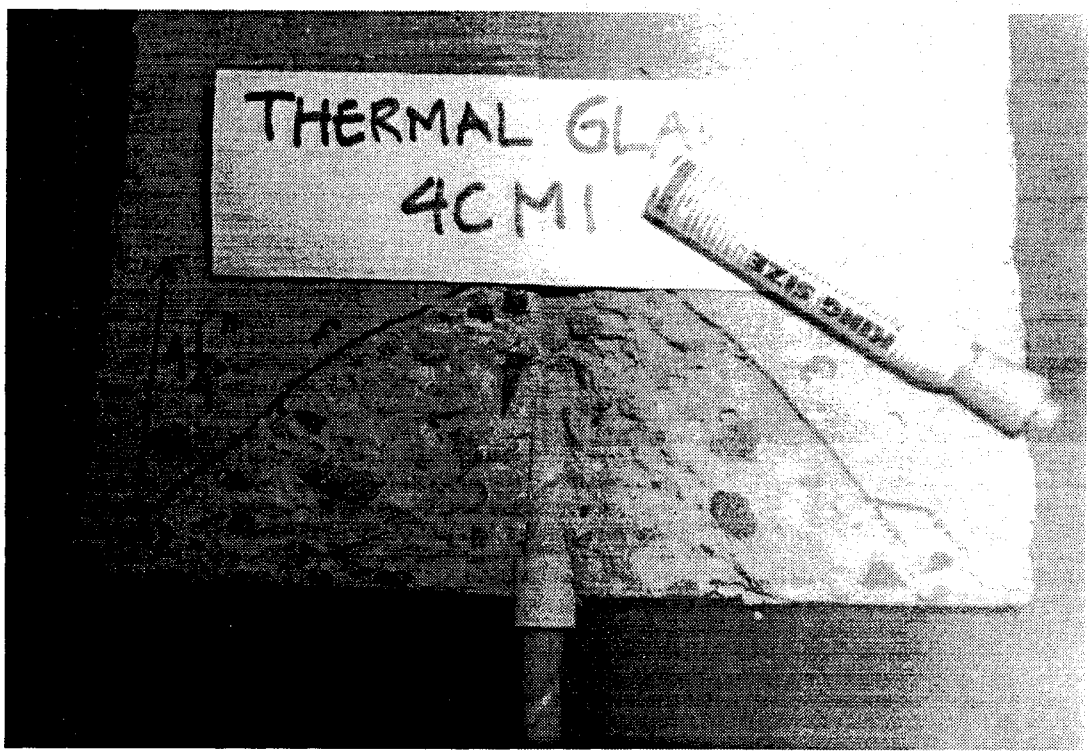

TG4AM1 and TG4CM1 Specimens

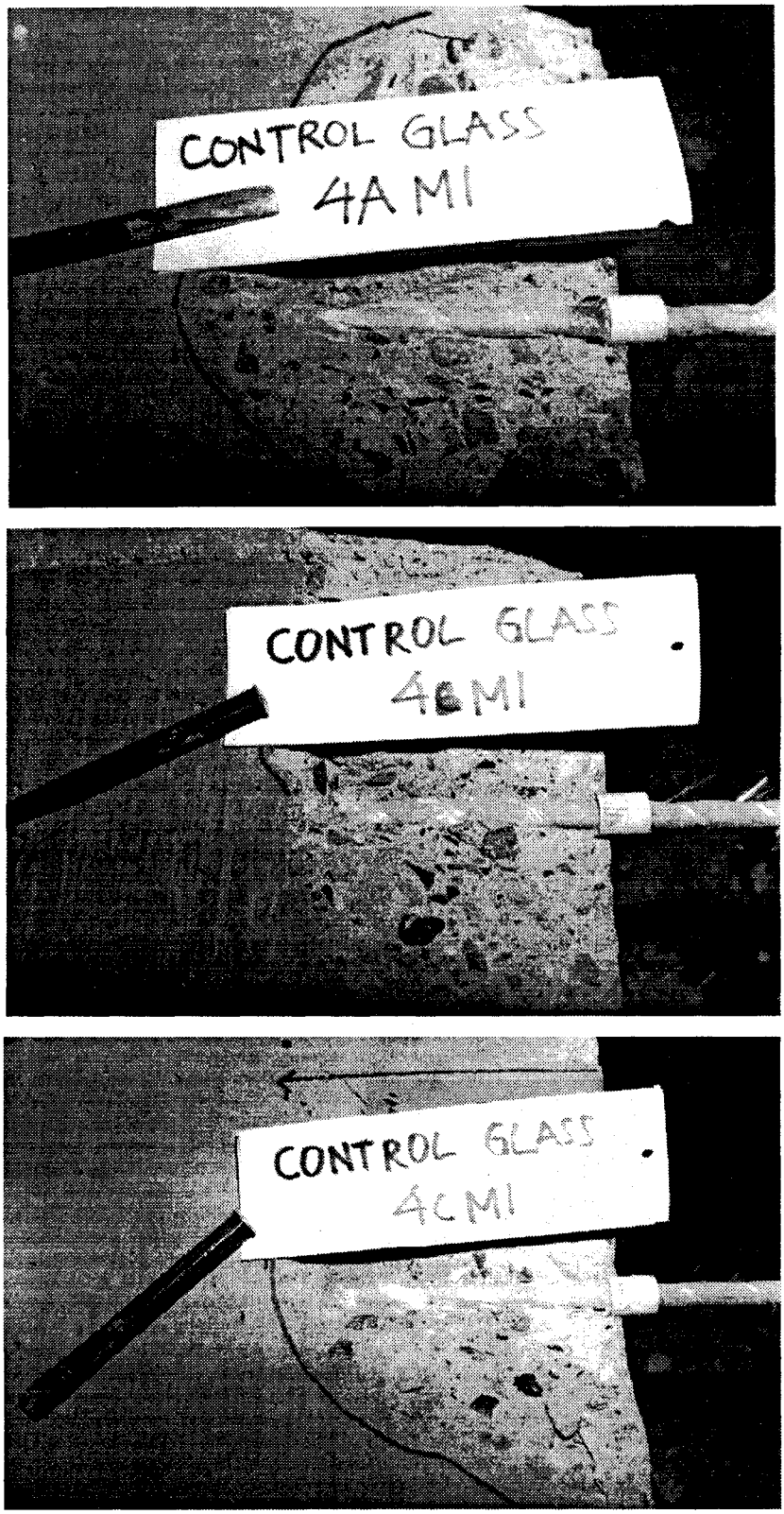

CG4AM1, CG4BM1, and CG4CM1 Specimens

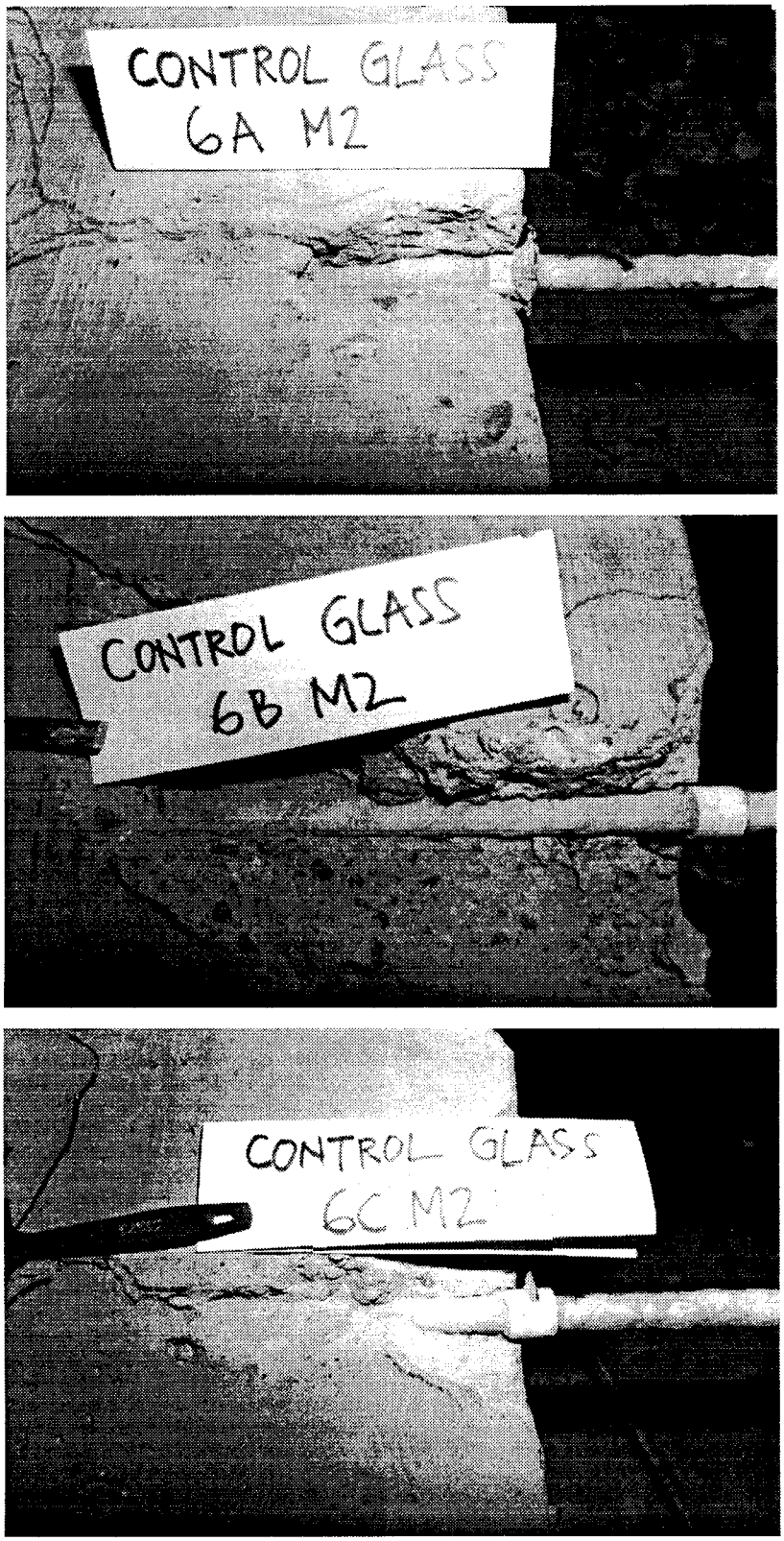

CG6AM2, CG6BM2, and CG6CM2 Specimens

TG6AM2. TG6BM2, and TG6CM2 Specimens

APPENDIX C

Free and Loaded End Slips During Mechanical Cycles

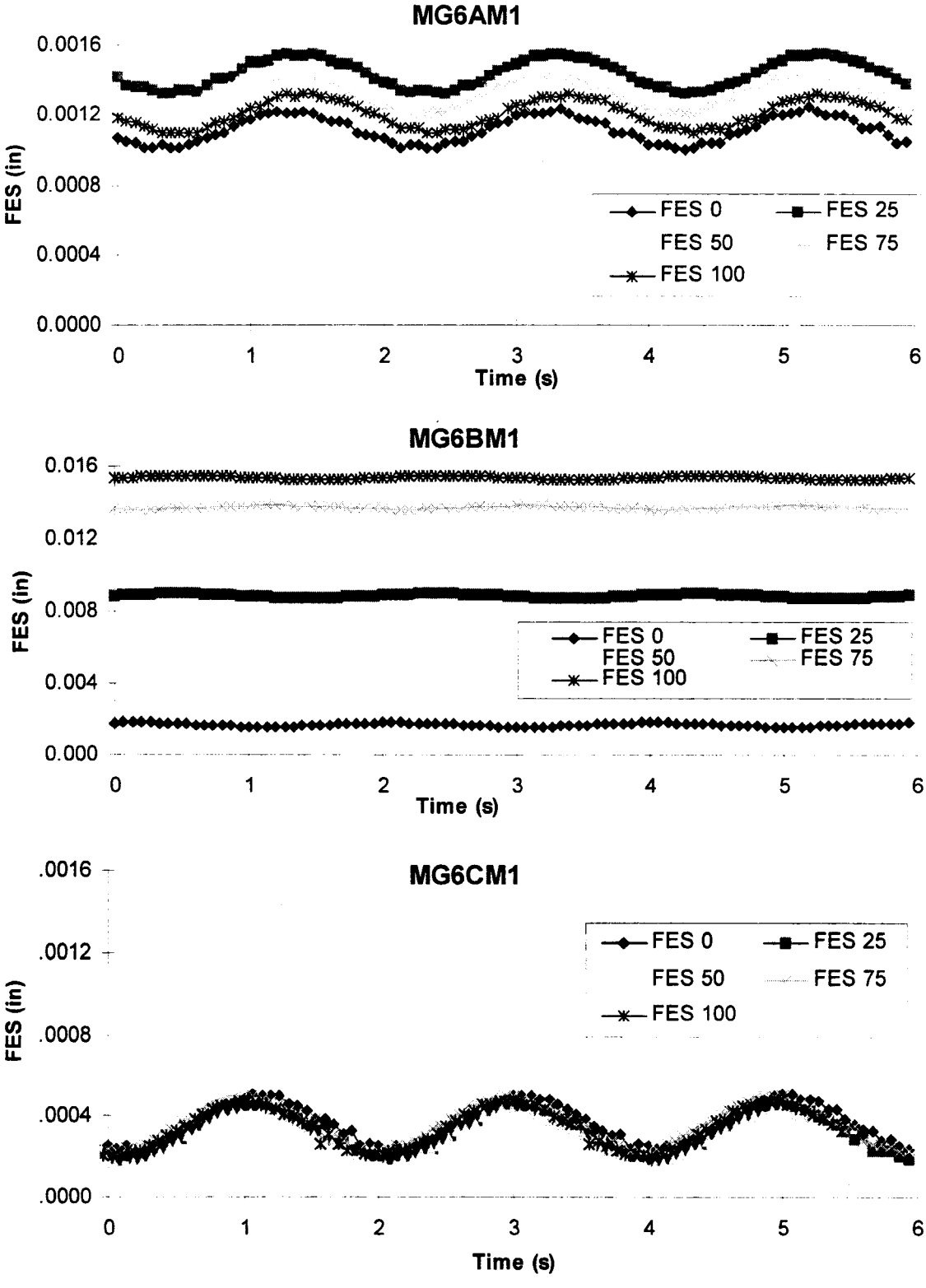

Mechanically Cycled GFRP Specimens: Free End Slip During Cycles

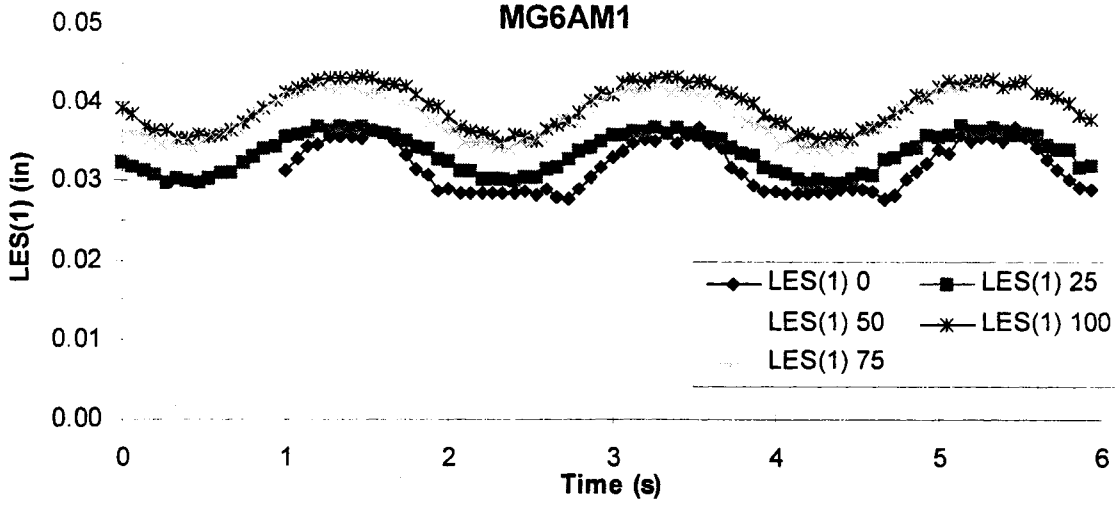

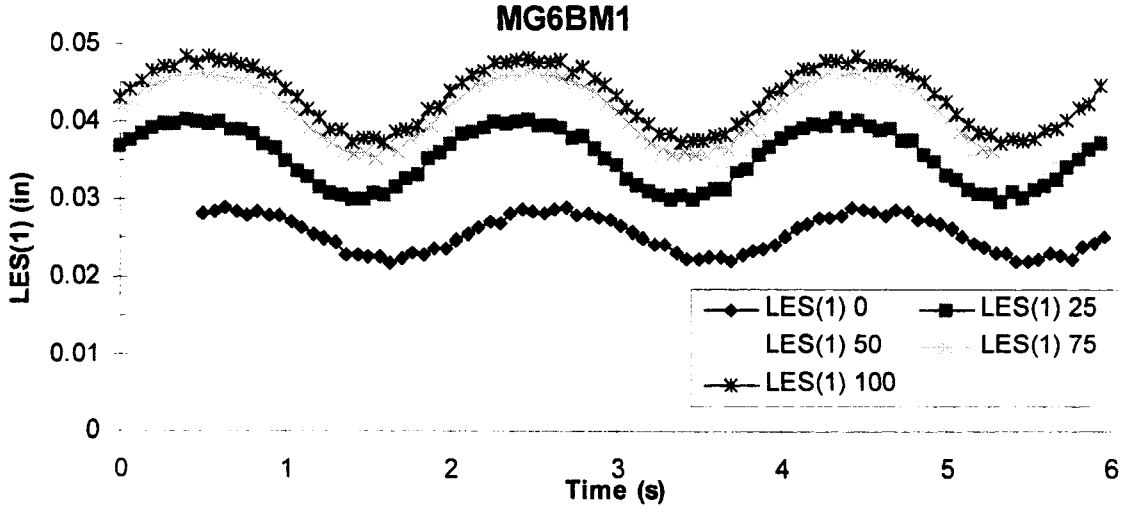

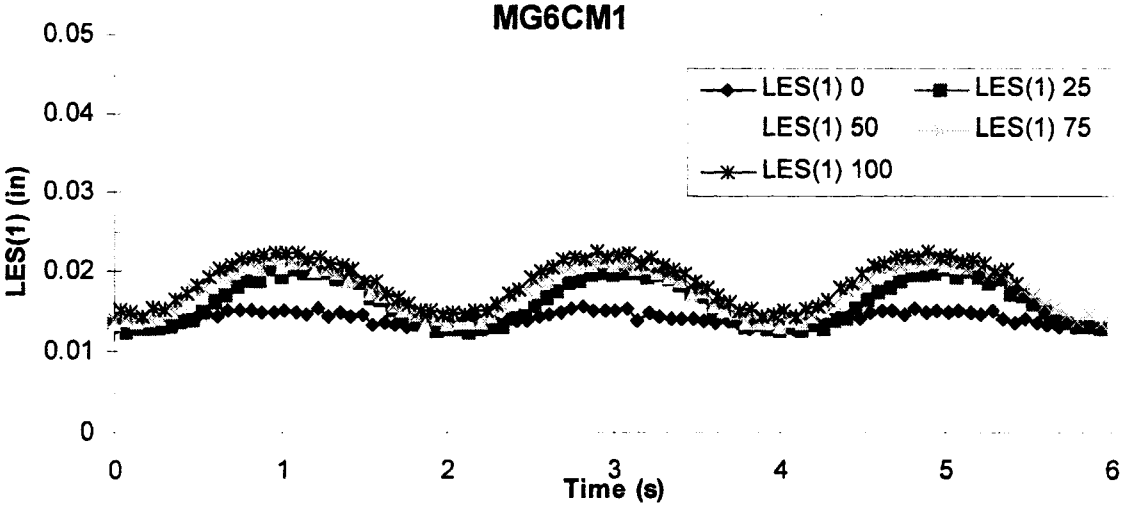

Mechanically Cycled GFRP Specimens: Loaded End Slip (1) During Cycles

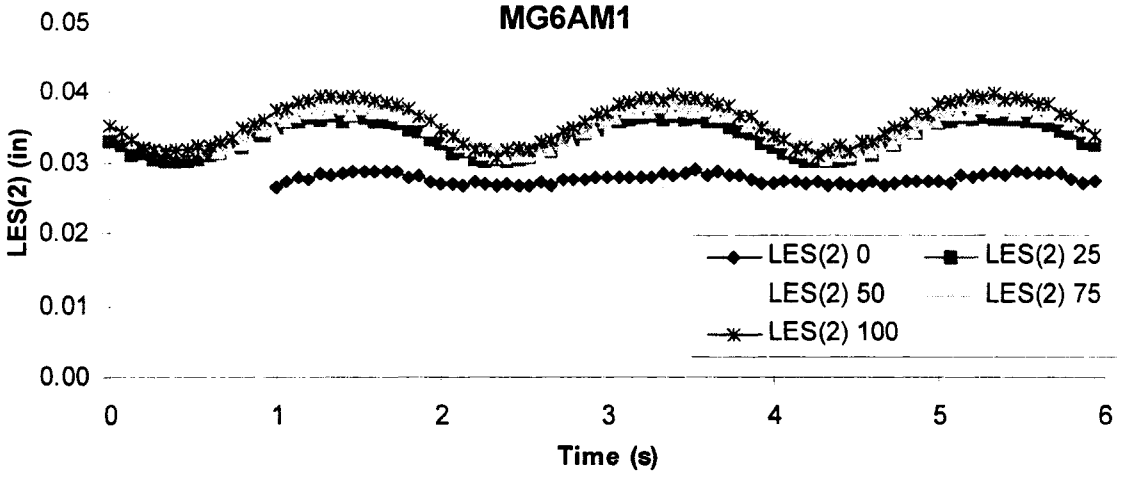

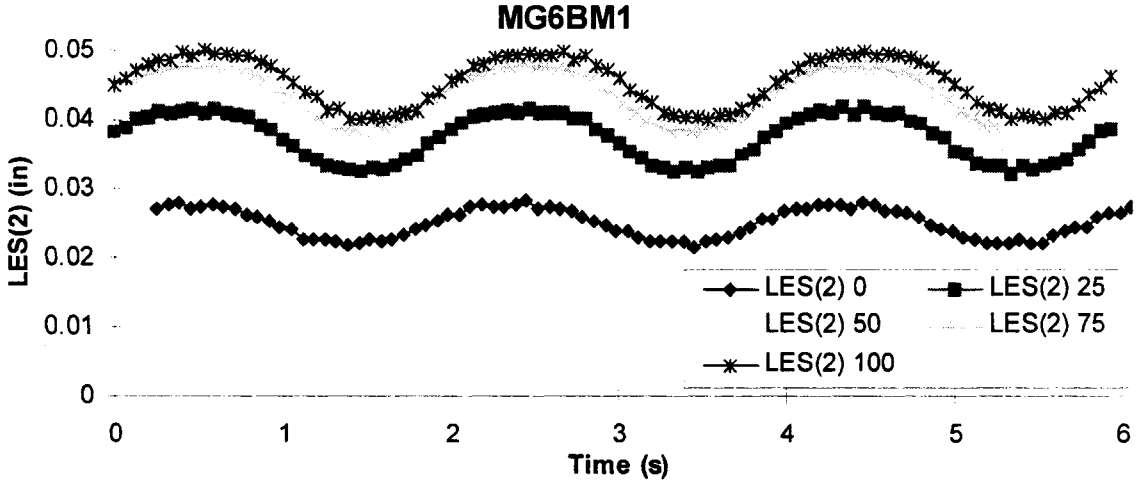

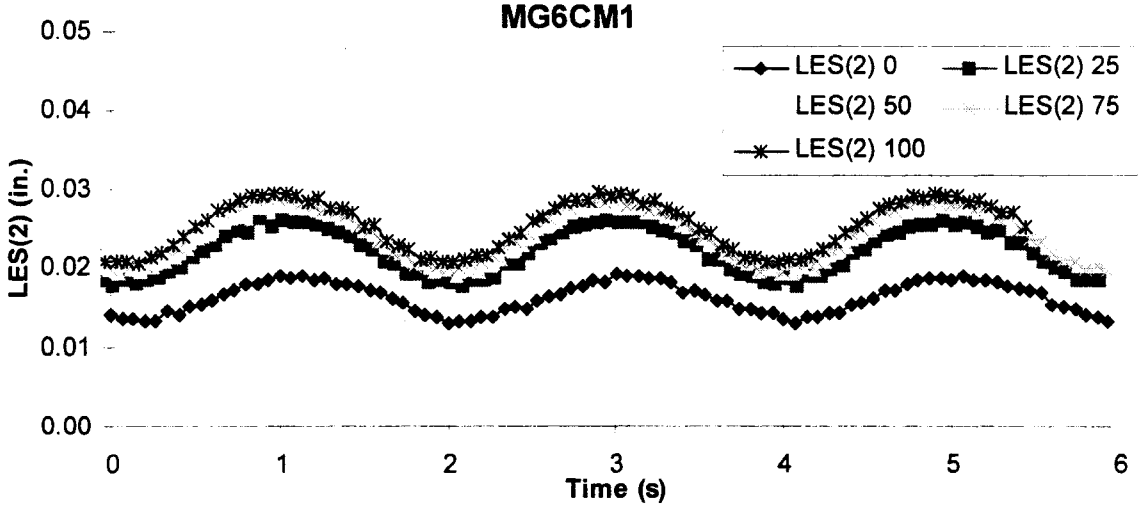

Mechanically Cycled GFRP Specimens: Loaded End Slip (2) During Cycles

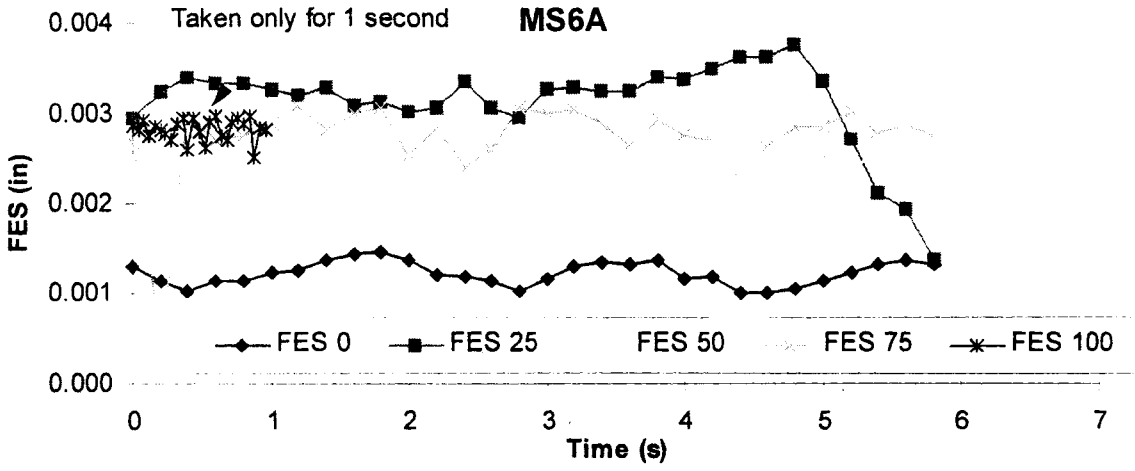

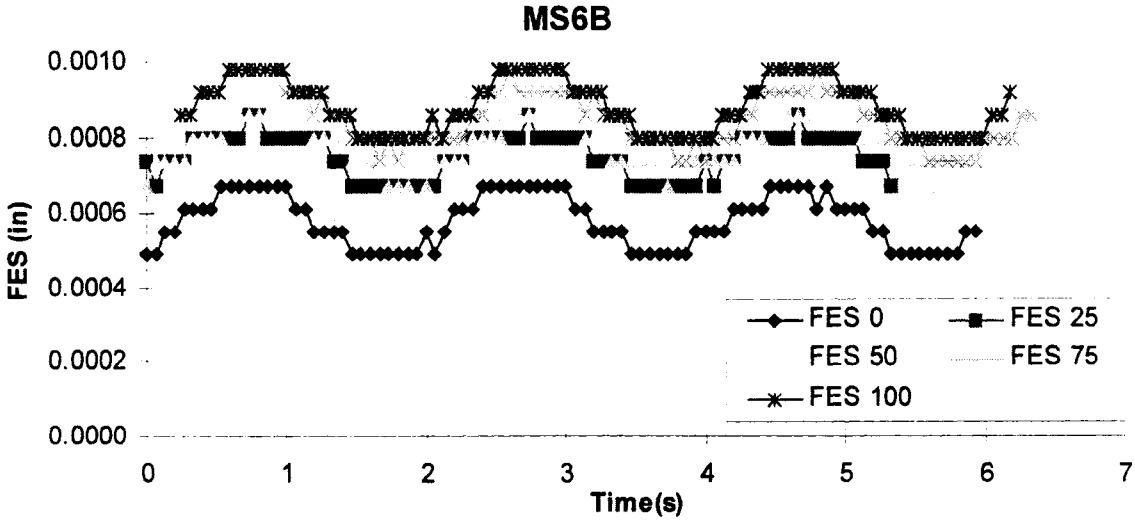

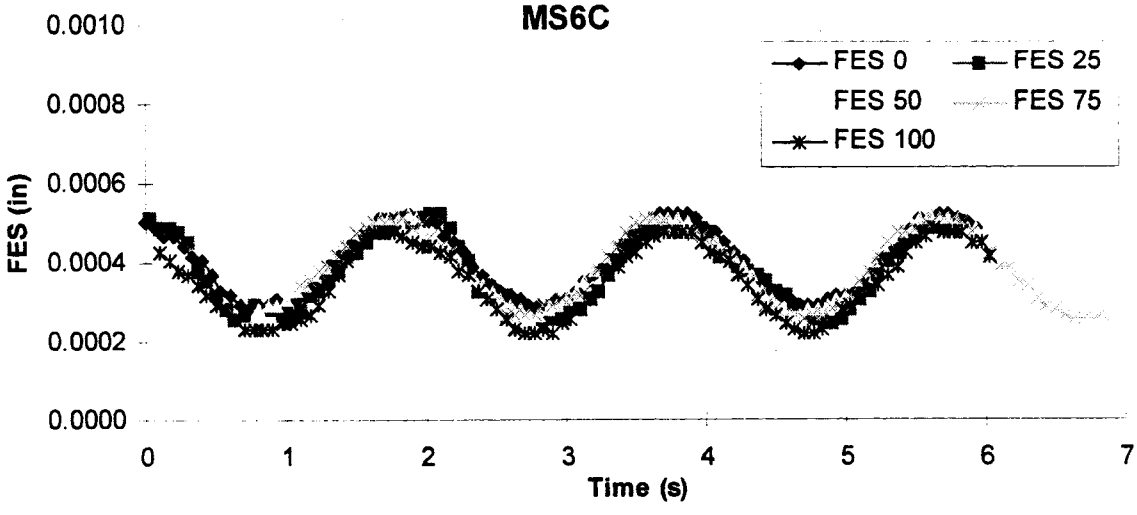

Mechanically Cycled Steel Specimens: Free End Slip During Cycles

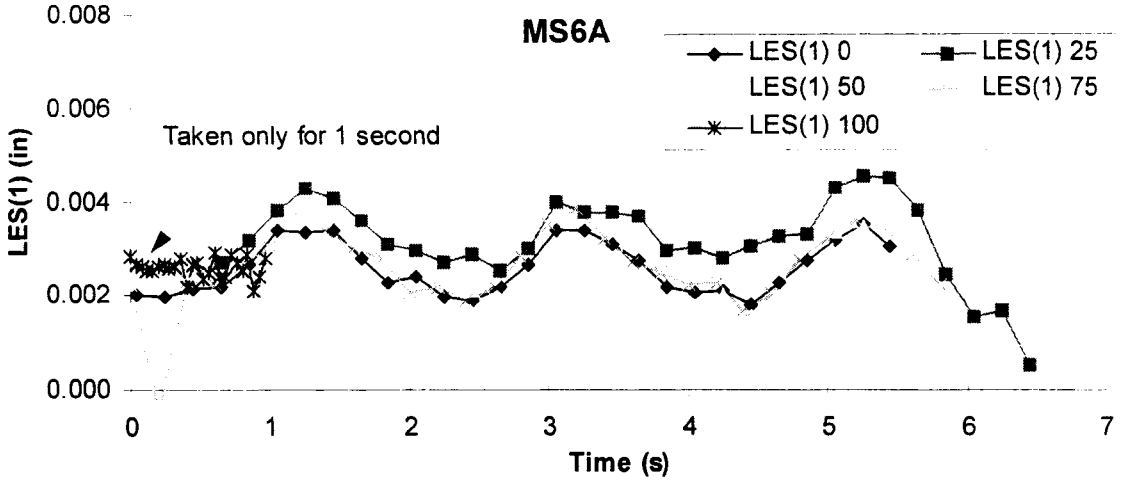

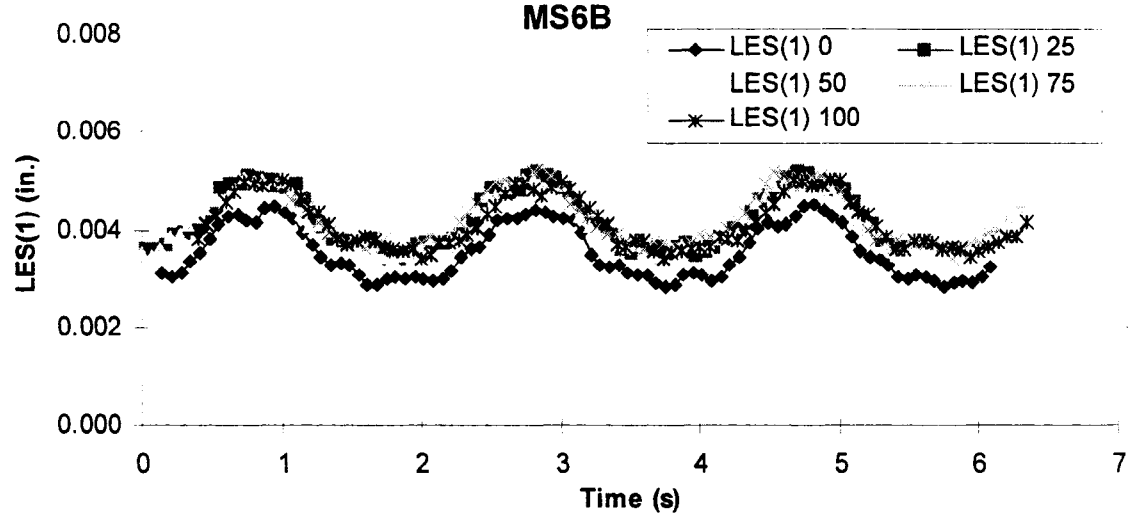

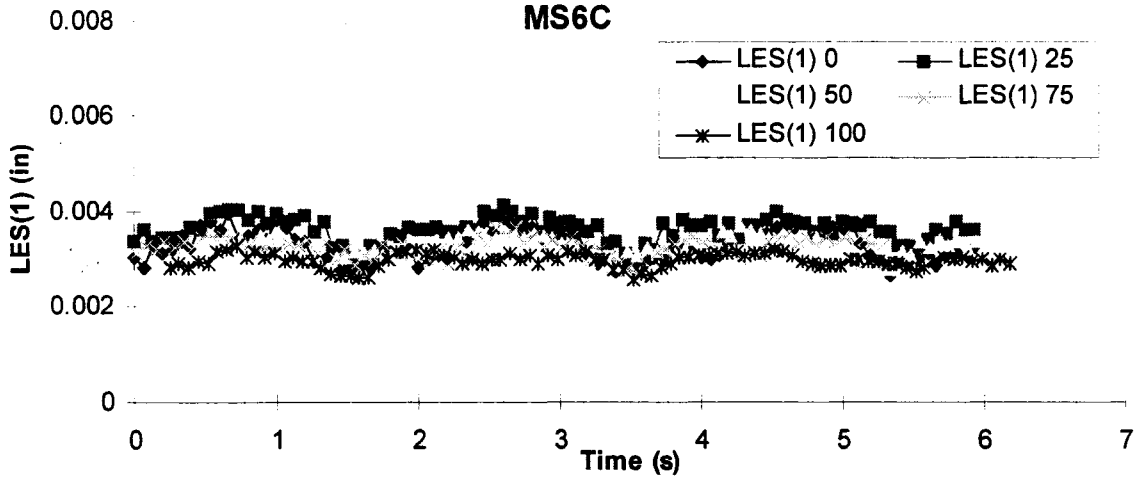

Mechanically Cycled Steel Specimens: Loaded End Slip (1) During Cycles

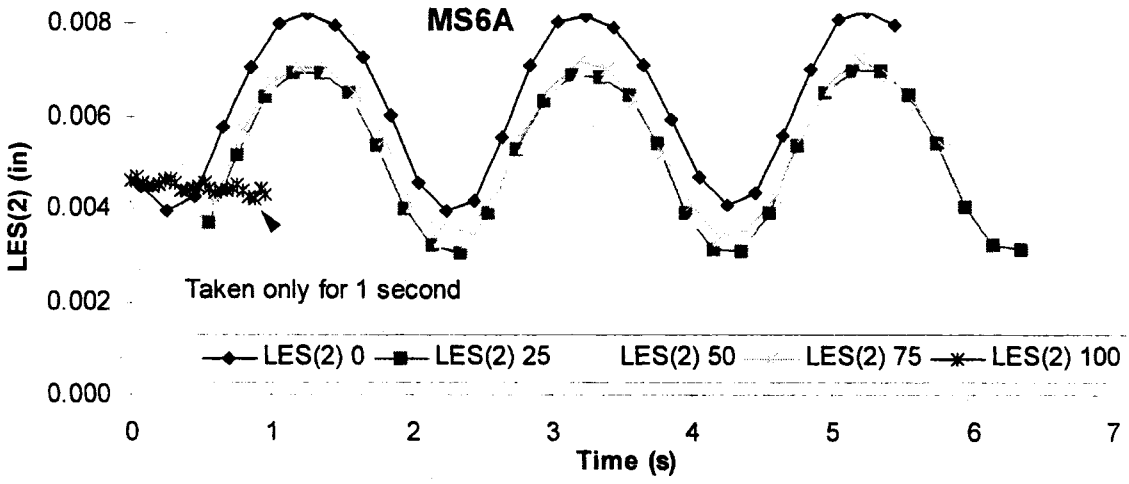

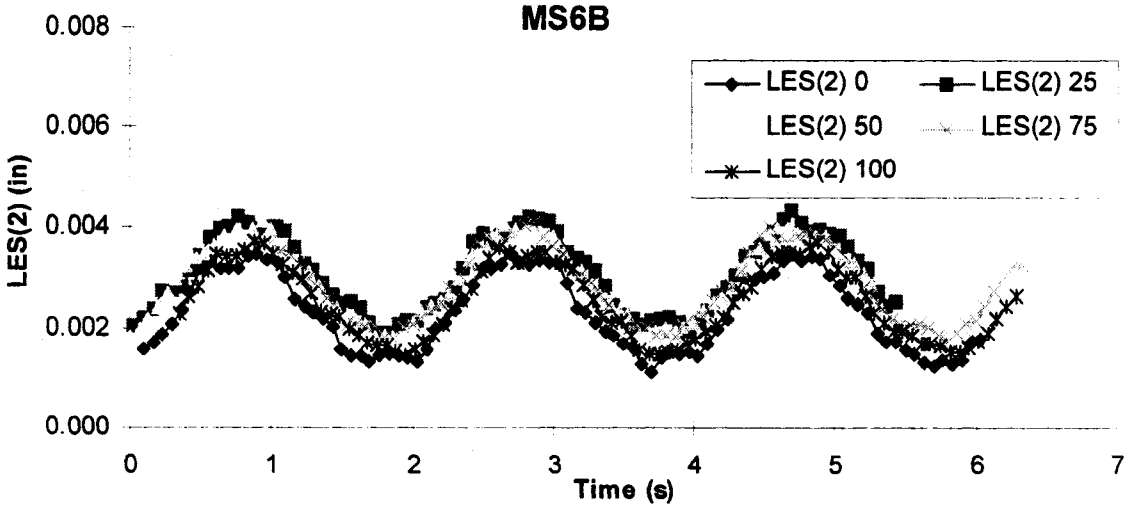

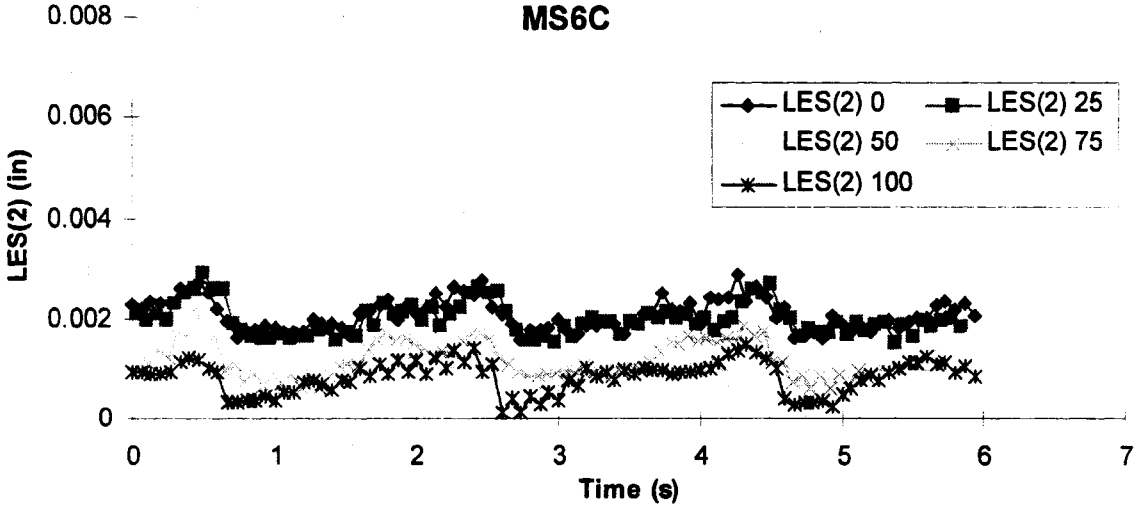

Mechanically Cycled Steel Specimens: Loaded End Slip (2) During Cycles